Impact of New Physics on Neutrino Mixing at Long Baseline Neutrino Experiments

A thesis submitted for the degree of

Doctor of Philosophy

Jogesh Rout

School of Physical Sciences

Jawaharlal Nehru University

New Delhi - 110067, India

July 2019

Declaration

This work has been carried out in School of Physical Sciences of the Jawaharlal Nehru University under the supervision of Dr. Poonam Mehta. The work reported in the thesis is original and has not been submitted earlier for any degree to any University.

Jogesh Rout

Jogesh Rout

July 2019

Poonam Mehta

Dr. Poonam Mehta
Supervisor
School of Physical Sciences
Jawaharlal Nehru University
New Delhi - 110067, India

Prof. Satyabrata Patnaik
Dean
School of Physical Sciences
Jawaharlal Nehru University
New Delhi - 110067, India

ii

Dedicated to

My brother

Acknowledgements

Firstly, I would like to express my sincere gratitude to my advisor, Prof. Poonam Mehta for her continuous support and encouragement during the course of my Ph.D study both academically and personally. She has been very patient with me and has motivated me to work hard. Her guidance has helped me throughout and at the time of writing of this thesis. I could not have imagined having a better advisor and mentor for my Ph.D study.

I would like to express my gratitude to all the teachers of SPS and in particular, Prof. Debashis Ghoshal, Prof. Subhasis Ghosh, Prof. Shankar Prasad Das and Prof. T. R. Seshadri for the wonderful courses during my Pre Ph.D. course work. I am also grateful to (late) Prof. Deepak Kumar and Prof. R. Rajaraman for useful discussions during the initial stages of my Ph.D. I would like to thank the members of my thesis advisory committee (Prof. Tanuja Mohanty and Prof. Anirban Chakraborti) for their guidance and support. I would like to thank Prof. Raj Gandhi for arranging my visit to HRI during which I attended a course on particle physics and learnt the subject from Prof. Anirban Basu and Prof. Satchidananda Naik. I would also like to thank the organisers for giving me an opportunity to participate in SERC school at BITS Hyderabad where I could learn the subject from the lecturers.

It gives me immense pleasure to thank my collaborators - Dr. Mehedi Masud, Prof. Laura Fields, Prof. Mary Bishai, Mr. Samiran Roy and Ms. Sheeba Shafaq. Also, a special thanks to Sheeba for her valuable help during the writing of this thesis. I would like to give a very special thanks to Dr. Mehedi Masud for the collaborative work as well as frequent and fruitful discussions that helped me in learning GLoBES package - an essential skill for working in neutrino physics. I would like to acknowledge fruitful discussions with Prof. Laura Fields on topics related to beam optimization and my friend, Dr. Biswa Ranjan Behera who helped me in all aspects during my visit to Fermilab on Rajendran Raja fellowship. I am also grateful to Prof. Sudhanwa Patra for hosting me at SOA, Bhubaneswar and IIT Bhilai, Raipur and for the useful discussions.

Some people arrive and make such a beautiful impact on your life, you can barely

remember what life was like without them. Some of those names are Bisu, Suchi, Nira, Bikash, Debi, Sukanta, Shiba, Kasi bhai, Mihir bhai, Shiba bhai, Jaga (Athgarh), Suchi (Athgarh), Archana, Deepti and Ranjan.

Next, I would like to mention that the time spent at JNU has been one of the most beautiful times of my life and which has thus become a "home away from home" for me during the past six years. I am lucky to have juniors like Samir, Chita, Dhiren, Dilip, Dev and Arpita. My classmates, a funny and bindas group, Umesh, Rahul, Pankaj, Sunil, Arijit, Nasir, Kishore and Kisan, you guys will be remembered for ever. My beloved seniors Pratyay da, Santosh Bhaiya, Ankita didi, Girish bhaiya, K. Kishore, Panchu bhaiya, Sarvan bhaiya, Yogi bhaiya, Dushyanta bhaiya, Manoj bhaiya who always supported me in all difficulties. SPS juniors Pawan, Amit, Neeraj, Ajit, Jagdish, Amar, Rahul, Bina, Vaibhav, Ali, Gopal, Kamlesh, Virender, Meghadeepa, Deepti, Ankit, Priyanka, Sanjiv and Tanmaya thanks to be very helpful. My hostelmates are so friendly and I will miss Dilip bhaiya, Rahul, Raju, Mehedi, Rakesh bhaiya, Rajib bhaiya, Dinesh, Deepak, Dibakar, Atique bhaiya, Zubair bhaiya, Pabitra bhaiya and my ideal Sujeet bhaiya.

It's now the turn for those who supported and encouraged me to reach at this level. My elder brother, Mr. Manguli Rout has always encouraged and supported me, both financially and morally throughout my journey. Without his support, I could not have arrived here. My parents have selflessly supported me and stood by me during this phase of my life even though they have little idea of research.

From the early stages, I cannot forget my tenth grade teachers, Mr. Pitabas and Mr. Laxman for their encouragement to improve my standards. During my bachelors, Dr. Suchismita Mohanty advised me to pursue a career in physics. During my masters at Utkal University, I was taught by Prof. Swapna Mahapatra and Prof. Karmadeva Maharana. They inspired me to take up research in the field of high energy physics and I would like to sincerely thank them.

Finally, I would like to acknowledge the infrastructural support from SPS. I would like to thank Bhupal Ji, Nikhil bhaiya, Saurabh bhaiya, Ashish bhaiya and Amita for their help and support. My research has been funded by UGC-BSR Fellowship.

List of Publications

Published

1. Can we probe intrinsic CP and T violations and nonunitarity at long baseline accelerator experiments?
   Jogesh Rout, Mehedi Masud, Poonam Mehta
   Phys. Rev. D 95, 075035 (2017).

2. Impact of New Physics on CP-Asymmetries at Long Baselines
   Jogesh Rout, Mehedi Masud, Poonam Mehta
   Springer Proc. Phys. 203 795 (2018).

Preprints

1. Impact of nonstandard interactions on beam optimization for CP violation sensitivity at DUNE
   Jogesh Rout, Laura Fields, Poonam Mehta
   under preparation.

2. Exploiting the second oscillation maximum at DUNE
   Sheeba Shafaq, Jogesh Rout, Mary Bishai, Poonam Mehta
   under preparation.

Acronyms

AGN Active Galactic Nuclei

BOTF Beam Optimization Task Force

CC Charged Current

CDR Conceptual Design Report

CP Charge conjugation Parity

CPT Charge conjugation Parity Time reversal

DUNE Deep Underground Neutrino Experiment

GRB Gamma Ray Bursts

ICARUS Imaging Cosmic And Rare Underground Signals

IH Inverted Hierarchy

INO India-based Neutrino Observatory

HK Hyper Kamiokande

KamLAND Kamioka Liquid Scintillator Antineutrino Detector

K2K KEK to Kamioka

LArTPC Liquid Argon Time Projection Chambers

LBL Long Baseline

LBNF Long Baseline Neutrino Facility

LEP Large Electron Positron Collider

LH Left-handed

LSND Liquid Scintillator Antineutrino Detector

MSW Mikheyev Smirnov Wolfenstein

NC Neutral Current

NH Normal Hierarchy

NOvA NuMI Off-Axis ν_e Appearance

NSI Non-standard Interactions

NuMI Neutrinos at the Main Injector

MINOS Main Injector Neutrino Oscillation Search

OPERA Oscillation Project with Emulsion-tRacking Apparatus

PMNS Pontecorvo Maki Nakagawa Sakata

PMTs Photo Multiplier Tubes

POT Protons on Target

RENO Reactor Experiment for Neutrino Oscillation

RH Right-handed

SBL Short Baseline

SBN Short Baseline Neutrino Program

SI Standard Interactions

SK Super Kamiokande

SM Standard Model

T Time reversal

T2K Tokai to Kamioka

T2HK Tokai to Hyper Kamiokande

Contents

List of Figures

List of Tables

Chapter 1

Introduction

This chapter serves as an introduction to the thesis and reviews the basic requirements necessary for studying impact of specific class of new physics (i.e. beyond the Standard Model (SM) of particle physics) scenarios which may leave their signatures in neutrino mixing at the long baseline (LBL) experiments. Presently, we know that the SM of particle physics is capable of successfully describing a large volume of experimental data. However it is no longer the case in the context of neutrino physics. Neutrino oscillations among the three active neutrino flavors have been vindicated by many categories of experiments such as solar, atmospheric, accelerator and reactor experiments which in turn implies that neutrinos have non-zero masses and the SM is inadequate. The present generation of neutrino oscillation experiments have been fairly successful in establishing neutrino oscillations and the next generation of experiments have been planned to answer some of the remaining unknowns in neutrino oscillation physics. In this thesis, we address some of the pertinent issues involving the impact of new physics in neutrino mixing at the future LBL experiments with main focus on the Deep Underground Neutrino Experiment (DUNE).

1.1 Neutrinos and the Standard Model

Since we wish to deal with topics beyond the SM of particle physics in this thesis, let us first describe what is SM. The SM of particle physics is a theory that gives a com-

prehensive description of fundamental constituents of matter and their interactions. This theory was devised by Glashow, Weinberg and Salam [1] and includes unified theory of electroweak interactions and the theory of strong interactions (quantum chromodynamics). We will give a brief description of the structure of the theory next.

1.1.1 Brief overview of the Standard Model

In the present section, we define the SM of elementary particles by introducing the particle content and parameters of this model. Our aim is to give only a short introduction here. In order to delve deeper into the subject touched upon here, we refer the reader to the seminal papers on the SM [1] and to the standard texts [2].

The SM is quantum field theory of electromagnetic, weak and strong interactions based on a gauge theory with an $\mathrm{SU(3)_c} \bigotimes \mathrm{SU(2)_L} \bigotimes \mathrm{U(1)_Y}$ gauge group. The $\mathrm{SU(3)_c}$ is the symmetry group of strong interactions where c is the colour quantum number carried by the gauge bosons that mediate strong interactions. The $\mathrm{SU(2)_L} \bigotimes \mathrm{U(1)_Y}$ is the symmetry group of electroweak interactions where L is left chirality and Y is the weak hypercharge defined below. SM comprises of three kinds of particles : the gauge bosons that mediate the interactions, fermions (quarks and leptons) and the Higgs sector.

Fermionic content of SM : The basic constituents of matter are the spin-half fermions which comprise of *the leptons* and *the quarks*. There are 3 generations of leptons and quarks in the SM.

$$l_{iL} \;:\; \begin{pmatrix} \nu_i \\ e_i \end{pmatrix}_L \quad e_{iR} \;;\; q_{iL} \;:\; \begin{pmatrix} u_{i\alpha} \\ d_{i\alpha} \end{pmatrix}_L \quad u_{i\alpha R} \quad d_{i\alpha R} \;;\quad i = 1,2,3 \quad \& \quad \alpha = 1,2,3$$

with i being the generation index and α being the colour index. In order to account for the V-A nature of the charged current (CC) weak interactions, the quarks and leptons transform according to left-handed (LH) doublet and right-handed (RH) singlet representations of $\mathrm{SU(2)_L}$. In order to account for the strong interactions of quarks, the quarks transform as triplets of $\mathrm{SU(3)_c}$ of colour, while the leptons are singlets under $\mathrm{SU(3)_c}$. The assignment of weak hypercharge corresponding to

the $U(1)_Y$ group to the various $SU(2)_L$ and $SU(3)_c$ multiplets is according to the charge formula : $Q = T_3 + Y$, where T_3, Y and Q denote the third component of weak isospin corresponding to $SU(2)_L$, weak hypercharge and the electric charge generators respectively. Note that electric charge is independent of colour, since no generator of $SU(3)_c$ appears in the charge formula. In Table 1.1 and Table 1.2 respectively, we have listed the three generations of leptons and quarks and their properties like mass (in units of MeV/c^2), electric charge (Q in units of $|e|$), the third component of the weak isospin ($T_3 = \pm 1/2$ for a weak isospin doublet and 0 for a singlet), the average charge of the weak isospin multiplet called the hypercharge assignments for fermions and the individual lepton family and baryon numbers.

Generation	Particles (Leptons)	Symbol	Mass (MeV/c^2)	Q	T_3	Y	Lepton no. L_e	L_μ	L_τ
I	Electron neutrino	ν_e	$< 3 \times 10^{-6}$	0	$+\frac{1}{2}$	$-\frac{1}{2}$	+1	0	0
	Electron	e^-	0.511	-1	$-\frac{1}{2}$	$-\frac{1}{2}$	+1	0	0
I	Electron	e_R^-	0.511	-1	0	-1	+1	0	0
II	Muon neutrino	ν_μ	< 0.19	0	$+\frac{1}{2}$	$-\frac{1}{2}$	0	+1	0
	Muon	μ^-	105.66	-1	$-\frac{1}{2}$	$-\frac{1}{2}$	0	+1	0
II	Muon	μ_R^-	105.66	-1	0	-1	0	+1	0
III	Tau neutrino	ν_τ	< 18	0	$+\frac{1}{2}$	$-\frac{1}{2}$	0	0	+1
	Tau	τ^-	1777	-1	$-\frac{1}{2}$	$-\frac{1}{2}$	0	0	+1
III	Tau	τ_R^-	1777	-1	0	-1	0	0	+1

Table 1.1: Properties of 6 known leptons in the SM. The corresponding anti-leptons have equal mass but opposite charge and additive quantum numbers.

Bosonic content of the SM : The scalar sector of the theory has one elementary particle called the *Higgs boson*. In the SM the Higgs boson transforms according to

Generation	Particles (Quarks)	Symbol	Mass (MeV/c^2)	Q	T_3	Y	Baryon no. B
I	Up	u	$1.5 - 4.5$	$+\frac{2}{3}$	$+\frac{1}{2}$	$+\frac{1}{6}$	1/3
	Down	d	$5 - 8.5$	$-\frac{1}{3}$	$-\frac{1}{2}$	$+\frac{1}{6}$	1/3
I	Up	u_R	$1.5 - 4.5$	$+\frac{2}{3}$	0	$+\frac{2}{3}$	1/3
	Down	d_R	$5 - 8.5$	$-\frac{1}{3}$	0	$-\frac{1}{3}$	1/3
II	Charm	c	$1000 - 1400$	$+\frac{2}{3}$	$+\frac{1}{2}$	$+\frac{1}{6}$	1/3
	Strange	s	$80 - 155$	$-\frac{1}{3}$	$-\frac{1}{2}$	$+\frac{1}{6}$	1/3
II	Charm	c_R	$1000 - 1400$	$+\frac{2}{3}$	0	$+\frac{2}{3}$	1/3
	Strange	s_R	$80 - 155$	$-\frac{1}{3}$	0	$-\frac{1}{3}$	1/3
III	Top	t	$174.3 \pm 5.1 \times 10^3$	$+\frac{2}{3}$	$+\frac{1}{2}$	$+\frac{1}{6}$	1/3
	Bottom	b	$4000 - 4500$	$-\frac{1}{3}$	$-\frac{1}{2}$	$+\frac{1}{6}$	1/3
III	Top	t_R	$174.3 \pm 5.1 \times 10^3$	$+\frac{2}{3}$	0	$+\frac{2}{3}$	1/3
	Bottom	b_R	$4000 - 4500$	$-\frac{1}{3}$	0	$-\frac{1}{3}$	1/3

Table 1.2: Properties of six known quarks in the SM. The corresponding anti-quarks have equal mass but opposite charge and additive quantum numbers.

doublet representation of $SU(2)_L$ while under $SU(3)_c$ it is a singlet. The complex scalar doublet is given by

$$\Phi = \begin{pmatrix} \phi^+ \\ \phi^0 \end{pmatrix}$$

The two complex scalars carry an electric charge $Q = +1, 0$ and a weak hypercharge $Y = Q - T_3 = 1/2$. Note that the Higgs boson is the only boson in the theory which is not a gauge boson.

In the gauge sector, we have *eight gluons* which are the gauge bosons of $SU(3)_c$ and are the mediators of strong interactions. For the broken $SU(2)_L \bigotimes U(1)_Y$, we have *three weak gauge bosons* : the $W^{\pm}$ and the Z and one photon (γ) which mediates the electromagnetic interactions. The gluons are chargeless and massless objects and carry colour quantum number. The $W^{\pm}$ are charged and massive particles while Z is electrically neutral but massive and the photon is both chargeless and massless.

The 8 gluons (g) and the 3 weak bosons ($W^{\pm}, Z$) are self-interacting but the photon (γ) is not. The properties of the gauge bosons and their interactions *etc* are listed in Table 1.3.

In a gauge invariant theory, none of the fields correspond to massive particles as global gauge invariance does not allow fermion mass terms while as local gauge invariance forbids any boson mass terms. Spontaneous symmetry breaking allows for the mass terms without sacrificing the renormalizability of the theory. The Higgs boson induces this spontaneous symmetry breaking of the gauge group $\mathrm{SU(3)_c} \bigotimes \mathrm{SU(2)_L} \bigotimes \mathrm{U(1)_Y}$ to $\mathrm{SU(3)_c} \bigotimes \mathrm{U(1)_Y}$.

Particles (Gauge bosons)	Symbol	Mass (in MeV/c^2)	Q	Symmetry	Interaction (strength)
8 Gluons	g	0	0	SU(3)	Strong (1)
Photons	γ	0	0	U(1)	Electromagnetic (10^{-2})
Intermediate vector bosons	$W^{\pm}$	80.423	± 1	SU(2)	Weak(10^{-5})
	Z^0	91.1876	0	SU(2)	Weak(10^{-5})

Table 1.3: Properties of gauge bosons and their interactions and underlying symmetries in SM.

A Remark concerning the mass of the neutrino : The neutrino sector in the SM has only LH neutrinos and RH anti-neutrinos which form doublets with corresponding charged leptons. With one Higgs field Φ in the theory, only the Yukawa couplings $\bar{l}_{iR} l_{iL} \Phi + h.c.$ are present in the SM and we have a global symmetry corresponding to lepton number conservation. Thus, neutrinos are massless in the SM. There are many possible extensions of the SM to give $m_\nu \neq 0$; they can be broadly categorized as

1. *Extension of the Higgs sector only :* Other scalars besides the Higgs doublet, Φ can join the lepton bilinear to form $\mathrm{SU(2)_L} \bigotimes \mathrm{U(1)_Y}$ gauge-invariant Yukawa

couplings. These can be triplet : H, singly charged singlet : h^+ and doubly charged singlet : R^{++}. For example, when the triplet, H develops a vacuum expectation value (v_H), a Majorana mass term for the neutrino, $(v_H f)\bar{\nu}^c_{iL}\nu_{iL}$, results.

2. *Extension of the lepton sector only :* The simplest scheme is obviously the addition of three neutral singlets, the RH neutrinos, ν_{eR}, $\nu_{\mu R}$ and $\nu_{\tau R}$ in the theory. These are singlets under $\mathrm{SU(3)_c}$ and $\mathrm{SU(2)_L}$ and carry no hypercharge. In this extension we get additional terms in the Lagrangian of the type : $D\bar{\nu}_{iL}\nu_{iR}+B\bar{\nu}^c_{iR}\nu_{iR}+h.c.$, where $D=(1/\sqrt{2})v_\Phi f$. A Majorana bare-mass term B is present because ν_R is totally neutral with respect to $\mathrm{SU(2)_L}\bigotimes\mathrm{U(1)_Y}$ group and we do not impose lepton number conservation on the theory. Thus in this extension we are naturally led to consider neutrino mass terms of the Dirac and Majorana types.

3. *Extension of both Higgs and lepton sectors :* This is the most general case where one adds new scalars like Higgs triplet mentioned above as well as RH singlet neutrinos to the theory. Here also, we can get neutrino mass terms of both Dirac and Majorana types.

1.1.2 Neutrino interactions within the Standard Model

Neutrinos interact and scatter off matter as described by the electroweak theory of SM [3, 4]. Neutrinos make excellent probes of hadronic matter. They are structureless, comparatively easy to generate in accelerators and their electroweak properties are well understood. One of the common methods of studying hadrons at quark level is by investigating the collisions of neutrinos with protons or neutrons in a fixed target. The effects of small interaction cross section for neutrinos has been overcome by modern experiments through the use of high-intensity beams coupled with massive detectors which give luminosities in the range of $10^{36}\mathrm{cm}^{-2}\mathrm{s}^{-1}$. Data samples in excess of one million events are now available, which allow measurements of strong and electroweak parameters comparable in precision to other fixed target and collider

determinations. In the SM, neutrinos interact only weakly with matter, either via the exchange of a W boson or of a Z boson. Neutrino-nucleon interactions dominate over neutrino-electron interaction, due to the small electron mass and the composite structure of the nucleon. The ratio $\sigma_{\nu-e}/\sigma_{\nu-p(n)}$ is of the order of m_e/m_p. The only exception is the $\nu_e - e$ interaction around E $= 6.3 \times 10^6$ GeV, where the resonant W boson production enhances the cross section by two orders of magnitude.

- **Charged Current interactions** are given by

$$\mathcal{L}_{CC} = \frac{g}{2\sqrt{2}}(J^+_\mu W^{+\mu} + J^-_\mu W^{-\mu}) \tag{1.1}$$

where the strength g is the $\mathrm{SU(2)_L}$ coupling constant and J^+_μ is the $V-A$ weak CC and can be written as

$$J^+_\mu \;=\; \sum_i \bar{\psi}_f \gamma_\mu (1-\gamma_5)\psi_i \tag{1.2}$$

Here $'i'$ stands for charged leptons $(e, \mu, \tau, d', s', b')$ and $'f'$ is the corresponding weak isospin partner $(\nu_e, \nu_\mu, \nu_\tau, u, c, t)$ respectively. In short-hand notation, we may simply write

$$J^+_\mu = (\bar{u}\, d')_{V-A} + (\bar{c}\, s')_{V-A} + (\bar{t}\, b')_{V-A} + (\bar{\nu}_e\, e)_{V-A} + (\bar{\nu}_\mu\, \mu)_{V-A} + (\bar{\nu}_\tau\, \tau)_{V-A} \tag{1.3}$$

For the low-energy four-fermion interaction, we generate the following effective Lagrangian

$$\mathcal{L}^{CC}_{eff} \;=\; \frac{-g^2}{2M^2_W} J^+_\mu J^{-\mu} \tag{1.4}$$

We can make the identification that g is related to the Fermi coupling constant G_F,

$$\frac{G_F}{\sqrt{2}} = \frac{g^2}{8M^2_W}$$

where M_W is the mass of the W boson.

- **Neutral Current interactions** are given by

$$\mathcal{L}_{NC} = e J^{em}_\mu A^\mu + \frac{g}{2\ \cos\Theta_W} J^0_\mu Z^\mu \tag{1.5}$$

where e is the QED coupling constant, g is the $\mathrm{SU(2)_L}$ coupling constant and Θ_W is the Weinberg angle. The electromagnetic and weak NC are given by

$$J_\mu^{em} = \sum_f Q_f \bar{f}\gamma_\mu f \tag{1.6}$$

$$\begin{aligned} J_\mu^0 &= \sum_f \left[g_L^f \bar{f}\gamma_\mu(1-\gamma_5)f + g_R^f \bar{f}\gamma_\mu(1+\gamma_5)f \right] \\ &= \sum_f \bar{f}\gamma_\mu(v_f - a_f\gamma_5)f \end{aligned} \tag{1.7}$$

where $'f'$ represents $(\nu_e, \nu_\mu, \nu_\tau, u, c, t)$ and their corresponding $\mathrm{SU(2)_L}$ partners. The sum is over 12 fermions (6 leptons and 6 quarks). We can express v_f and a_f in terms of g_L^f and g_R^f as

$$v_f = g_L^f + g_R^f = T_3^f - 2\ Q_f\ \sin^2\Theta_W \quad ; \quad a_f = g_L^f - g_R^f = T_3^f \tag{1.8}$$

where Q_f and T_3^f denotes the electric charge and the third component of the weak isospin of the LH fermion f_L respectively and Θ_W is the Weinberg angle. The electroweak charges of leptons and quarks in the SM are listed in Table 1.1 and Table 1.2 respectively. We can generate low-energy four-fermion interactions corresponding to the product of NC,

$$\mathcal{L}_{eff}^{NC} = \frac{-g^2}{2M_W^2} J_\mu^0 J^{0\mu} \tag{1.9}$$

where $M_Z \cos\Theta_W = M_W$ has been used, M_Z being the mass of Z-boson.

We see that the weak CC is exclusively LH as opposed to the weak NC which contains a RH component. This is why the RH quarks and charged leptons are in weak isospin singlets. The gauge bosons $W^\pm$ connect leptons within a family *e.g.* $(\bar{\psi}_{\nu_e}\psi_e W^+ + \text{h.c.})$. We can assign an additive "lepton family number" to each of the leptons : electron number, L_e is equal to 1 for e^- and ν_e, -1 for e^+ and $\bar{\nu}_e$, etc. As can be seen from the form of the weak CC and NC, the weak interactions conserve this lepton family number, which means ν_e induced interaction always has a e^- or ν_e in the final state for example. An important consequence of this is that in the SM neutrinos *cannot change flavor by any means.*

1.2 Neutrino mass and mixing

As mentioned above, neutrinos are strictly massless in the SM, but we now know that neutrinos oscillate due to non-zero masses and mixing. Using the extensions of SM as explained in Section 1.1.1, we describe how to generate the neutrino mass in Dirac case as well as in Majorana case [3, 4]. The Dirac case is identical to that of any other charged leptons so the mechanism of mass generation is identical but one cannot explain the extreme smallness. However, since neutrinos are neutral, they can be their own antiparticle and this corresponds to Majorana case. If neutrinos are Majorana type, one can easily explain the smallness via the seesaw mechanism [5] which has been a very attractive idea. One can also account for the observed baryon asymmetry of the Universe through baryogenesis via leptogenesis [6].

The vanishingly small mass of neutrinos makes it very difficult to distinguish between different types of massive neutrinos and it is currently not known whether neutrinos are Majorana or Dirac particles. The most promising way of finding this out is through the experiments on neutrinoless double beta decay [7].

1.2.1 Dirac and Majorana mass terms

Neutrino mass can be generated with the same Higgs mechanism that gives masses to quarks and charged leptons in the SM. The only extension of the SM that is needed is the introduction of RH components $\nu_{\alpha R}$ of the neutrino fields ($\alpha = e, \mu, \tau$). The RH neutrino fields are called sterile neutrinos because they do not participate in weak interactions as well as strong and electromagnetic interactions, as all neutrino fields; their only interaction is gravitational. On the other hand, there is a way to make neutrinos massive without assuming the existence of the RH neutrino (ν_R), by assuming that the RH particle could be a manifestation of the LH particle [8]. The Majorana relation, which relates the two, is

$$\nu_R = C\bar{\nu_L}^T \tag{1.10}$$

where C is the charge conjugation matrix. Now there are, in general, two types of mass terms that arise from renormalizable terms:

$$-\mathcal{L}_{M_\nu} = \underbrace{M_{D\alpha\beta}\overline{\nu_{\alpha L}}\nu_{\beta R}}_{\text{Dirac}} + \underbrace{\frac{1}{2}M_{N\alpha\beta}\overline{\nu^c_{\alpha L}}\nu_{\alpha L}}_{\text{Majorana}} + \text{h.c.} \tag{1.11}$$

The first term is a Dirac mass term. It has the following properties:

- Since it transforms as the doublet representation of $\mathrm{SU(2)_L}$, it is generated after spontaneous electroweak symmetry breaking from the Yukawa interactions of the form $Y'^{\nu}_{\alpha\beta}\ \bar{L}_{\alpha L}\ \tilde{\Phi}\ \nu'_{\beta R}$, analogous to the charged fermion masses.
- Since it has a neutrino field and an antineutrino field, the total lepton number is conserved.
- M_D is a complex $3 \times m$ matrix.

The second term in Eq. 1.11 is a Majorana mass term. It is different from the Dirac mass term in the following aspects

- It is a singlet of the SM gauge group. Therefore, it can appear as a bare mass term.
- Since it involves two neutrino fields, it breaks lepton number conservation by two units. More generally, such a term is allowed only if the neutrinos carry no additive conserved charge. This is the reason that such terms are not allowed for any charged fermions which, by definition, carry $\mathrm{U(1)_{EM}}$ charges.

1.2.2 Neutrino mixing

The mass term for charged leptons and neutrinos can be written via the Yukawa coupling. It is invariant under $\mathrm{SU(2)_L} \bigotimes \mathrm{U(1)_Y}$ gauge symmetry. The vacuum expectation value of Higgs field and the Yukawa coupling combinedly gives the masses for leptons in SM as follows

The Lagrangian for charged leptons masses and the Dirac neutrinos masses are given by

$$\mathcal{L}_{H,L} \ = \ -\sum_{\alpha,\beta=e,\mu,\tau} Y'^{l}_{\alpha\beta}\ \bar{L}_{\alpha L}\ \Phi\ l'_{\beta R} - \sum_{\alpha,\beta=e,\mu,\tau} Y'^{\nu}_{\alpha\beta}\ \bar{L}_{\alpha L}\ \tilde{\Phi}\ \nu'_{\beta R} + \text{h.c} \tag{1.12}$$

where $Y'^{l}_{\alpha\beta}$ and $Y'^{\nu}_{\alpha\beta}$ are Yukawa couplings for charged leptons and neutrinos respectively, $L_{\alpha L}$ is the left chiral field of lepton, Φ is the Higgs field, $l'_{\beta R}$ is the right chiral field of charged lepton and $\nu'_{\beta R}$ is the sterile state included for neutrinos. The lepton doublet field is represented as,

$$L_{\alpha L} = \begin{pmatrix} \nu'_{\alpha L} \\ l'_L \end{pmatrix} \quad \text{where} \quad l' = (e', \mu', \tau') \quad \text{and} \quad \nu'_\alpha = (\nu'_e, \nu'_\mu, \nu'_\tau)$$

Using the vacuum expectation value of Higgs field,

$$\langle \Phi \rangle = \frac{1}{\sqrt{2}} \begin{pmatrix} 0 \\ v_\Phi \end{pmatrix} \tag{1.13}$$

and

$$\mathcal{L}_{H,L} = -\frac{v_\Phi}{\sqrt{2}} \left[\bar{l}'_L \; Y'^{l} \; l'_R + \bar{\nu}'_L \; Y'^{\nu} \; \nu'_R \right] + \text{h.c.} \tag{1.14}$$

The array of RH neutrino field is

$$\nu'_R = \begin{pmatrix} \nu'_{eR} \\ \nu'_{\mu R} \\ \nu'_{\tau R} \end{pmatrix}$$

Here we clearly see that the mass matrix for charge lepton as well as neutrino are not diagonalized. The diagonalization of Y'^{l} and Y'^{ν} can be obtained by appropriate 3×3 unitary matrices [3]. These unitary matrices must be different for charge leptons and neutrinos of different chiral fields. With the below mentioned diagonalization method,

$$V_L^{l\dagger} \; Y'^{l} \; V_R^{l} = \; Y^{l} \quad \text{and} \quad V_L^{\nu\dagger} \; Y'^{\nu} \; V_R^{\nu} = \; Y^{\nu} \tag{1.15}$$

the Lagrangian for charge lepton mass and neutrino mass is

$$\mathcal{L}_{H,L} = -\frac{v_\Phi}{\sqrt{2}} \left[\bar{l}_L \; Y^{l} \; l_R + \bar{n}_L \; Y^{\nu} \; \nu_R \right] + \text{h.c.} \tag{1.16}$$

where

$$l_L = V_L^{l\dagger} l'_L \equiv \begin{pmatrix} e_L \\ \mu_L \\ \tau_L \end{pmatrix}, \; l_R = V_R^{l\dagger} l'_R \equiv \begin{pmatrix} e_R \\ \mu_R \\ \tau_R \end{pmatrix}, \; n_L = V_L^{\nu\dagger} \nu'_L \equiv \begin{pmatrix} \nu_{1L} \\ \nu_{2L} \\ \nu_{3L} \end{pmatrix} \text{ and}$$

$$n_R = V_R^{\nu\dagger}\nu'_R \equiv \begin{pmatrix} \nu_{1R} \\ \nu_{2R} \\ \nu_{3R} \end{pmatrix}$$

So after diagonalization, we get a new state called mass eigenstate. Now we use this mass eigenstates expression in weak CC interaction where the fermion flavor eigenstates are formed from the mixing of mass eigenstates. The Lagrangian for CC is govern by,

$$\mathcal{L}^{CC} = -\frac{g}{2\sqrt{2}} J^\mu W_\mu + \text{h.c.} \tag{1.17}$$

where W_μ is the bosonic field, g is the gauge coupling and J^μ is the weak current. The current in mass eigenstate basis can be written as

$$\begin{aligned} J^\mu &= 2\left(\bar{e_L}' \ \bar{\mu_L}' \ \bar{\tau_L}'\right)\gamma^\mu \begin{pmatrix} \nu'_{1L} \\ \nu'_{2L} \\ \nu'_{3L} \end{pmatrix} = 2\left(\bar{e_L} \ \bar{\mu_L} \ \bar{\tau_L}\right)\gamma^\mu V_L^{l\dagger} V_L^\nu \begin{pmatrix} \nu_{1L} \\ \nu_{2L} \\ \nu_{3L} \end{pmatrix} \\ &= 2\left(\ \bar{e_L} \ \bar{\mu_L}\bar{\tau_L}\right)\gamma^\mu U \begin{pmatrix} \nu_{1L} \\ \nu_{2L} \\ \nu_{3L} \end{pmatrix} \end{aligned} \tag{1.18}$$

where $U = V_L^{l\dagger} V_L^\nu$ is the mixing matrix.

Now we choose one basis where the fermion fields has a diagonal mass matrix and the another basis projects U on the other fermion field. This leads to fermion mixing because of the non-diagonal mixing matrix, U i.e. fermion changes it's flavor from one generation to another. One choice is projection of U on charged lepton flavor i.e. mixing of different charge lepton flavors but this is not possible because mass of charge lepton is defined by it's flavor. Hence we must choose the second option where the charge leptons are flavor states with definite masses and the neutrino mass eigenstates mix to form flavor states.

Physical parameters in mixing matrix :

A general unitary $N \times N$ matrix has N^2 independent real parameters, out of which, $\frac{N(N-1)}{2}$ are mixing angles and $\frac{N(N+1)}{2}$ are phases. Hence the three flavor lepton mixing matrix can be written with three mixing angles and six phases and the two flavor

mixing matrix with one mixing parameter and three phases. Not all these phases have physical effect which can be explained from the weak CC process in leptonic sector. The global phase transformations of the lepton fields of the type,

$$l_\alpha \to e^{i\psi^l_\alpha} l_\alpha, \quad n_j \to e^{i\psi^n_j} n_j \tag{1.19}$$

makes the Lagrangian invariant. So the weak charge-current for N flavors is given as

$$J^\mu = 2 \sum_{\alpha=1}^{N} \sum_{j=1}^{N} \bar{l}_{\alpha L} \gamma^\mu e^{-i\psi^l_\alpha} U_{\alpha j} e^{i\psi^n_j} n_{jL}$$

The above equation can be expressed as

$$J^\mu = 2 \underbrace{e^{-i(\psi^l_1 - \psi^n_1)}}_{1} \sum_{\alpha=1}^{N} \sum_{j=1}^{N} \bar{l}_{\alpha L} \gamma^\mu \underbrace{e^{-i(\psi^l_\alpha - \psi^l_1)}}_{N-1} U_{\alpha j} \underbrace{e^{i(\psi^n_j - \psi^n_1)}}_{N-1} n_{jL}$$

where the arbitrary phase, $e^{-i(\psi^l_1 - \psi^n_1)}$ has been factorized from the current and the number written underneath the underbrace indicates the independent number of phases that can be chosen to eliminate phases of mixing matrix. So from the above equation, it is clear that,

$$1 + (N-1) + (N-1) = 2N - 1 \tag{1.20}$$

arbitrary phases of leptonic mixing matrix can be eliminated. So for two flavor case, 2N-1=2×2-1=3 phases and the three flavor case, 2N-1=2×3-1=5 phases can be eliminated from the mixing matrix.

For the simplest case of 2 flavors [3], we have

$$U = \begin{pmatrix} \cos\theta\, e^{i\omega_1} & \sin\theta\, e^{i(\omega_2+\eta)} \\ -\sin\theta\, e^{i(\omega_1-\eta)} & \cos\theta\, e^{i\omega_2} \end{pmatrix} \tag{1.21}$$

in terms of one mixing angle and three phases ω_1, ω_2 and η. The equivalent form

$$U = \begin{pmatrix} e^{i\omega_1} & 0 \\ 0 & e^{i\omega_2} \end{pmatrix} \begin{pmatrix} e^{i\eta} & 0 \\ 0 & 1 \end{pmatrix} \begin{pmatrix} \cos\theta & \sin\theta \\ -\sin\theta & \cos\theta \end{pmatrix} \begin{pmatrix} e^{-i\eta} & 0 \\ 0 & 1 \end{pmatrix} \tag{1.22}$$

shows explicitly that all three phases can be eliminated by rephasing the lepton fields as

$$e_L \to e^{i(\omega_1+\eta)} e_L \quad , \quad \mu_L \to e^{i\omega_2} \mu_L \quad \text{and} \quad \nu_{eL} \to e^{i\eta} \nu_{eL} \tag{1.23}$$

Hence, we obtain the mixing matrix U without the unphysical phases

$$U = \begin{pmatrix} \cos\theta & \sin\theta \\ -\sin\theta & \cos\theta \end{pmatrix} \tag{1.24}$$

Since two flavor case has only three independent phases in mixing matrix, so all three phases eliminate in rephasing but the three flavor has six phases in mixing matrix, so one phase remains in the mixing matrix. This is why two flavor case has no CP violation.

In the general case of N flavors, the mixing matrix, U consists of $(N-1)(N-2)/2$ Dirac-type CP-violating phases. We have $(N-1)$ additional Majorana-type phases, if neutrino is a Majorana particle. However, the Majorana phases do not affect neutrino oscillations.

1.2.3 Parametrization of the mixing matrix

For the three-flavor case, the mixing matrix can be written as

$$U = \begin{pmatrix} U_{e1} & U_{e2} & U_{e3} \\ U_{\mu 1} & U_{\mu 2} & U_{\mu 3} \\ U_{\tau 3} & U_{\tau 3} & U_{\tau 3} \end{pmatrix} \tag{1.25}$$

The mixing matrix can be written as product of rotation matrices about the three axes [3, 4, 9] as given below (see Fig. 1.1)

$$U = V_{23} W_{13} V_{12} D \equiv V D \tag{1.26}$$

where

$$V_{12} = \begin{pmatrix} c_{12} & s_{12} & 0 \\ -s_{12} & c_{12} & 0 \\ 0 & 0 & 1 \end{pmatrix} \quad W_{13} = \begin{pmatrix} c_{13} & 0 & s_{13}e^{-i\delta_{13}} \\ 0 & 1 & 0 \\ -s_{13}e^{i\delta_{13}} & 0 & c_{13} \end{pmatrix} \quad V_{23} = \begin{pmatrix} 1 & 0 & 0 \\ 0 & c_{23} & s_{23} \\ 0 & -s_{23} & c_{23} \end{pmatrix} \tag{1.27}$$

and $D = diag(1, e^{i\phi_1/2}, e^{i\phi_2/2})$. The phase δ_{13} in W_{13} is the usual Dirac-type CP-violating phase, whereas the phases ϕ_1 and ϕ_2 are present only in the Majorana case. It immediately follows that Majorana phases have no effect on the neutrino

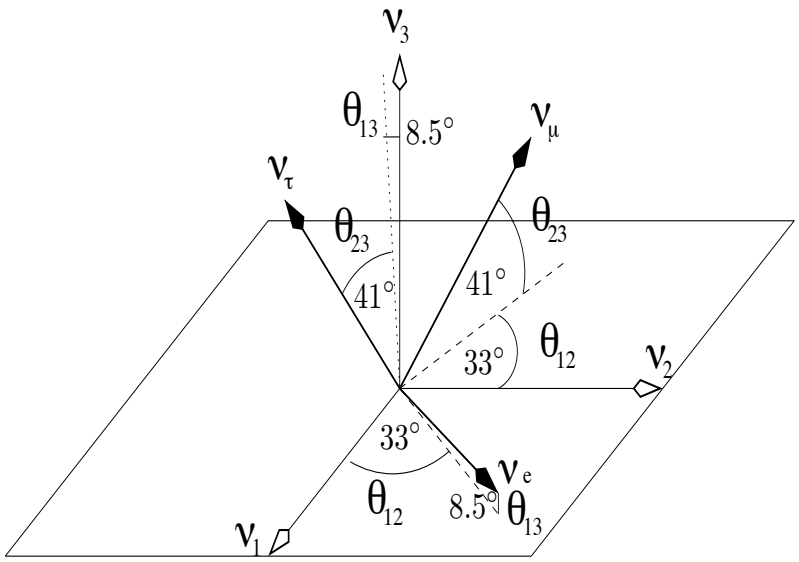

Figure 1.1: Neutrino mixing angles depicted as a product of Euler angles for the case when $\delta_{13} = 0$. Taken from [10].

oscillations and therefore one can omit the factor D and write $U = V$ and we get the (3×3) unitary matrix for the case of 3 flavors

$$U = \begin{pmatrix} c_{12}c_{13} & s_{12}c_{13} & s_{13}e^{-i\delta_{13}} \\ -s_{12}c_{23} - c_{12}s_{23}s_{13}e^{i\delta_{13}} & c_{12}c_{23} - s_{12}s_{23}s_{13}e^{i\delta_{13}} & s_{23}c_{13} \\ s_{12}s_{23} - c_{12}c_{23}s_{13}e^{i\delta_{13}} & -c_{12}s_{23} - s_{12}c_{23}s_{13}e^{i\delta_{13}} & c_{23}c_{13} \end{pmatrix} \quad (1.28)$$

where $c_{ij} = \cos\theta_{ij}$, $s_{ij} = \sin\theta_{ij}$. This is referred as the Pontecorvo-Maki-Nakagawa-Sakata (PMNS) matrix [11]. For Majorana neutrinos, U contains two furthur multiplicative phase factors, but these donot enter in oscillation phenomena. Note that there are only 3 angles and 1 phase involved, so we can furthur shorten the indices of the cos and sin terms for simplicity sake, we write c_{12} as c_1, c_{23} as c_2 and c_{13} as c_3, s_{12} as s_1, s_{23} as s_2 and s_{13} as s_3 respectively and get

$$U = \begin{pmatrix} c_1c_3 & s_1c_3 & s_3e^{-i\delta_{13}} \\ -s_1c_2 - c_1s_2s_3e^{i\delta_{13}} & c_1c_2 - s_1s_2s_3e^{i\delta_{13}} & s_2c_3 \\ s_1s_2 - c_1c_2s_3e^{i\delta_{13}} & -c_1s_2 - s_1c_2s_3e^{i\delta_{13}} & c_2c_3 \end{pmatrix} \quad (1.29)$$

The properties that the matrix U satisfies are :

$$\begin{aligned} U^{\dagger} &= U^{-1} \\ \Sigma_i U_{\alpha i} U^{\star}_{\beta i} &= \delta_{\alpha\beta} \end{aligned} \tag{1.30}$$

where $\delta_{\alpha\beta}$ is the Kronecker delta, $\delta_{\alpha\beta} = 1$ only for $\alpha = \beta$ and zero otherwise.

1.3 Neutrino oscillations - Theory

The possibility of neutrino oscillations was raised in 1957 by Pontecorvo [12] and the experimental confirmation of neutrino oscillations was rewarded with a Nobel prize in 2015 [13]. In this Section, the neutrino oscillation framework is presented and the analytic computation of neutrino oscillation probability is detailed.

Evolution equation for mixed neutrinos

In the present section, we derive the equation for neutrino oscillations [14]. The Dirac spinor ν_i which describes the neutrino mass eigenstate i obeys the Dirac and thus the Klein-Gordon equation $(\partial_t^2 - \nabla^2 + m_i^2)\nu_i = 0$. Writing an equation for all mass eigenstates

$$(\partial_t^2 - \nabla^2 + M^2)\Psi = 0 \tag{1.31}$$

where

$$M^2 = \begin{pmatrix} m_1^2 & 0 & 0 \\ 0 & m_2^2 & 0 \\ 0 & 0 & m_3^2 \end{pmatrix} \text{ and } \Psi \equiv \begin{pmatrix} \nu_1 \\ \nu_2 \\ \nu_3 \end{pmatrix} \tag{1.32}$$

Eq. 1.31 may be written in any desired flavor basis. If we wish to express it in the basis of weak-interaction eigenstates, we can use

$$\begin{pmatrix} \nu_e \\ \nu_\mu \\ \nu_\tau \end{pmatrix} = U \begin{pmatrix} \nu_1 \\ \nu_2 \\ \nu_3 \end{pmatrix} \tag{1.33}$$

The mass matrix transforms according to $M^2 \rightarrow UM^2U^{\dagger}$ and will not be diagonal any more. Since U is a unitary matrix, $U^{\dagger} = U^{-1}$. Expanding the neutrino fields in

plane waves of the form $\Psi(t,x) = \Psi_k(t)e^{-i(\vec{k}\cdot\vec{x})}$ for which Eq. 1.31 is

$$(\partial_t^2 + k^2 + M^2)\Psi_k(t) = 0 \tag{1.34}$$

We cannot assume a temporal variation here ($e^{-i\omega t}$) because there are three different branches of the dispersion relation with $w_i^2 = k^2 + m_i^2$. A mixed neutrino cannot simultaneously have a fixed energy and a fixed momentum. Assuming very relativistic neutrinos, for which $k = |\vec{k}| \gg m_i$, one may linearize Eq. 1.34 by virtue of $(\partial_t^2 + k^2) = (i\partial_t + k)(-i\partial_t + k)$. For each mass eigenstate $i\partial_t \to \omega_i \approx k$ and one needs to keep the exact expression only in the second factor where the difference between energy and momentum appears. Thus $\partial_t^2 + k^2 \approx 2k(-\partial_t + k)$, leading to the Schrödinger-type equation

$$i\partial_t\Psi_k = \Omega_k\Psi_k \qquad \text{where} \quad \Omega_k \equiv \left(k + \frac{M^2}{2k}\right) \tag{1.35}$$

This implies that Ψ which was originally a set of neutrino Dirac spinors, has been reinterpreted as a vector of positive-energy probability amplitudes. For negative-energy states (antineutrinos) a global minus sign appears in Eq. 1.35. The Schrödinger equation (Eq. 1.35) describes a spatially homogeneous system with a nonstationary temporal evolution. The more often encountered situation is the one with a stationary neutrino flux such as that from a reactor or the Sun with a nontrivial spatial variation. Then it is useful to expand $\Psi(t,x)$ in components of fixed frequency $\Psi_\omega(x)e^{i\omega t}$, yielding

$$(-\omega^2 - \nabla^2 + M^2)\Psi_\omega(x) = 0 \tag{1.36}$$

In the relativistic limit and restricting the spatial variation to the z-direction one obtains in full analogy to the previous case

$$i\partial_z\psi_\omega = -K_\omega\Psi_\omega \quad \text{where} \quad K_\omega \equiv \left(\omega - \frac{M^2}{2\omega}\right) \tag{1.37}$$

This equation describes the spatial variation of a neutrino beam propagating in the positive z-direction with a fixed energy ω.

In what follows, we describe neutrino oscillations in vacuum and then go on to describe neutrino oscillations in matter [3, 4].

1.3.1 Neutrino oscillations in vacuum

The probability of transition of neutrino from $\nu_\alpha \to \nu_\beta$ is given by the absolute square of the overlap of the observed flavor state $|\nu_\beta\rangle$, with the time-evolved initially produced flavor state, $|\nu_\alpha\rangle$. In vacuum, the evolution operator involves just the Hamiltonian H_0 of a free particle, yielding the following result for the probability that a (relativistic) weak neutrino eigenstate ν_α becomes ν_β after propagating a distance L :

$$\begin{aligned} P(\nu_\alpha \to \nu_\beta) &= |\langle\nu_\beta|e^{-iH_0L}|\nu_\alpha\rangle|^2 \\ &= \Sigma_{i,j} U_{\alpha i} U^\star_{\beta i} U^\star_{\alpha j} U_{\beta j}\, e^{-i\delta m^2_{ij} L/2E} \\ &= P_{\rm CP-even}(\nu_\alpha \to \nu_\beta) \;+\; P_{\rm CP-odd}(\nu_\alpha \to \nu_\beta) \end{aligned} \tag{1.38}$$

The CP-even and CP-odd contributions are

$$\begin{aligned} P_{\rm CP-even}(\nu_\alpha \to \nu_\beta) &= P_{\rm CP-even}(\bar\nu_\alpha \to \bar\nu_\beta) \\ &= \delta_{\alpha\beta} \;-\; 4\,\Sigma_{i>j}\, Re(U_{\alpha i} U^\star_{\beta i} U^\star_{\alpha j} U_{\beta j})\, \sin^2(\frac{\delta m^2_{ij} L}{4E}) \end{aligned} \tag{1.39}$$

$$\begin{aligned} P_{\rm CP-odd}(\nu_\alpha \to \nu_\beta) &= -P_{\rm CP-odd}(\bar\nu_\alpha \to \bar\nu_\beta) \\ &= 4\,\Sigma_{i>j}\, Im(U_{\alpha i} U^\star_{\beta i} U^\star_{\alpha j} U_{\beta j})\, \sin(\frac{\delta m^2_{ij} L}{4E})\, \cos(\frac{\delta m^2_{ij} L}{4E}) \\ &= 2\,\Sigma_{i>j}\, Im(U_{\alpha i} U^\star_{\beta i} U^\star_{\alpha j} U_{\beta j})\, \sin(\frac{\delta m^2_{ij} L}{2E}) \end{aligned} \tag{1.40}$$

so that

$$\begin{aligned} P(\bar\nu_\alpha \to \bar\nu_\beta) &= P(\nu_\beta \to \nu_\alpha) \\ &= P_{\rm CP-even}(\nu_\alpha \to \nu_\beta) \;-\; P_{\rm CP-odd}(\nu_\alpha \to \nu_\beta) \end{aligned} \tag{1.41}$$

where, by CPT invariance, $P(\nu_\alpha \to \nu_\beta) = P(\bar\nu_\beta \to \bar\nu_\alpha)$ and hence for $\beta = \alpha$, $P(\bar\nu_\alpha \to \bar\nu_\alpha) = P(\nu_\alpha \to \nu_\alpha)$. For the CP-transformed reaction $\bar\nu_\alpha \to \bar\nu_\beta$ and the T-reversed reaction $\nu_\beta \to \nu_\alpha$, the transition probabilities will be the same except that the sign of the imaginary term is reversed. In vacuum, the CP-even and CP-odd contributions are even and odd, respectively, under time reversal : $\alpha \leftrightarrow \beta$. In above

equations, $\delta m^2_{ij} = m^2_i - m^2_j$ is the mass squared difference of the two neutrino states and the combination

$$\frac{\delta m^2_{ij} L}{4E} \quad = \quad 1.267 \times \frac{\delta m^2_{ij}(\mathrm{eV}^2) L(\mathrm{km})}{E(\mathrm{GeV})} \tag{1.42}$$

in units where $\hbar = c = 1$ and δm^2_{ij} is expressed in eV^2 and (L,E) are in (km, GeV).

Two flavor case

We begin in the lepton flavor framework in which the charged lepton mass matrix is diagonalized. Define the two-flavor eigenstates ν_α and ν_β, and their mass eigenstates, ν_1 and ν_2 of masses m_1 and m_2, respectively. The mixing matrix U is given by an orthogonal rotation matrix in two dimension relating the flavor states to the mass eigenstates.

$$\begin{pmatrix} \nu_\alpha \\ \nu_\beta \end{pmatrix} = U \begin{pmatrix} \nu_1 \\ \nu_2 \end{pmatrix}, \qquad U = \begin{pmatrix} \cos\theta & \sin\theta \\ -\sin\theta & \cos\theta \end{pmatrix} \tag{1.43}$$

where θ is the mixing angle. The states are orthonormalized within their own spaces, i.e.,

$$\langle \nu_j | \nu_k \rangle = \delta_{jk}; \qquad j,k = \alpha, \beta; \text{ or } 1,2 \tag{1.44}$$

It should be noted that in an experiment, neutrinos are always produced as flavor eigenstates. The time evolution of a flavor state can be simply expressed in terms of the time evolution of the mass eigenstates which enter into the flavor state at $t = 0$,

$$\begin{pmatrix} \nu_\alpha(t) \\ \nu_\beta(t) \end{pmatrix} \quad = \quad U \begin{pmatrix} \nu_1(t) \\ \nu_2(t) \end{pmatrix} = U \begin{pmatrix} e^{-iE_1 t}\nu_1 \\ e^{-iE_2 t}\nu_2 \end{pmatrix} = U \begin{pmatrix} e^{-iE_1 t} & 0 \\ 0 & e^{-iE_2 t} \end{pmatrix} U^\dagger \begin{pmatrix} \nu_\alpha \\ \nu_\beta \end{pmatrix} \tag{1.45}$$

Suppose the neutrino flavor state ν_α is produced, then at time t we have

$$\nu_\alpha(t) \quad = \quad (\cos^2\theta e^{-iE_1 t} + \sin^2\theta e^{-iE_2 t})\nu_\alpha + \cos\theta \sin\theta\,(-e^{-iE_1 t} + e^{-iE_2 t})\nu_\beta \tag{1.46}$$

The probability of finding the original flavor, referred to as the **survival probability**, is

$$\begin{aligned} P(\nu_\alpha \to \nu_\alpha) = |\langle \nu_\alpha | \nu_\alpha(t) \rangle|^2 &= 1 \; - \; \sin^2(2\theta) \, \sin^2 \left(\frac{E_2 - E_1}{2} \, t \right) \\ &= 1 \; - \; \sin^2(2\theta) \, \sin^2 \left(1.267 \, \delta m^2(\mathrm{eV}^2) \, \frac{\mathrm{L(km)}}{\mathrm{E(GeV)}} \right) \end{aligned} \tag{1.47}$$

and the probability of finding the other flavor, referred to as the **appearance probability**, is

$$P(\nu_\alpha \to \nu_\beta) = \sin^2(2\theta) \, \sin^2 \left(1.267 \, \delta m^2(\mathrm{eV}^2) \, \frac{\mathrm{L(km)}}{\mathrm{E(GeV)}} \right) \tag{1.48}$$

Here we take the approximation $E_j \approx |p| + m_j^2/2E$ and denote $\delta m^2 = m_2^2 - m_1^2$. The characteristic behaviour of this expression as a function of $\sin^2(2\theta)$ and δm^2 is the following : for large δm^2, the argument of the sine function is large and hence oscillates rapidly in even a very small energy range. The energy average of the sine function involved becomes 1/2, hence we have

$$\sin^2(2\theta) \approx 2 \, P(\nu_\alpha \to \nu_\beta)$$

We give the expressions for three flavor case in vacuum.

Three flavor case

$$\begin{aligned} P(\nu_\mu \to \nu_e) \;\; = \;\; & 4 \, (\, c_{13}^2 \, s_{23}^2 \, s_{13}^2 \; + \; \mathcal{J} \sin \Delta_{21} \,) \, \sin^2 \frac{\Delta_{31}}{2} \\ + \;\; & 2 \, (\, c_{12} \, c_{23} \, c_{13}^2 \, s_{12} \, s_{23} \, s_{13} \, \cos \delta_{13} \; - \; c_{13}^2 \, s_{12}^2 \, s_{23}^2 \, s_{13}^2 \,) \, \sin \Delta_{21} \, \sin \Delta_{31} \\ + \;\; & 4 \, (\, c_{12}^2 \, c_{23}^2 \, c_{13}^2 \, s_{12}^2 \; + \; c_{13}^2 \, s_{12}^4 \, s_{23}^2 \, s_{13}^2 \; - \; 2 \, c_{12} \, c_{23} \, c_{13}^2 \, s_{12}^3 \, s_{23} \, s_{13} \, \cos \delta_{13} \\ - \;\; & \mathcal{J} \sin \Delta_{31} \,) \sin^2 \frac{\Delta_{21}}{2} \\ + \;\; & 8 \, (\, c_{12} \, c_{23} \, c_{13}^2 \, s_{12} \, s_{23} \, s_{13} \, \cos \delta_{13} \; - \; c_{13}^2 \, s_{12}^2 \, s_{23}^2 \, s_{13}^2 \,) \, \sin^2 \frac{\Delta_{21}}{2} \, \sin^2 \frac{\Delta_{31}}{2} \end{aligned} \tag{1.49}$$

Here, $\mathcal{J} = c_{12} \, c_{23} \, c_{13}^2 \, s_{12} \, s_{23} \, s_{13} \, \sin \delta_{13}$ is called **Jarlskog factor** [15] which is an invariant quantity that measures CP violation in the neutrino sector. The abbreviations $s_{ij} = \sin \theta_{ij}$, $c_{ij} = \cos \theta_{ij}$ and $\Delta_{ij} = \delta m_{ij}^2 \, L/2 \, E$ are used. The probability

expression for the CP-transformed reaction $\bar{\nu}_\mu \to \bar{\nu}_e$ and the T-reversed reaction $\nu_e \to \nu_\mu$ is the same except for the fact that the $\mathcal{J}$ terms will have the opposite sign since $\delta_{13} \to -\delta_{13}$.

$$\begin{aligned}
P(\nu_\mu \to \nu_\tau) &= 4\left(c_{23}^2\, c_{13}^4\, s_{23}^2 \;-\; \mathcal{J} \sin\Delta_{21} \right) \sin^2\frac{\Delta_{31}}{2} \\
&+ 2\Big(c_{12}\, c_{23}\, c_{13}^2\, s_{12}\, s_{23}\, s_{13}\, (s_{23}^2 - c_{23}^2)\, \cos\delta_{13} \;-\; c_{12}^2\, c_{23}^2\, c_{13}^2\, s_{23}^2 \\
&+ c_{23}^2\, c_{13}^2\, s_{12}^2\, s_{23}^2\, s_{13}^2 \Big) \sin\Delta_{21}\, \sin\Delta_{31} \\
&+ 4\Big(c_{12}^4\, c_{23}^2\, s_{23}^2 \;+\; c_{23}^2\, s_{12}^4\, s_{23}^2\, s_{13}^4 \;+\; c_{12}^2\, s_{12}^2\, s_{13}^2\, (s_{23}^4 \;+\; c_{23}^4) \\
&- 2\, c_{12}^3\, c_{23}\, s_{12}\, s_{23}\, s_{13}\, (s_{23}^2 - c_{23}^2)\, \cos\delta_{13} \\
&+ 2\, c_{12}\, c_{23}\, s_{12}^3\, s_{23}\, s_{13}^3\, (s_{23}^2 - c_{23}^2)\, \cos\delta_{13} \\
&- 4\, c_{12}^2\, c_{23}^2\, s_{12}^2\, s_{23}^2\, s_{13}^2\, \cos^2\delta \\
&+ \mathcal{J} \sin\Delta_{31} \Big) \sin^2\frac{\Delta_{21}}{2} \\
&+ 8\Big(c_{12}\, c_{23}\, c_{13}^2\, s_{12}\, s_{23}\, s_{13}\, (s_{23}^2 - c_{23}^2)\, \cos\delta_{13} \;-\; c_{12}^2\, c_{23}^2\, c_{13}^2\, s_{23}^2 \\
&+ c_{23}^2\, c_{13}^2\, s_{12}^2\, s_{23}^2\, s_{13}^2 \Big) \sin^2\frac{\Delta_{21}}{2}\, \sin^2\frac{\Delta_{31}}{2}
\end{aligned} \tag{1.50}$$

The probability expression for the CP-transformed reaction $\bar{\nu}_\mu \to \bar{\nu}_\tau$ and the T-reversed reaction $\nu_\tau \to \nu_\mu$ is the same except for the fact that the $\mathcal{J}$ terms will have the opposite sign.

Notice that the CP-odd terms (i.e. the terms involving $\mathcal{J}$) for $\nu_\mu \to \nu_\tau$ (Eq. 1.50) transition are the same as for $\nu_\mu \to \nu_e$ case (Eq. 1.49), except that they have opposite sign.

$$\begin{aligned}
P(\nu_e \to \nu_\tau) &= 4\,(\, c_{23}^2\, c_{13}^2\, s_{13}^2 \;+\; \mathcal{J} \sin\Delta_{21}\,)\, \sin^2\frac{\Delta_{31}}{2} \\
&- 2\,(\, c_{12}\, c_{23}\, c_{13}^2\, s_{12}\, s_{23}\, s_{13}\, \cos\delta_{13} \;+\; c_{23}^2\, c_{13}^2\, s_{12}^2\, s_{13}^2\,)\, \sin\Delta_{21}\, \sin\Delta_{31} \\
&+ 4\,(\, c_{12}^2\, c_{13}^2\, s_{12}^2\, s_{23}^2 \;+\; c_{23}^2\, c_{13}^2\, s_{12}^4\, s_{13}^2 \;+\; 2\, c_{12}\, c_{23}\, c_{13}^2\, s_{12}^3\, s_{23}\, s_{13}\, \cos\delta_{13} \\
&- \mathcal{J} \sin\Delta_{31}\,) \sin^2\frac{\Delta_{21}}{2} \\
&- 8\,(\, c_{12}\, c_{23}\, c_{13}^2\, s_{12}\, s_{23}\, s_{13}\, \cos\delta_{13} \;+\; c_{23}^2\, c_{13}^2\, s_{12}^2\, s_{13}^2\,)\, \sin^2\frac{\Delta_{21}}{2}\, \sin^2\frac{\Delta_{31}}{2}
\end{aligned} \tag{1.51}$$

The probability expression for the CP-transformed reaction $\bar{\nu}_e \to \bar{\nu}_\tau$ and the T-reversed reaction $\nu_\tau \to \nu_e$ is the same except for the fact that the $\mathcal{J}$ terms will have the opposite sign. Note that the above expression for $P(\nu_e \to \nu_\tau)$ can be obtained from the expression for $P(\nu_\mu \to \nu_e)$ (see Eq. 1.49) by simply making the replacement $s_{23} \leftrightarrow c_{23}$.

We note that the CP-odd terms (i.e. the terms involving $\mathcal{J}$) for $\nu_e \to \nu_\tau$ (Eq. 1.51) transition are the same (both in magnitude as well as in sign) as for $\nu_\mu \to \nu_e$ case (Eq. 1.49). Thus, we can write

$$P_{CP-odd}(\nu_\mu \to \nu_e) = - P_{CP-odd}(\nu_\mu \to \nu_\tau) = P_{CP-odd}(\nu_e \to \nu_\tau) \tag{1.52}$$

This implies that measurement of CP violation in one channel is enough to establish CP violation in the leptonic sector. This nice feature breaks down when we have sterile neutrinos in the game.

1.3.2 Neutrino oscillations in matter

Two flavor case

Wolfenstein pointed out that the patterns of neutrino oscillation might be significantly affected if the neutrinos travel through a material medium rather than in vacuum [16]. That is is due to the fact that normal matter has electrons but no muons or taons at all. Thus a ν_e beam encounters both CC and NC interactions with electrons in the matter, while ν_μ or ν_τ beam interacts via NC interactions with the electron with the same strength as ν_e (since NC interaction is flavor blind) as shown in the Fig. 1.2. Interactions modify the effective mass that a particle exhibits while travelling through a medium. Since ν_e interacts differently, the modification of the effective mass of ν_e is different than the other flavors neutrinos (see Appendix A.1 for a detailed derivation of the matter potential.).

Let us first recapitulate the case of vacuum oscillation in a way that is most suitable for the generalization to matter oscillation. If the two mass eigenstates are ν_1 and ν_2, the evolution equation for these states in mass eigenstate basis can be

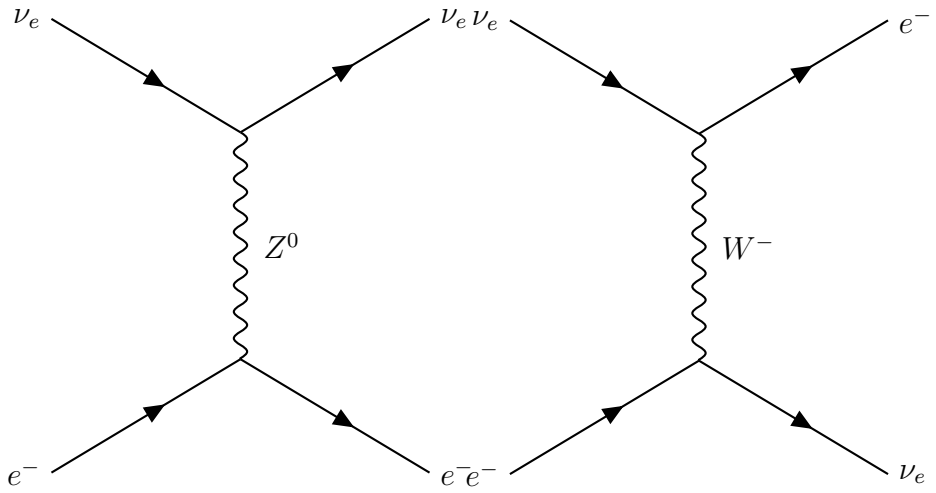

Figure 1.2: NC (left) and CC (right) interaction of ν_e with e in Earth matter.

written as

$$i\frac{d}{dt}\begin{pmatrix}\nu_1(t)\\ \nu_2(t)\end{pmatrix} = H\begin{pmatrix}\nu_1(t)\\ \nu_2(t)\end{pmatrix} \tag{1.53}$$

where H is diagonal in this basis :

$$H = \begin{pmatrix}E_1 & 0\\ 0 & E_2\end{pmatrix} \simeq |p| + \begin{pmatrix}m_1^2/2|p| & 0\\ 0 & m_2^2/2|p|\end{pmatrix} \tag{1.54}$$

Now we know that

$$\begin{pmatrix}\nu_e(t)\\ \nu_\mu(t)\end{pmatrix} = U\begin{pmatrix}\nu_1(t)\\ \nu_2(t)\end{pmatrix}, \qquad U = \begin{pmatrix}\cos\theta & \sin\theta\\ -\sin\theta & \cos\theta\end{pmatrix} \tag{1.55}$$

So, we can write down the evolution equation in flavor basis,

$$i\frac{d}{dt}\begin{pmatrix}\nu_e(t)\\ \nu_\mu(t)\end{pmatrix} = H'\begin{pmatrix}\nu_e(t)\\ \nu_\mu(t)\end{pmatrix} \tag{1.56}$$

where $H' = UHU^\dagger$ and is given by

$$H' = |p| + \frac{m_1^2 + m_2^2}{4|p|} + \frac{\delta m^2}{4|p|}\begin{pmatrix}-\cos 2\theta & \sin 2\theta\\ \sin 2\theta & \cos 2\theta\end{pmatrix} \tag{1.57}$$

Here $\delta m^2 = m_2^2 - m_1^2$. The diagonalising angle θ is given by

$$\tan 2\theta = \frac{2H'_{12}}{H'_{22} - H'_{11}} \tag{1.58}$$

We now consider the problem when neutrinos are travelling through matter. For simplicity, we assume that the density of the background matter is constant and uniform, with n_e, n_p, n_n denoting the number of electrons, protons and neutrons per unit volume. Elastic scattering off these particles change the effective masses of neutrinos, whose magnitude we will now estimate.

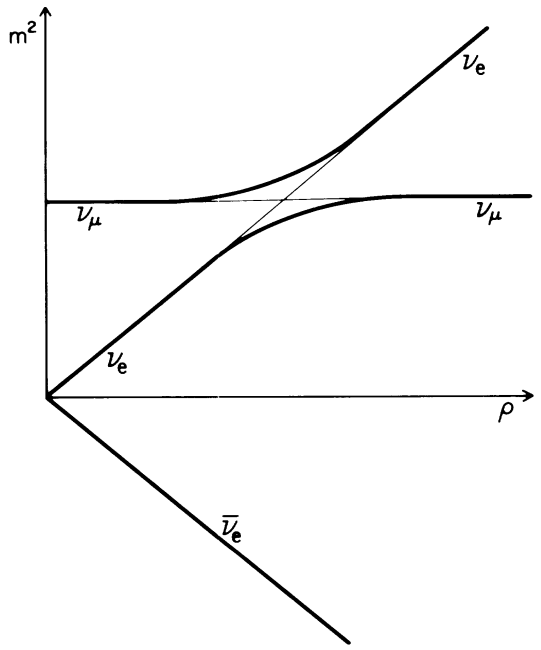

Figure 1.3: The masses of two flavors of neutrinos as a function of density. The curves approach each other near the resonant density. The electron-antineutrino mass is also shown. Taken from Bethe [17] (see also [16]).

In the presence of matter, we can write down the evolution equation in flavor basis as,

$$i\frac{d}{dt}\begin{pmatrix}\nu_e(t)\\ \nu_\mu(t)\end{pmatrix} = H^m \begin{pmatrix}\nu_e(t)\\ \nu_\mu(t)\end{pmatrix} \tag{1.59}$$

where $H^m = UHU^\dagger$ and is given by

$$H^m = |p| + \frac{m_1^2 + m_2^2}{4|p|} - \frac{1}{\sqrt{2}}G_F n_n + \frac{\delta m^2}{4|p|}\begin{pmatrix} -\cos 2\theta + \frac{4|p|}{\delta m^2}\sqrt{2}G_F n_e & \sin 2\theta \\ \sin 2\theta & \cos 2\theta \end{pmatrix} \tag{1.60}$$

The effective mixing angle in matter, θ^m is given by

$$\tan 2\theta^m = \frac{2H_{12}^m}{H_{22}^m - H_{11}^m} = \frac{\delta m^2 \sin 2\theta}{\delta m^2 \cos 2\theta - A} \tag{1.61}$$

or, equilvalently,

$$\sin 2\theta^m = \frac{\delta m^2 \sin 2\theta}{\sqrt{(\delta m^2 \cos 2\theta - A)^2 + (\delta m^2 \sin 2\theta)^2}} \tag{1.62}$$

Here

$$A = 2\sqrt{2} G_F n_e E = 1.54 \times 10^{-4} \text{eV}^2 Y_e \rho(\text{g/cm}^3) E(\text{GeV})$$

(see Appendix A.1) where n_e is the electron number density. Thus, the effective mixing angle changes inside matter. When $A = \delta m^2 \cos 2\theta$, we obtain $\theta^m = \pi/4$ and ν_e and ν_μ mix maximally. This is referred to as the Mikheyev0-Smirnov-Wolfenstein (MSW) matter resonance effect [16] (see also Bethe [17]). The condition for resonance is given by

$$E_{res} \simeq \frac{\delta m^2 \cos 2\theta}{2\sqrt{2} G_F n_e} \tag{1.63}$$

The effective masses in matter are given by

$$(m_{1,2}^m)^2 = \frac{A}{2} \mp \frac{1}{2}\sqrt{(\delta m^2 \cos 2\theta - A)^2 + (\delta m^2 \sin 2\theta)^2} \tag{1.64}$$

These are shown in Fig. 1.3 as a function of the density. The m^2 for the two mass states is depicted along the y-axis in arbitrary units. The light black line depicts the crossing of levels at $A = A_{res}$. The complete conversion of one flavor into another takes place at the resonance. The difference between the two mass splittings becomes minimum when the resonance condition is satisfied.

Therefore, the oscillation amplitude in matter is enhanced if $\delta m^2 > 0$ and a resonance occurs (i.e. the amplitude reaches its maximal value of unity at the critical value of density i.e., $\sin^2 2\theta^m = 1$, even if $\sin^2 2\theta$ is small). For neutrinos, we get **enhancement for** $\delta m^2 > 0$ and **suppression for** $\delta m^2 < 0$. However, for anti-neutrinos, $A \to -A$ and the effect is opposite i.e., the oscillation amplitude is **enhanced if** $\delta m^2 < 0$ and **suppressed if** $\delta m^2 > 0$. This can also be seen from Fig. 1.3. In the case of two flavor neutrino oscillation in matter, the following points are worth mentioning :

1. The oscillation probabilities are modified for transitions involving a ν_e and $\overline{\nu}_e$ if the neutrinos propagate through the matter, and the modification depends upon the sign of δm^2. We have written down the expression for $\nu_e \to \nu_\mu$ where we have written the matter term as $A = 2\sqrt{2}G_F n_e E$, but for $\overline{\nu}_e \to \overline{\nu}_\mu$ oscillations, $A \to -A$. Note that in matter, the anti-neutrino transition probabilities are **not** the same as the corresponding neutrino transition probabilities (i.e., $P(\nu_\alpha \to \nu_\beta) \neq P(\overline{\nu}_\alpha \to \overline{\nu}_\beta)$).

2. We need $\delta m^2 > 0$ for neutrinos and $\delta m^2 < 0$ for anti-neutrinos inorder to get the resonance. For $\sin^2 2\theta << 1$ and $A \approx \delta m^2 > 0$, the oscillation probability for neutrinos is enhanced and that for anti-neutrinos is suppressed due to matter effects. For $\sin^2 2\theta << 1$ and $-A \approx \delta m^2 < 0$, the oscillation probability for anti-neutrinos is enhanced and that for neutrinos is suppressed due to matter effects. Thus, a comparison of the $\nu_e \to \nu_\mu$ CC rate with the $\bar{\nu}_e \to \bar{\nu}_\mu$ CC rate discriminates between the two signs of δm^2.

Three Flavor case

In the 3 neutrino oscillation scenario, the neutrino evolution in vacuum is described by two mass parameters (δm^2_{21}, δm^2_{31}), three mixing angles (θ_{12}, θ_{13}, θ_{23}) and a complex phase (δ_{13}). In matter, we also need to consider the coherent forward elastic scattering of the neutrinos with the medium described by the matter potential $V_{mat} = \sqrt{2}G_F n_e(x)\mathrm{diag}(1,0,0)$, where n_e is the electron density through the neutrino trajectory.

The analytic computation of probability in matter with standard interactions (SI) has been carried out by many authors [18–23].

For LBL experiments, the oscillation probabilities in matter can be written down in terms of the small hierarchy parameter $r_\lambda \equiv \delta m^2_{21}/\delta m^2_{31}$ and the small $\sin 2\theta_{13}$

upto the second order as [21]

$$\begin{aligned} P(\nu_e \to \nu_\mu) &= 4\, s_{13}^2\, s_{23}^2 \frac{\sin^2(r_A-1)\Delta}{(r_A-1)^2} + r_\lambda^2\, \sin^2 2\theta_{12}\, c_{23}^2 \frac{\sin^2 r_A\Delta}{r_A^2} \\ &+ 2\, r_\lambda\, s_{13}\, \sin 2\theta_{12}\, \sin 2\theta_{23} \cos(\Delta - \delta_{13})\, \frac{\sin r_A\Delta}{r_A}\, \frac{\sin(r_A-1)\Delta}{r_A-1} \end{aligned} \tag{1.65}$$

$$\begin{aligned} P(\nu_e \to \nu_\tau) &= 4\, s_{13}^2\, c_{23}^2 \frac{\sin^2(r_A-1)\Delta}{(r_A-1)^2} + r_\lambda^2\, \sin^2 2\theta_{12}\, s_{23}^2 \frac{\sin^2 r_A\Delta}{r_A^2} \\ &- 2\, r_\lambda\, s_{13}\, \sin 2\theta_{12}\, \sin 2\theta_{23} \cos(\Delta - \delta_{13})\, \frac{\sin r_A\Delta}{r_A}\, \frac{\sin(r_A-1)\Delta}{r_A-1} \end{aligned} \tag{1.66}$$

$$\begin{aligned} P(\nu_\mu \to \nu_\tau) &= \sin^2 2\theta_{23}\, \sin^2\Delta - r_\lambda\, c_{12}^2\, \sin^2 2\theta_{23}\, \Delta\, \sin 2\Delta + r_\lambda^2\, c_{12}^4\, \sin^2 2\theta_{23}\, \Delta^2\, \cos 2\Delta \\ &- \frac{1}{2r_A}\, r_\lambda^2\, \sin^2 2\theta_{12}\, \sin^2 2\theta_{23} \left(\sin\Delta\, \frac{\sin r_A\Delta}{r_A}\, \cos(r_A-1)\Delta - \frac{\Delta}{2}\, \sin 2\Delta \right) \\ &+ \frac{2}{r_A-1}\, s_{13}^2\, \sin^2 2\theta_{23} \left(\sin\Delta\, \cos r_A\Delta\, \frac{\sin(r_A-1)\Delta}{r_A-1} - \frac{r_A}{2}\Delta\, \sin 2\Delta \right) \\ &+ 2\, r_\lambda\, s_{13}\, \sin 2\theta_{12}\, \sin 2\theta_{23}\, \sin\delta_{13}\, \sin\Delta\, \frac{\sin r_A\Delta}{r_A}\, \frac{\sin(r_A-1)\Delta}{r_A-1} \\ &- \frac{2}{r_A-1}\, r_\lambda\, s_{13}\, \sin 2\theta_{12}\, \sin 2\theta_{23}\, \cos 2\theta_{23}\, \cos\delta_{13}\, \sin\Delta \\ &\times \left(r_A \sin\Delta - \frac{\sin r_A\Delta}{r_A}\, \cos(r_A-1)\Delta \right) \end{aligned} \tag{1.67}$$

Here $\Delta \equiv \delta m_{31}^2 L/4E$ and $r_A \equiv \pm(2\sqrt{2}G_F n_e E)/\delta m_{31}^2$. The sign of the second term is determined by choosing $\nu_e \to \nu_\mu$ (positive) or $\nu_\mu \to \nu_e$ (negative) as the oscillation channel, and the sign of r_A is determined by the sign of δm_{31}^2 and choosing neutrinos or anti-neutrinos. This formula shows that close to the resonance condition $r_A \approx 1$ especially the first term can be enhanced by matter effects. Therefore it is most affected by the sign of δm_{31}^2. In addition, CP effects are only present in the second and third terms. Depending on which quantity should be measured, one or two of the terms will act as signal and the rest of the terms will act as background.

1.3.3 Neutrino oscillations as a probe of discrete symmetries and their violation

We will follow the discussion on violation of discrete symmetries in neutrino oscil-

lations as presented in [24, 25]. Under CP transformation, parity is reversed and

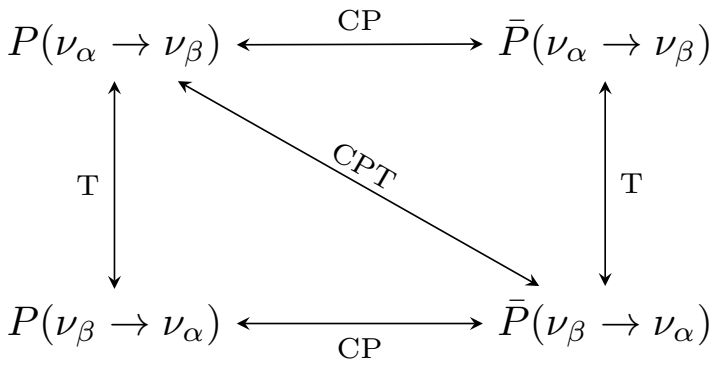

Figure 1.4: Depiction of CP, T, and CPT transformations in neutrino oscillations.

neutrinos are replaced by their antiparticles ($\nu_{\alpha,\beta} \leftrightarrow \bar{\nu}_{\alpha,\beta}$), which leads to the complex conjugation of $U_{\alpha i}$:

$$\begin{aligned} CP: \qquad & \nu_{\alpha,\beta} \longleftrightarrow \bar{\nu}_{\alpha,\beta} \\ & \Longleftrightarrow U_{\alpha i} \to U^{\star}_{\alpha i} \qquad (\{\delta_{13}\} \to -\{\delta_{13}\}) \end{aligned} \tag{1.68}$$

Time reversal transformation interchanges the initial and final evolution times t_0 and t, i.e. corresponds to evolution "backwards in time". The interchange $t_0 \rightleftharpoons t$ is equivalent to the complex conjugation of the exponential factors in the oscillation amplitude. Since the transition probability only depends on the modulus of the amplitude, this is equivalent to the complex conjugation of the factors $U_{\beta i}$ and $U^{\star}_{\alpha i}$, which inturn amounts to interchanging $\alpha \rightleftharpoons \beta$. Thus instead of the evolution "backwards in time" one can consider evolution forward in time, but between the interchanged initial and final flavors:

$$\begin{aligned} T: \qquad & t_0 \rightleftharpoons t \Longleftrightarrow \nu_\alpha \longleftrightarrow \nu_\beta \\ & \to U_{\alpha i} \to U^{\star}_{\alpha i} \qquad (\{\delta_{13}\} \to -\{\delta_{13}\}) \end{aligned} \tag{1.69}$$

Under the combined action of CP and T,

$$\begin{aligned} CPT: \qquad & \nu_{\alpha,\beta} \longleftrightarrow \bar{\nu}_{\alpha,\beta} \quad \& \quad t_0 \rightleftharpoons t \quad (\nu_\alpha \leftrightarrow \nu_\beta) \\ & \to P(\nu_\alpha \to \nu_\beta) \to P(\bar{\nu}_\beta \to \bar{\nu}_\alpha) \end{aligned} \tag{1.70}$$

From CPT invariance it follows that CP violation implies T violation and vice versa.

CP and T violation can be characterized by the probability differences,

$$\Delta P^{CP}_{\alpha\beta} \equiv P(\nu_\alpha \to \nu_\beta) - P(\bar{\nu}_\alpha \to \bar{\nu}_\beta)$$
$$\Delta P^{T}_{\alpha\beta} \equiv P(\nu_\alpha \to \nu_\beta) - P(\nu_\beta \to \nu_\alpha) \tag{1.71}$$

From CPT invariance, it follows that CP- and T-violating probability differences coincide, and that the survival probabilities have no CP asymmetry:

$$\Delta P^{CP}_{\alpha\beta} = \Delta P^{T}_{\alpha\beta} \;\; ; \Delta P^{CP}_{\alpha\alpha} = 0 \tag{1.72}$$

CP and T violations are absent in the 2 flavor case, so any observable violation in these symmetries in neutrino oscillations in vacuum would be a pure ≥ 3 flavor effect.

In the 3 flavor case, there is only one CP-violating Dirac-type phase δ_{13} and so only one CP-odd (and T-odd) probability difference:

$$\Delta P^{CP}_{e\mu} = \Delta P^{CP}_{\mu\tau} = \Delta P^{CP}_{\tau e} \equiv \Delta P \tag{1.73}$$

where

$$\Delta P = -4 c_{12}\, c_{23}\, c^2_{13}\, s_{12}\, s_{23}\, s_{13}\, \sin\delta_{13} \left[\sin(\Delta_{12}) \;+\; \sin(\Delta_{23}) \;+\; \sin(\Delta_{31}) \right] \tag{1.74}$$

It vanishes

- when at least one $\delta m^2_{ij} = 0$ (i.e. if $\delta m^2_{21} = 0$, then $\delta m^2_{31} = -\delta m^2_{23}$ since $\delta m^2_{32} = \delta m^2_{31} - \delta m^2_{21}$ and sin is an odd function.)
- when at least one $\theta_{ij} = 0$ or 90 degrees
- when $\delta_{13} = 0$ or 180 degrees
- in the averaging regime
- in the limit $L \to 0$ (as L^3)

Clearly, this quantity is very difficult to observe.

CP violation in matter

For neutrino oscillations in matter, CP transformation (substitution $\nu_\alpha \leftrightarrow \bar{\nu}_\alpha$) implies not only complex conjugating the leptonic mixing matrix, but also flipping the sign of the matter-induced neutrino potentials :

$$CP: \qquad U_{\alpha i} \to U^{\star}_{\alpha i} \qquad (\{\delta_{13}\} \to -\{\delta_{13}\}), \quad V(r) \to -V(r) \tag{1.75}$$

It can be shown that *in matter with an arbitrary density profile, as well as in vacuum, the action of time reversal on neutrino oscillations is equivalent to interchanging the initial and final neutrino flavors.* It is also equivalent to complex conjugating $U_{\alpha i}$, and replacing the matter density profile by the reverse one:

$$T: \qquad U_{\alpha i} \to U^{\star}_{\alpha i} \qquad (\{\delta_{13}\} \to -\{\delta_{13}\}), \quad V(r) \to \tilde{V}(r) \tag{1.76}$$

Here

$$\tilde{V}(r) = \sqrt{2} G_F \tilde{n}(r) \tag{1.77}$$

$\tilde{n}(r)$ being the reverse profile, i.e. the profile that corresponds to the interchanged positions of the neutrino source and detector. In the case of symmetric matter density profiles (e.g., matter of constant density), $\tilde{n}(r) = n(r)$.

It is to be noted that the very presence of matter violates C, CP and CPT. Thus even in the absence of the CP-violating phases $\{\delta_{13}\}$, CP violation would be observed. This extrinsic CP violation may complicate the study of the intrinsic one.

Unlike in vacuum, CP violation in neutrino oscillations in matter exists even in the 2-flavor case (in the case of 3 or more flavors, even when all $\{\delta_{13}\} = 0$) :

$$P(\nu_\alpha \to \nu_\beta) \neq P(\bar{\nu}_\alpha \to \bar{\nu}_\beta) \tag{1.78}$$

This is actually a well-known fact - for example, the MSW effect can enhance the $\nu_e \leftrightarrow \nu_\mu$ oscillations, and suppress the $\bar{\nu}_e \leftrightarrow \bar{\nu}_\mu$ ones, or vice versa. Moreover, in matter, the survival probabilities are not CP-invariant:

$$P(\nu_\alpha \to \nu_\alpha) \neq P(\bar{\nu}_\alpha \to \bar{\nu}_\alpha) \tag{1.79}$$

To extricate the intrinsic CP violation from the matter induced one in the LBL experiments, we would need to measure the energy dependence of the oscillated signal, or the signals at two baselines, which is an unfavorable condition. Some of the alternatives are :

- LBL experiments at relatively low energies and moderate baselines ($E \sim 0.1-1$ GeV, $L \sim 100 - 1000$ km.)
- Indirect measurements through
  1. CP-even terms $\sim \cos\delta_{13}$
  2. Area of leptonic unitarity angle.

Due to the experimental indistinguishability of low-energy ν_μ and ν_τ,CP violation cannot be studied in the supernova neutrino experiments.

Since CPT is not conserved in matter, CP and T violations are no longer directly connected (although some relations between them still exist). Therefore, T violation on neutrino oscillation in matter is not linked with the CP violation. Its characteristic features are :

- Matter does not necessarily induce T violation (only asymmetric matter with $\tilde{n}(r) \neq n(r)$ does).
- There is no T violation (either fundamental or matter-induced) in the 2-flavor case. This is a simple consequence of unitarity. For example, for the (ν_e, ν_μ) system one has :

$$\begin{aligned} P(\nu_e \to \nu_e) + P(\nu_e \to \nu_\mu) &= 1 \\ P(\nu_e \to \nu_e) + P(\nu_\mu \to \nu_e) &= 1 \end{aligned} \tag{1.80}$$

  from which $P(\nu_e \to \nu_\mu) = P(\nu_\mu \to \nu_e)$.
- In the 3-flavor case, there is only one T-odd probability difference for ν's (and only one for $\bar{\nu}'$s), irrespective of the matter density profile :

$$\Delta P^T_{e\mu} = \Delta P^T_{\mu\tau} = \Delta P^T_{\tau e} \tag{1.81}$$

  This is a consequence of 3-flavor unitarity.

The matter-induced T violation is an interesting pure $\geq$ 3f matter effect, absent in symmetric matter (in particular, in constant-density matter). It does not vanish in the regime of complete averaging of neutrino oscillations. It may fake the fundamental T violation and complicate its study, i.e. the extraction of δ_{13} from the experiment. The matter-induced T-violation vanishes when either $U_{e3} = 0$ or $\delta m^2_{21} = 0$ (i.e., in the 2 flavor limits), and so is doubly suppressed by both these small parameters. This implies that the perturbation theory can be used to obtain analytic expressions for the T-odd probability differences.

1.4 Status of neutrino oscillations and future goals

Various experiments using solar, atmospheric, reactor and accelerator neutrinos in the past few decades have verified that neutrinos oscillate among the three flavors while conserving the lepton number. The latest global fit [26] (see also [9]) to the world oscillation data directs us to two important aspects regarding mass and mixing in the neutrino sector, namely

- *Tiny masses with mild or no hierarchy :* From the best-fit values [26] of the two mass-squared splittings[1],

$$\delta m^2_{sol} = 7.39 \times 10^{-5}\text{eV}^2 \; ; \quad \delta m^2_{atm} = 2.52 \; (-2.51) \times 10^{-3}\text{eV}^2 \tag{1.82}$$

  one can deduce some information on the mass pattern of neutrinos even though the oscillation data can not tell anything about absolute mass scale. For normal hierarchy (NH), $m_1 \sim 0, m_2 \sim \sqrt{\delta m^2_{sol}}, m_3 \sim \sqrt{\delta m^2_{atm}}$ while for inverted hierarchy (IH), $m_3 \sim 0, m_2 \sim \sqrt{\delta m^2_{atm}}, m_1 \sim \sqrt{\delta m^2_{atm}}$. Currently, we donot know whether the hierarchy is normal or inverted. From this one can conclude that unlike the case with quarks or charged leptons, the hierarchy is relatively mild between the two heavy masses: for NH, $m_3/m_2 \simeq 6$ and for IH and the degenerate case, we have $m_2/m_1 \simeq 1$.

[1] The bracketed values correspond to IH.

- *Nearly tri-bimaximal mixing pattern :* The best-fit values for the mixing angles in the PMNS mixing matrix are

$$\sin^2\theta_{12} = 0.31 \; ; \quad \sin^2\theta_{23} = 0.58 \; ; \quad \sin^2\theta_{13} = 0.022 \; (0.023) \tag{1.83}$$

  Thus the mixing in the neutrino sector is close to tri-bi-maximal (one maximal, one large and one small) mixing as opposed to three small mixings present in the quark sector [27].

Both these observations reveal that the leptonic sector is quite asymmetric with respect to the quark sector and neutrinos (unlike quarks and charged leptons) which are allowed to be Majorana-type particle due to its neutral character are natural candidate to explain this inferred asymmetry.

The oscillation experiments have clearly established that at least two of the neutrinos are massive however the question of how they attain their masses still eludes us. Neutrinos are massless in the SM hence any theoretical explanation of the observed phenomena of neutrino oscillations necessarily requires physics beyond the SM. This is done by either extending the fermionic spectrum of the SM or giving up gauge invariance and/or renormalizability. The simplest and the most elegant possibility of generating neutrino masses is through the seesaw mechanism [5] in which one trades the tininess of the neutrino masses with heaviness of the high scale heavy fields. In addition, the seesaw mechanism is attractive as it has the ingredients for generating the baryon asymmetry of the Universe via leptogenesis [6].

In Table 1.4 and 1.5, we summarize the present status of the known three flavor neutrino oscillation parameters [26] obtained from a global analysis of data available from solar, atmospheric, reactor and accelerator experiments. The unknown parameters are sign(δm^2_{31}) and δ_{13}.

These results have delineated the **primary goals of neutrino oscillation research** over the coming decade, and these can be summarized below :

- Improved precision on the mass squared differences ($\delta m^2_{21}, \delta m^2_{31}$) and mixing angles ($\theta_{12}, \theta_{23}, \theta_{13}$).

- Determination of the hierarchy of neutrino masses or sign(δm^2_{31}).

- The presence, or otherwise, absence of CP violation in the leptonic sector and the value of δ_{13}.

The experimental realization of the above mentioned goals is a complex task. Hence a large number of neutrino experiments are underway or being planned to work towards achieving these aims. For a recent review, see [28].

Parameter	True value	3σ range	3σ Precision
θ_{12} [deg]	33.82	31.61 - 36.27	14%
θ_{13} [deg]	8.61	8.22 - 8.99	8.9%
θ_{23} (NH) [deg]	49.6	40.9 - 52.2	27%
θ_{23} (IH) [deg]	49.8	41.2 - 52.1	27%
δm^2_{21} [eV^2]	7.39×10^{-5}	[6.79 - 8.01] $\times 10^{-5}$	16%
δm^2_{31} (NH) [eV^2]	$+2.52 \times 10^{-3}$	[2.42 - 2.62]$\times 10^{-3}$	7.8%
δm^2_{31} (IH) [eV^2]	-2.51×10^{-3}	-[2.41 - 2.61] $\times 10^{-3}$	7.8%
δ_{13} (NH) [deg]	-145	$-\pi, \pi$	
δ_{13} (IH) [deg]	-76	$-\pi, \pi$	

Table 1.4: Current best-fit values, 3σ allowed range and precision of neutrino oscillation parameters obtained from global analysis of data [26] without the inclusion of tabulated χ^2 data on atmospheric neutrinos provided by the Super-Kamiokande collaboration (SK-atm). The precision is computed using $2(x^{up} - x^{low})/(x^{up} + x^{low})$ where x^{up} and x^{low} are the upper and lower bounds on the parameter x at 3σ level.

1.5 Neutrino oscillations - Experiments

In the present section, we give a brief description of different neutrino experiments. We first give a short description of how neutrinos are produced in the different kinds of sources and how different detector technologies are useful to detect neutrinos of different flavors.

Parameter	True value	3σ range	3σ Precision
θ_{12} [deg]	33.82	31.61 - 36.27	14%
θ_{13} [deg]	8.61	8.22 - 8.98	8.9%
θ_{23} (NH) [deg]	49.7	40.9 - 52.2	24%
θ_{23} (IH) [deg]	49.7	41.2 - 52.1	24%
δm^2_{21} [eV^2]	7.39×10^{-5}	[6.79 - 8.01] $\times 10^{-5}$	16%
δm^2_{31} (NH) [eV^2]	$+2.52 \times 10^{-3}$	[2.43 - 2.62]$\times 10^{-3}$	7.6%
δm^2_{31} (IH) [eV^2]	-2.51×10^{-3}	-[2.41 - 2.61] $\times 10^{-3}$	7.6%
δ_{13} (NH) [deg]	-143	$-\pi, \pi$	
δ_{13} (IH) [deg]	-80	$-\pi, \pi$	

Table 1.5: **Current best-fit values, 3σ allowed range and precision of neutrino oscillation parameters obtained from global analysis of data [26] with the inclusion of tabulated χ^2 data on atmospheric neutrinos provided by the Super-Kamiokande collaboration (SK-atm). The precision is computed using $2(x^{up} - x^{low})/(x^{up} + x^{low})$ where x^{up} and x^{low} are the upper and lower bounds on the parameter x at 3σ level.**

1.5.1 Sources of neutrinos

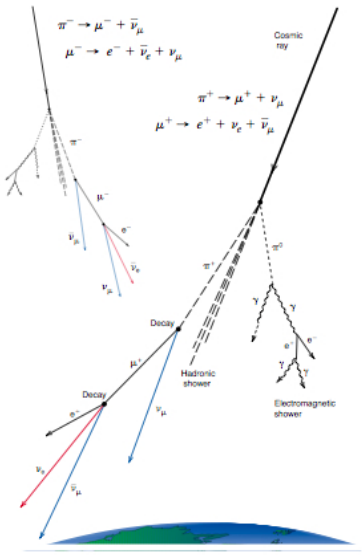

Figure 1.5: **Atmospheric neutrinos. Taken from [29].**

1. *Atmospheric neutrinos :-* These result from interactions of cosmic rays hitting atmospheric nuclei, thereby producing mesons (pions and kaons) which further decay to give rise to $\nu_\mu, \bar{\nu}_\mu, \nu_e$ and $\bar{\nu}_e$ as given below

$$\pi^+, K^+ \rightarrow \mu^+\nu_\mu \text{ (2 body decays of } \pi^+, K^+ \text{ giving } \mu^+ \text{ which further decays)}$$
$$\downarrow$$
$$e^+\bar{\nu}_\mu\nu_e \text{ (Branching Fraction} \approx 100\%)$$

The total number of muon-type neutrinos is expected to be twice as large as the total number of electron-type neutrinos. Atmospheric neutrinos have energies $\in$ 100 MeV $-$100 GeV. Fig. 1.5 shows a schematic of atmospheric neutrinos. The flux is fairly well understood and falls steeply as $E^{-2.7}$ at energies above 1 GeV [30–32].

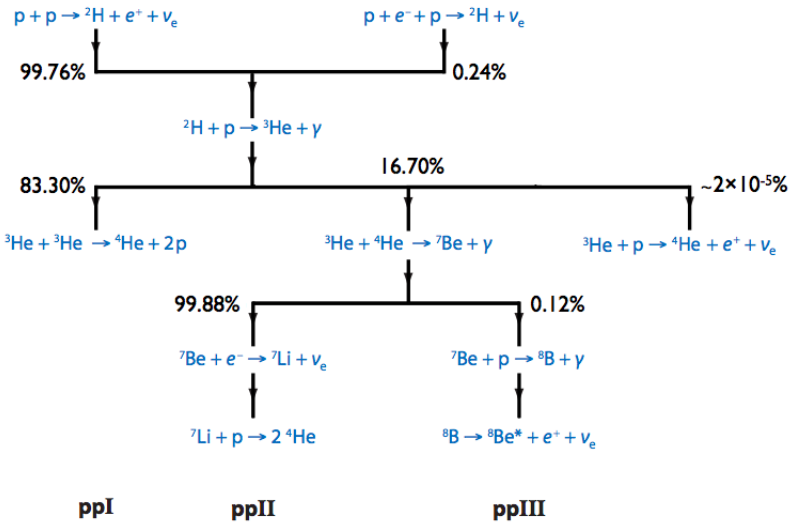

Figure 1.6: Solar neutrinos produced via the pp chain. Taken from [34].

2. *Solar neutrinos :* The Sun releases energy in nuclear fusion reactions taking place in the core of the Sun where hydrogen is burnt to ^{4}He. Solar neutrinos are essentially electron neutrinos and are produced in the Sun as a result of the thermonuclear reactions via the pp chain (Fig. 1.6 shows a schematic of the pp chain which is the dominant energy generation mechanism in the Sun) and the CNO cycle. In order to compute the fluxes of these neutrinos and energy spectra, one needs a detailed model of the Sun which involves explaining

not only present solar structure but also the evolution of the Sun from initial ignition of hydrogen nuclear fusion to present day. The specific solar models incorporate many observed parameters such as the solar surface luminosity, mass and age of the Sun. The best model available is the Standard Solar Model [33].

3. *Astrophysical neutrinos :* At the very high end of the energy spectrum, it is possible to produce neutrinos in astrophysical sources such as gamma ray bursts (GRB) or active galactic nuclei (AGN) jets. Interaction of protons with the ambient photons (pion photoproduction in the $p\gamma$ interaction) or protons (pp interaction) within the source produces charged pions which then decay to give rise to muons and muon neutrinos. Depending on the energy, the muons thus produced may also decay further to give muon neutrinos and electron neutrinos. Typically (in pion beam source), the flux of muon neutrinos is twice the flux of electron neutrinos. These neutrinos are of order PeV ($= 10^{15}$ eV) in energy and these are referred to as ultra high energy neutrinos [35].

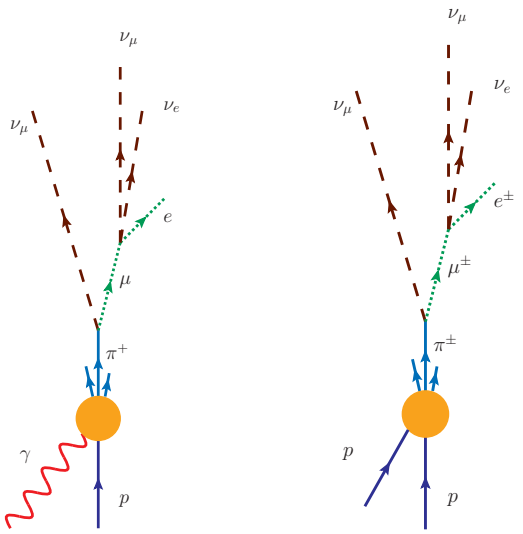

Figure 1.7: Astrophysical neutrinos produced via the $p\gamma$ or pp interaction.

4. *Conventional Beams :-* These correspond to neutrino beams produced in terrestrial accelerators and are advantageous over the other neutrino sources as they provide much greater control of the source. It is possible to adjust the

energy spectrum of neutrinos produced. Also, neutrinos may be delivered in a controlled fashion by allowing for better background rejection. A conventional beam is obtained by first bombarding the target with high energy protons which produces mesons (mostly pions and some kaons) which are focused into an evacuated decay region where they decay to produce neutrinos. This technique inherently makes a beam which contains dominantly muon type with some admixture of electron type neutrinos.

A beam of either neutrinos or antineutrinos can be selected by removing either negatively or positively charged mesons from the beamline. Let us consider that positively charged mesons (π^+, K^+) are selected. The main decay channels are

$\pi^+ \rightarrow \mu^+\nu_\mu$ (Branching Fraction $\approx 99.99\%$)

$K^+ \rightarrow \mu^+\nu_\mu$ (Branching Fraction $\approx 63.4\%$)

$K^0_L \rightarrow \pi + \mu + \nu_\mu$ (Branching Fraction $\approx 27.0\%$)

Due to the relatively longer lifetime of muons ($\tau \simeq 2.2\ \mu$s), the muons produced in the decay of mesons stop before decaying so these are not crucial source of muon neutrinos. For example, in the NuMI beam tunnel (L = 677 m) approximately 70% of 10 GeV π^+ would decay, while only 1% of the 10 GeV μ^+ would decay. However the neutrino beam produced in this way is not pure. It has a small (0.5-1.0 %) admixture of ν_e coming from the kaon 3 body decay and the decay of daughter muons (μ^+) produced in 2 body decays of pions and kaons (π^+, K^+). The main 3 body decay channels that result in ν_e contamination are :

$K_L \rightarrow \pi e \nu_e$ (Branching Fraction $\approx 40\%$)

$K^+ \rightarrow \pi^0 e^+ \nu_e$ (Branching Fraction $\approx 4.9\%$)

$\pi^+, K^+ \rightarrow \mu^+\nu_\mu$ (2 body decays of π^+, K^+ giving μ^+ which furthur decays)

$\downarrow$

$e^+\bar{\nu}_\mu\nu_e$ (Branching Fraction $\approx 100\%$)

It should be noted that muon decay is mainly responsible for the ν_e component of the beam.

The oscillation channels that can be studied are : $\nu_\mu \rightarrow \nu_e$, $\nu_\mu \rightarrow \nu_\tau$ and $\nu_\mu \rightarrow \nu_\mu$. If the neutrino energy is below the tau detection threshold of 3.46 GeV, the main appearance channel is $\nu_\mu \rightarrow \nu_e$. But one has to eliminate the backgrounds which arise from (i) ν_e contamination in the beam, (ii) Fake electrons from NC π^0. A beam of either neutrinos or antineutrinos can be selected by removing either negatively or positively charged mesons from the beamline. Fluxes of neutrino beams are parametrized in terms of number of protons on target (POT) per year. Conventional beams have POT of about 10^{20} per year. Examples : OPERA [36], ICARUS [37].

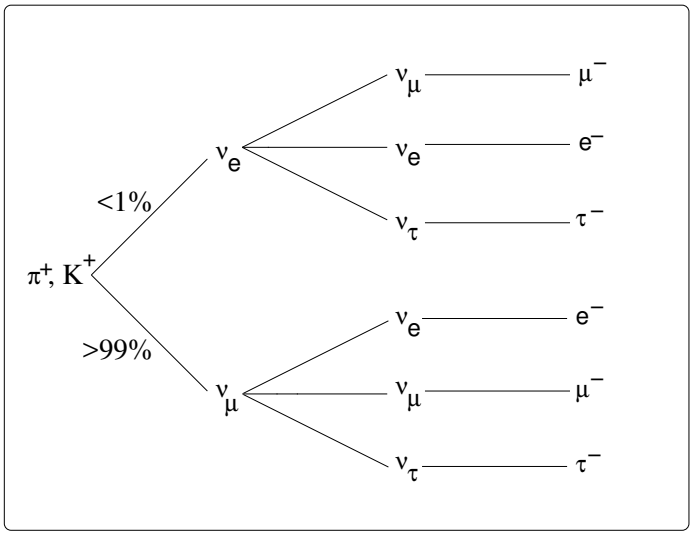

Figure 1.8: The decay of mesons (pions and kaons) gives a beam of ν_μ.

5. *Superbeam :-* Tehnologically upgraded version of coventional beam is referred to as superbeam. The proton fluxes are expected to higher by a factor of 10 to 50 as compared to the conventional beams. The source power for superbeams is $\simeq 10^{21}$ POT per year. The ν_e contamination is expected to be reducible to $\leq 0.2\%$ in future superbeams. Examples : NOvA [38], T2K [39].

6. *Reactor neutrinos :-* Reactors produce an isotropic flux of electron antineutrinos ($\bar{\nu}_e$) with energies of the order of MeV. Since the initial flavor of the neu-

trino is $\bar{\nu}_e$, one is mainly interested in disappearance measurement i.e., $\bar{\nu}_e \to \bar{\nu}_e$ with low energy neutrinos and one is able to access smaller values of the neutrino mass squared difference. Examples : CHOOZ [40], D-CHOOZ [41], Palo Verde [42], KamLAND [43], Daya Bay [44], RENO [45].

7. *Neutrino Factory beams :-* These are based on muon storage rings where it will be possible to capture roughly 10^{20} muons (of either sign) per year. These are created by the decays of high energy muons which are stored in elongated rings. A neutrino factory is a muon storage ring with a long straight section in which some fraction of the high energy accelerated muons ($\sim 20 - 50$ GeV) decay in the straight sections thereby creating a well-collimated neutrino beam along the direction of the straight section (see Fig. 1.9) [46]. The advantages over a conventional neutrino beam are :

   - the resulting neutrino spectrum is well-known.
   - both ν_e and ν_μ beams are available.
   - there is no contamination.
   - the required proton energy is more modest (since much of the neutrino energy comes from adding energy to the muons in recirculating linacs)
   - there is no long decay tunnel (the entire length of the ring may only be $\sim$ 200 m).

   For $\mu^- \to \nu_\mu e^- \bar{\nu}_e$ decays, the observable channels are $\nu_\mu \to \nu_e, \nu_\mu, \nu_\tau$ and $\bar{\nu}_e \to \bar{\nu}_e, \bar{\nu}_\mu, \bar{\nu}_\tau$

1.5.2 Detectors

We now describe some important detectors that have been used in neutrino oscillation experiments and their properties.

1. *Water Cerenkov Detector*: In this case, the detecting element is purified water. When charged particles passes through water, it produces Cerenkov light which

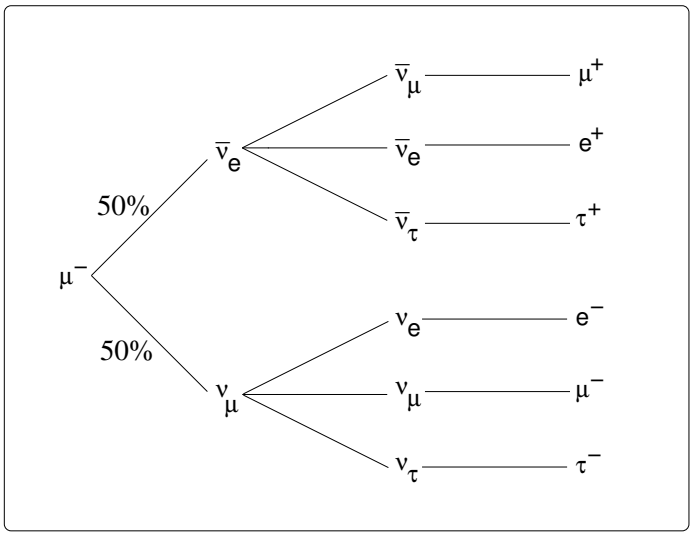

Figure 1.9: The decay of μ^- at a neutrino factory leads to ν_μ and $\bar{\nu}_e$. All oscillation channels are accessible in this case.

gets detected by the Photo Multiplier Tubes (PMTs) surrounding the water. The pattern of Cerenkov light emission allows one to identify whether it was due to electrons (positrons) or muons (antimuons). For highly energetic particles, the energy reconstruction is harder due to the large number of particles produced in the hadron shower produced in deep inelastic scattering. Charge of the particle cannot be identified. Examples : SK [47], HK [48], MEMPHYS [49].

2. *Liquid Argon Detector*: Liquid Argon acts as the detecting medium. The tracks produced by charged particles are identified in the liquid. The pattern allows us to detect the particle. This detector has excellent particle identification capability as well as good calorimetry. There is no magnetic field hence it is not possible to distinguish between particles and corresponding anti-particles. Examples : ICARUS [37].

3. *Liquid scintillator Detector*: In this case, the detecting medium is dilute liquid scintillator such as mineral oil and b-PBD is used for detection of charged particles. The scintillation light produced by a charged particle is detected by the PMT. Here again the charge of the particle cannot be identified due to the absence of magnetic field. Examples : LSND [54], D-CHOOZ [41].

Experiment	Detector (mass)	Source	L (km)	< E > (GeV)	Location
K2K [50]	Water Cerenkov (50 Kt)	Conventional Beam	250	1.4	SK, Japan
MINOS [51]	Iron Calorimeter (5.4 Kt)	Atmospheric Conventional Beam	15-13000 735	1-100 3, ∼8, ∼11	Soudan, US
ICARUS [37]	Liquid Argon TPC (2.35 Kt)	Conventional Beam	732	17	LNGS, Europe
OPERA [36]	Emulsion Cloud Chamber (1.65 Kt)	Conventional Beam	735	17	LNGS, Europe
T2K [39]	Water Cerenkov (50 Kt)	Superbeam (Off-axis)	295	0.76	Kamioka, Japan
NOvA [38]	Liquid Scintillator (50 Kt)	Superbeam (Off-axis)	812	2.22	US
T2HK [48]	Water Cerenkov (1 Mt)	Atmospheric Superbeam	15-13000 295	1-100 4.0	Japan
DUNE [52]	LArTPC (40 Kt)	Atmospheric Superbeam	15-13000 1300	1-100 0.8, 2.5	US
INO [53]	Iron Calorimeter (50 - 100 Kt)	Atmospheric Superbeam/NF	15-13000 TBD	1-100 TBD	India

TBD → To be decided.

Table 1.6: General features such as detector type, neutrino source, baseline (L), average energy ($\langle E \rangle$) and location of the some of the experiments.

4. *Iron Calorimeter*: Iron Calorimeters consist of iron (steel) modules interspersed with sensitive elements in which charged particles deposit energy. These detectors are good for observing ν_μ and $\bar{\nu}_\mu$ but not ν_e and $\bar{\nu}_e$. One can distinguish between μ^- and μ^+ if a magnetic field is added. Examples : MINOS [51], INO [53].

5. *Emulsion Detector*: The above detector types are not useful to detect τ. If one employs emulsion films (50 μm thick), it is possible to observe the trajectories of τ and its decay products. These films are interleavened with 1 mm thick lead plates to provide a large (1.8 Kt) target mass. In addition to the emulsion films, the detector also contains a magnetic spectrometer which measures the charge

and the momentum of muons going through it. Examples : OPERA [36].

Experiment	Channel	Physics potential
K2K	$\nu_\mu \to \nu_{\mu,e}$	**Beam:** $\lvert\delta m^2\rvert = 2.8 \times 10^{-3}\text{eV}^2$, $\sin^2 2\theta_{23} < 0.13$ at 90% C.L.
[50]		
MINOS	$\nu_\mu \to \nu_{\mu,e}$	**Atm:** Compare ν_μ and $\bar{\nu}_\mu$ osc. : CPT test
[51]		**Beam:** $\lvert\delta m^2_{32}\rvert = 2.41^{+0.09}_{-0.10} \times 10^{-3}\text{eV}^2$, $\sin^2 2\theta_{23} = 0.950^{+0.035}_{-0.036}$
ICARUS	$\nu_\mu \to \nu_{e,\mu,\tau}$	**Beam:** τ, e appearance, proton decay
[37]		$\lvert\delta m^2_{32}\rvert$, $\sin^2\theta_{23}$, $\sin^2 2\theta_{13}$ precision as in MINOS
OPERA	$\nu_\mu \to \nu_{e,\mu,\tau}$	**Beam:** τ, e appearance, proton decay
[36]		$\lvert\delta m^2_{32}\rvert$, $\sin^2\theta_{23}$, $\sin^2 2\theta_{13}$ precision as in MINOS
T2K	$\nu_\mu \to \nu_{e,\mu}$	**Beam:** e appearance
[39]		$\lvert\delta m^2_{32}\rvert = 2.463^{+0.071}_{-0.074} \times 10^{-3}\text{eV}^2$, $\sin^2\theta_{23} = 0.526^{+0.032}_{-0.036}$
NOvA	$\nu_\mu \to \nu_{e,\mu}$	**Beam:** e appearance
		Search for sterile ν
[38]		$\Delta m^2_{32} = 2.44 \times 10^{-3}\text{eV}^2$, $\sin^2\theta_{23} = 0.56$, $\delta_{13} = 1.21\pi$ (NH)
T2HK	$\nu_\mu \to \nu_{e,\mu,\tau}$	**Atm:** Possible τ appearance, L/E dip
[48]		**Beam:** $\sin^2\theta_{13}$ sensitivity below 10^{-3}
		Sign δm^2_{32}, δ_{13}
DUNE	$\nu_\mu \to \nu_{\mu,e}$	**Beam:** precise measurement of δ_{13}, mass ordering
[52]	$\bar{\nu}_\mu \to \bar{\nu}_{\mu,e}$	**Beam:** Octant of θ_{23}
INO	$\nu_\mu \to \nu_\mu$	**Atm:** L/E dip, CPT test
[53]		Sign Δm^2_{32}
		$\lvert\Delta m^2_{32}\rvert$, $\sin^2\theta_{23}$ precision as in MINOS
		Beam: $\lvert\Delta m^2_{32}\rvert$, $\sin^2\theta_{23}$, $\sin^2 2\theta_{13}$ precision, δ_{CP}

Table 1.7: Physics potential of the various neutrino experiments.

1.5.3 Long baseline neutrino experiments

LBL neutrino experiments are terrestrial accelerator experiments in which one produces conventional beams or superbeams as depicted in Fig. 1.10 (for reviews on LBL neutrino experiments, see [55, 56]). As mentioned earlier, the neutrino beams are produced by the decay of charged pions and kaons generated by a high energy

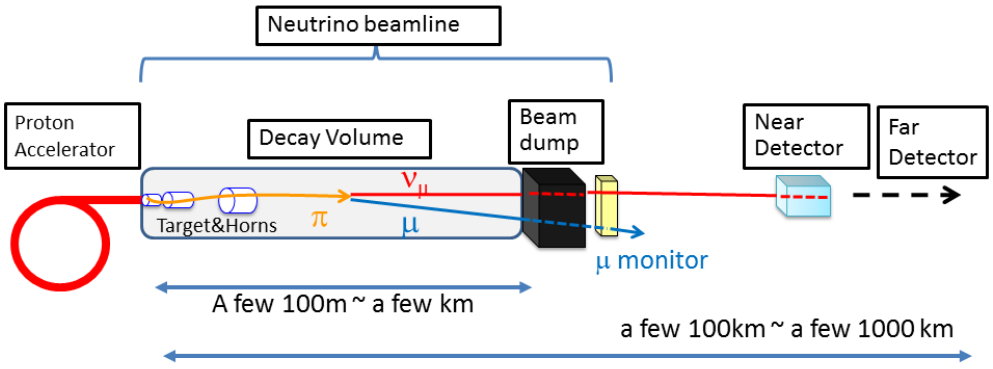

Figure 1.10: Schematic of an accelerator beam line. Taken from [57].

proton beam hitting a target. The positive and negative mesons are sign-selected and focussed by large acceptance magnetic lenses into a long evacuated decay tunnel where the muon neutrinos (or antineutrinos) are generated. In case of positive charge selection, we have a ν_μ beam with a few percent contamination of $\bar{\nu}_\mu$ (from decay of π^-, K^-, K^0) and about 1% contamination of ν_e and $\bar{\nu}_e$ (from three body decay of $K^\pm, K^0$ and μ).

In order to fulfil the needs of search for CP violation, one needs to push the conventional beams to their ultimate limits (i.e. superbeams) and gigantic neutrino detectors must be built. All LBL experiments mainly produce muon (anti)neutrinos at source which propagate to detector. So there are mainly two kinds of oscillation channels, disappearance channel (survival of muon (anti)neutrinos) and appearance channel (appearance of electron (anti)neutrino). The disappearance channel is most sensitive to θ_{23} and mass hierarchy while the appearance channel is sensitive to θ_{13} and the CP phase, δ_{13} and also to the mass hierarchy [52].

The first generation of LBL experiments were KEK to Kamioka (K2K), Main injector neutrino oscillation search (MINOS), MINOS+, Oscillation Project with Emulsion-tRacking Apparatus (OPERA) and Imaging Cosmic And Rare Underground Signals (ICARUS). Tokai to Kamioka (T2K) and NuMI Off-Axis ν_e Appearance (NOνA) are the second generation LBL experiments and DUNE and Tokai to Hyper-Kamiokande (T2HK) are the third generation LBL experiments. We have listed some of the past, present and future LBL experiments (see Table 1.6 and 1.7

for a comprehensive summary of some experiments.)

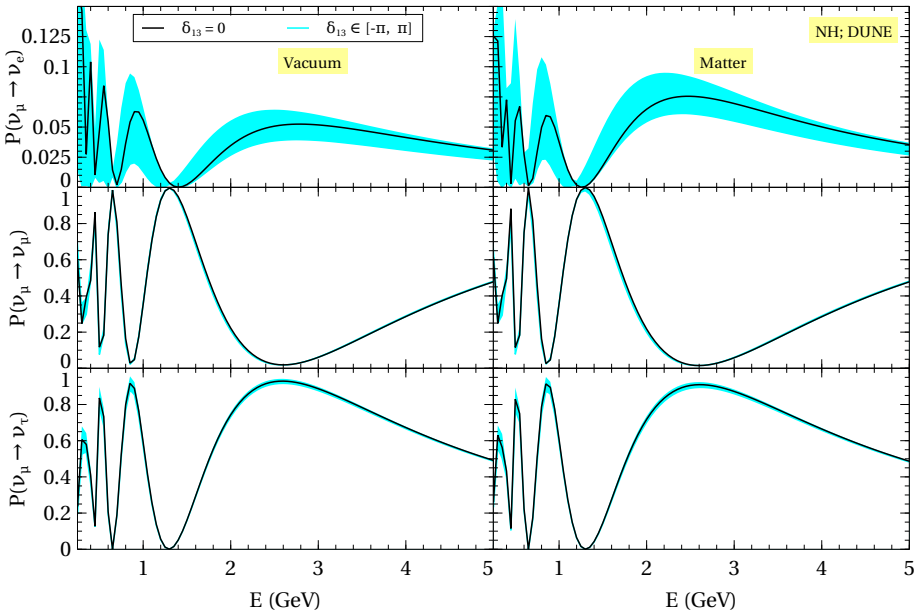

Figure 1.11: Oscillation probabilities for $\nu_\mu \to \nu_e$ (top row), $\nu_\mu \to \nu_\mu$ (middle row) and $\nu_\mu \to \nu_\tau$ (bottom row) as a function of E for a fixed baseline of 1300 km in vacuum (left) and in matter (right). The oscillation parameters have been taken from the Table 1.5. The solid line is for $\delta_{13} = 0$. The bands indicate the variation in probability due to the variation of δ_{13} in the allowed range which is indicated in the plot.

Since the neutrinos are mainly produced in the ν_μ flavor at the LBL experiments, the oscillation channels that are accessible at a LBL experiment are $\nu_\mu \to \nu_e$, $\nu_\mu \to \nu_\mu$ and $\nu_\mu \to \nu_\tau$. In order to facilitate a smooth and clear understanding of the results presented in Chapter 2, we numerically obtain the relevant probabilities in Fig. 1.11 and Fig 1.12 using General Long Baseline Experiment Simulator (GLoBES) software [79] both for the case of vacuum and standard matter interactions for a fixed baseline of 1300 km. In Fig. 1.11, we show the neutrino oscillation probability for $\nu_\mu \to \nu_e$, $\nu_\mu \to \nu_\mu$ and $\nu_\mu \to \nu_\tau$ channels as a function of E in vacuum and in matter (assuming SI) for the case of NH. The CP asymmetry in the $\nu_\mu \to \nu_e$ channel is plotted against energy for fixed baseline of 1300 km in Fig. 1.12. The following salient features emerge from Fig. 1.11 and Fig. 1.12

- **Unitarity :-** At each value of E, one can check that the probabilities for the

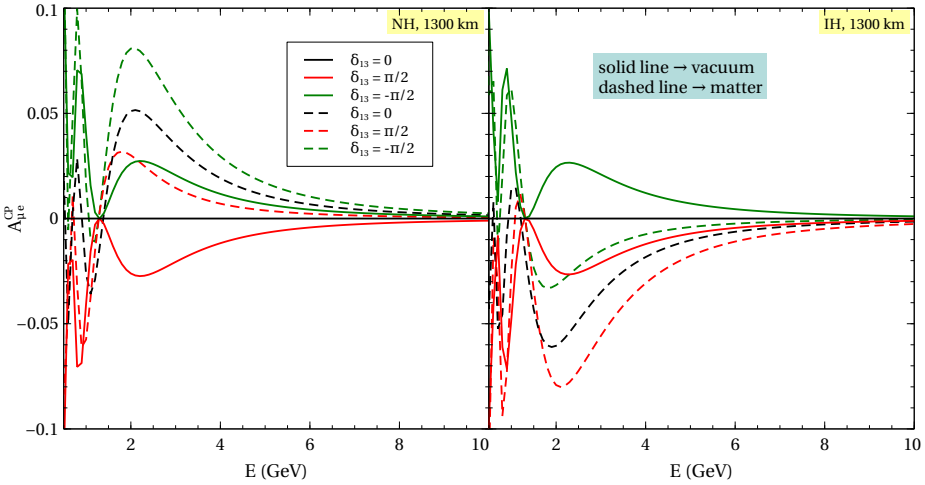

Figure 1.12: CP asymmetry in the $\nu_\mu \to \nu_e$ channel as a function of E for a fixed baseline of 1300 km in vacuum and in matter. The oscillation parameters have been taken from Table 1.5.

three channels add up to 1 *i.e.*,

$$P(\nu_\mu \to \nu_e) + P(\nu_\mu \to \nu_\mu) + P(\nu_\mu \to \nu_\tau) = 1$$

This is expected from unitarity of the mixing matrix (Eq. 1.28). The muon survival probability is large and approaches unity which in turn makes the $\nu_\mu \to \nu_\tau$ probability also large approaching unity. The $\nu_\mu \to \nu_e$ probability on the other hand is much smaller than the other two. In the region of interest for LBL experiments, $\nu_\mu \to \nu_e$ probability can take values upto around ~ 0.05.

- $\nu_\mu \to \nu_e$ **channel :** If we look at the leading oscillatory term of $P(\nu_\mu \to \nu_e)$, we get oscillation maxima at

$$\begin{aligned} \frac{\Delta m^2_{31} L}{4E} &= (2n-1)\frac{\pi}{2} \\ \frac{L}{E} &\simeq (2n-1)\frac{\pi}{2}\left(\frac{1}{1.267}\right)\left(\frac{2.52\times 10^{-3}\ \text{eV}^2}{\Delta m^2_{31}}\right) \\ \frac{L}{E} &\simeq (2n-1)\times 500\ \frac{\text{km}}{\text{GeV}} \end{aligned} \tag{1.84}$$

where n is an integer and $n = 0, 1, \ldots$ stands for first, second, ... oscillation maxima occurring at $L/E \simeq 500, 1500, \ldots$ km/GeV and so on. It may be possible to observe the higher ($n > 1$) oscillation maximas when the baselines are

comparatively longer (so that the energies at which higher maximas occur are not too small). For $L = 1300$ km, the energy for first oscillation maximum is $E \simeq 2.6$ GeV and the energy for second oscillation maximum is $E \simeq 0.8$ GeV. The LBL neutrino experiments are typically planned to exploit the first oscillation maximum of the $\nu_\mu \to \nu_e$ probability (i.e. $L/E \simeq 500\ km/GeV$) and the neutrino flux is typically tuned to be peaked at a value of energy corresponding the first oscillation maximum for the baseline under consideration. This enhances the sensitivity of those experiments to neutrino oscillation parameters.

At the first peak, the probability in the neutrino channel reaches a value of ~ 0.05 in vacuum (for $\delta_{13} = 0$) which gets enhanced to ~ 0.075 (for $\delta_{13} = 0$) in matter for NH due to the matter effect. One can clearly see that the band of allowed probabilities when δ_{13} is varied is also higher than the vacuum case.

For CP violation discussion, one needs to study the probability differences between the neutrino and the antineutrino channels (Fig. 1.12). In vacuum, when $\delta_{13} = 0$, we get the same values for probabilities in neutrino and antineutrino channels. This is expected since the only term that distinguishes neutrinos from antineutrinos is the CP phase (δ_{13}). However, when δ_{13} is non-zero, one gets non-zero CP asymmetry which becomes largest when $\delta_{13} = \pm\pi/2$. This can be understood from the $\sin\delta_{13}$ dependence of the CP asymmetry (see Eq. 1.73). This is referred to as **intrinsic CP** effect. The CP asymmetry in vacuum is also independent of the neutrino mass hierarchy as expected.

However, the scenario in matter (assuming SI) is quite different. Even when $\delta_{13} = 0$, one gets non-zero CP asymmetry the sign of which depends on the choice of hierarchy as can be seen in Fig. 1.12. One gets non-zero CP asymmetry also when $\delta_{13} \neq 0$ but again the sign of the asymmetry is hierarchy dependent. The asymmetry at $\delta_{13} = 0$ arises purely due to the fact that matter is CP asymmetric which induces **extrinsic CP** effects. In general, there are two components in the CP asymmetry and it is very hard to disentangle the two contributions. This issue has been discussed at length in Chapter 2.

- $\nu_\mu \to \nu_\mu$ **channel :-** The muon survival probability can be very large at some energies but it has almost no dependence on the value of δ_{13}. This is due to the fact that the CP odd term ($\propto \sin\delta_{13}$) vanishes. There is almost no impact of Earth matter on this channel for this baseline of $\mathcal{O}(1000)$ km. Matter effects are crucial for longer baselines [22, 23].

- $\nu_\mu \to \nu_\tau$ **channel :-** Like the muon survival probability, this can be very large at some energies but it has almost no dependence on the value of δ_{13}. Earth matter effects are also small at the baseline of $\mathcal{O}(1000)$ km. This is no longer true for longer baselines [22, 23]. Also, detection of tau neutrinos is not very easy so this appearance channel is not very useful.

The $\nu_\mu \to \nu_e$ **channel** is termed as the **golden channel** [19] since the information about the neutrino oscillation parameters are mainly extracted through this channel at the LBL experiments. The dependence due to the CP odd term ($\propto \sin\delta_{13}$) primarily manifests itself in the $\nu_\mu \to \nu_e$ channel.

1.6 New physics scenarios

Unification of all fundamental interactions observed in nature has been the dream of particle physicists. SM of particle physics has been a big step in this direction which successfully unified weak and electromagnetic interactions. But as has been well discussed in literature, the SM despite all successes also leave many questions unanswered. The SM also has known and well emphasized problems like naturalness, hierarchy etc. associated with it. So there are very strong reasons to believe that SM is a effective theory valid upto a certain energy scale ($\sim$ 1 TeV), and beyond this scale some new physics should take over.

As is already mentioned in the introduction, the SM is clearly inadequate to explain the phenomena of neutrino oscillations and masses. One is therefore interested in possible extensions of SM, which can accommodate the masses of neutrinos in a natural way. Here we will describe the possible candidates for new physics (theories

beyond the SM) either by enlarging the particle content of the SM or via new type of interactions.

1.6.1 Non-standard interactions

Effects due to new physics in neutrino oscillations can be very conveniently described by nonstandard interactions (NSI). The idea of NSI emerged in the seminal paper by Wolfenstein [16] in order to explain the idea of flavor change of neutrinos for the case of massless neutrinos. It is now well established by present data that neutrinos oscillate due to nonzero masses and mixing. However there can be subleading effects due to NSI which can be probed in neutrino oscillation experiments. The possibility of detection of NSI and their interference with standard neutrino oscillation measurements has triggered a considerable interest in the community in the recent years. For recent reviews on NSI, see [58–61].

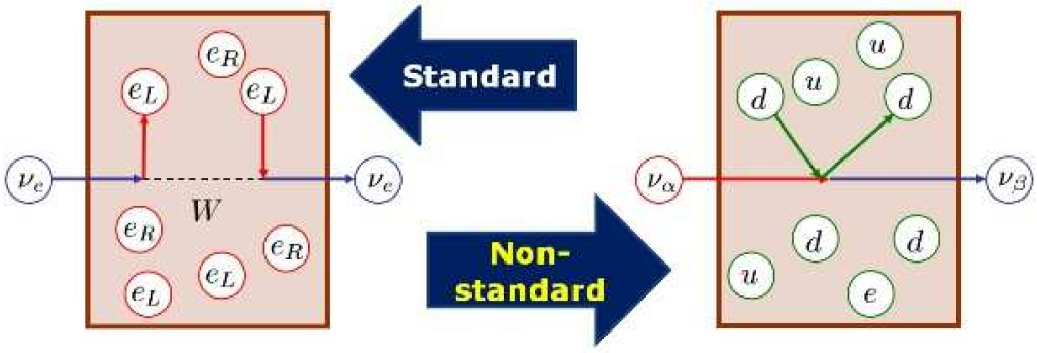

Figure 1.13: A cartoon depicting interactions (SI and NSI). Taken from Ohlsson [58].

At low energies ($E \ll M_{ew}$, where M_{ew} is the electroweak scale), we can parametrize a wide class of new physics scenarios in a model independent way by using effective four-fermion interactions. In general, NSI can influence both via CC interactions or NC interactions. See Fig. 1.13 for a cartoon depicting SI and NSI. It is known that CC interactions affect processes only at the source or the detector and these are clearly discernible at near detectors. On the other hand, the NC interactions affect the propagation of neutrinos which can be studied only at far detectors. We are interested in NSI that alter the propagation of neutrinos, we shall consider only the

NC type of interactions. The effective Lagrangian describing the NC type neutrino NSI is given by

$$\mathcal{L}_{NSI} = -2\sqrt{2}G_F\varepsilon^{fC}_{\alpha\beta}\ [\bar{\nu}_\alpha\gamma^\mu P_L\nu_\beta]\ [\bar{f}\gamma_\mu P_C f] \tag{1.85}$$

where f represents the first generation SM fermion (e, u, d). The requirement of coherence in the interaction preserves the flavor of the background fermion. Second or third generation fermions do not affect oscillation experiments since matter does not contain them. $P_L = (1-\gamma_5)/2$ and $P_C = (1\pm\gamma_5)/2$. In general, the NSI terms can be complex.

The new NC interaction terms can affect the neutrino oscillation physics either by causing the flavor of neutrino to change i.e. flavor changing interaction or, by having a non-universal scattering amplitude of NC for different neutrino flavors i.e. flavor preserving interaction. Even though in the Lagrangian, NSI coupling of the neutrino is with first generation fermions, it turns out that phenomenologically, only the sum (incoherent) of all the individual contributions from different scatterers contribute to the coherent forward scattering of neutrinos in matter. If we normalize to the n_e, the effective NSI parameter for neutral Earth matter (there are 2 nucleons (one proton and one neutron) per electron for neutral Earth matter) is

$$\varepsilon_{\alpha\beta} \quad = \quad \sum_{f=e,u,d}\frac{n_f}{n_e}\varepsilon^f_{\alpha\beta} = \varepsilon^e_{\alpha\beta} + 2\varepsilon^u_{\alpha\beta} + \varepsilon^d_{\alpha\beta} + \frac{n_n}{n_e}(2\varepsilon^d_{\alpha\beta} + \varepsilon^u_{\alpha\beta}) = \varepsilon^e_{\alpha\beta} + 3\varepsilon^u_{\alpha\beta} + 3\varepsilon^d_{\alpha\beta} \tag{1.86}$$

where n_n and n_f are neutron number density and density of fermion f in that medium respectively. If we normalize to either up or down quark abundance (assume isoscalar composition of matter) instead, there is a relative factor of 3 which will need to be incorporated accordingly. Also, $\varepsilon^f_{\alpha\beta} = \varepsilon^{fL}_{\alpha\beta} + \varepsilon^{fR}_{\alpha\beta}$ which encodes the fact that NC type NSI matter effects are sensitive to the vector sum of NSI couplings.

We next give the current constraints on the NC type NSI parameters. Eq. 1.86 is the combination of NSI terms that impact neutrino oscillations. Typically, as in [62], the constraints are set on individual NSI terms, for example, $\varepsilon^{fL}_{\alpha\beta}$ or $\varepsilon^{fR}_{\alpha\beta}$ where the coupling is to either of the fermions (e, u, d) individually. This complicates the extraction of constraints on effective $\varepsilon_{\alpha\beta}$. One could take a conservative approach

and use the most stringent constraint in the individual NSI terms (say, use $|\varepsilon^{u}_{\mu e}|$) to constrain the effective term (say, $|\varepsilon_{\mu e}|$) and that leads to

$$|\varepsilon_{\alpha\beta}| \; < \; \begin{pmatrix} 0.06 & 0.05 & 0.27 \\ 0.05 & 0.003 & 0.05 \\ 0.27 & 0.05 & 0.16 \end{pmatrix} \tag{1.87}$$

However, if we assume that the errors on individual NSI terms are uncorrelated, one can (as in Ref. [63]) deduce model-independent bounds on effective NC NSI terms

$$\varepsilon_{\alpha\beta} \lesssim \left\{ \sum_{C=L,R} [(\varepsilon^{eC}_{\alpha\beta})^2 + (3\varepsilon^{uC}_{\alpha\beta})^2 + (3\varepsilon^{dC}_{\alpha\beta})^2] \right\}^{1/2}$$

This approach for the Earth matter leads to

$$|\varepsilon_{\alpha\beta}| \; < \; \begin{pmatrix} 4.2 & 0.33 & 3.0 \\ 0.33 & 0.068 & 0.33 \\ 3.0 & 0.33 & 21 \end{pmatrix} \tag{1.88}$$

Note that the values mentioned in Eq. 1.88 are larger by one or two orders of magnitude than the bounds of Eq. 1.87.

Additionally, two experiments have tried to constrain NSI parameters. There is no evidence in favour of NSI in the SK NSI search for atmospheric neutrinos crossing the Earth and the study led to upper bound on NSI parameters [64] given by $|\varepsilon_{\mu\tau}| < 0.033, |\varepsilon_{\tau\tau} - \varepsilon_{\mu\mu}| < 0.147$ (at 90% CL) in a two flavor hybrid model [58]. The off-diagonal NSI parameter $\varepsilon_{\mu\tau}$ is constrained $-0.20 < \varepsilon_{\mu\tau} < 0.07$ (at 90% CL) from MINOS data in the framework of two flavor neutrino oscillations [65, 66]. Additionally, the allowed ranges of NSI parameters have been recently extracted using global analysis of neutrino data in Ref. [67].

In presence of NSI, the effective Hamiltonian in the ultra-relativistic limit is given by

$$H \;\; = \;\; H_{\rm vac} + H_{\rm SI} + H_{\rm NSI} \tag{1.89}$$

where $H_{\rm vac}$ is the vacuum Hamiltonian and $H_{\rm SI},\; H_{\rm NSI}$ are the effective Hamiltonians

in presence of SI alone and NSI respectively. Thus,

$$H = \frac{1}{2E}\left\{ U \begin{pmatrix} 0 & & \\ & \delta m^2_{21} & \\ & & \delta m^2_{31} \end{pmatrix} U^\dagger + A(x) \begin{pmatrix} 1+\varepsilon_{ee} & \varepsilon_{e\mu} & \varepsilon_{e\tau} \\ \varepsilon_{e\mu}{}^\star & \varepsilon_{\mu\mu} & \varepsilon_{\mu\tau} \\ \varepsilon_{e\tau}{}^\star & \varepsilon_{\mu\tau}{}^\star & \varepsilon_{\tau\tau} \end{pmatrix} \right\} \tag{1.90}$$

where $A(x) = 2E\sqrt{2}G_F n_e(x)$ is the standard CC potential due to the coherent forward scattering of neutrinos. The perturbative expressions for oscillation probability including effects due to NSI have been computed in [68–70].

The oscillation probability for $\nu_e \to \nu_\mu$ can be obtained as

$$\begin{aligned} P(\nu_e \to \nu_\mu) \simeq\ & 4s^2_{13}s^2_{23}\left[\frac{\sin^2(1-r_A)\lambda L/2}{(1-r_A)^2}\right] \\ & + 8s_{13}s_{23}c_{23}(|\varepsilon_{e\mu}|c_{23}c_\chi - |\varepsilon_{e\tau}|s_{23}c_\omega)\, r_A \left[\frac{\sin r_A\lambda L/2}{r_A}\ \frac{\sin(1-r_A)\lambda L/2}{(1-r_A)}\ \cos\frac{\lambda L}{2}\right] \\ & + 8s_{13}s_{23}c_{23}(|\varepsilon_{e\mu}|c_{23}s_\chi - |\varepsilon_{e\tau}|s_{23}s_\omega) r_A \left[\frac{\sin r_A\lambda L/2}{r_A}\ \frac{\sin(1-r_A)\lambda L/2}{(1-r_A)}\ \sin\frac{\lambda L}{2}\right] \\ & + 8s_{13}s^2_{23}(|\varepsilon_{e\mu}|s_{23}c_\chi + |\varepsilon_{e\tau}|c_{23}c_\omega) r_A \left[\frac{\sin^2(1-r_A)\lambda L/2}{(1-r_A)^2}\right] \end{aligned} \tag{1.91}$$

$$\text{where} \quad \lambda \equiv \frac{\delta m^2_{31}}{2E} \quad ; \quad r_\lambda \equiv \frac{\delta m^2_{21}}{\delta m^2_{31}} \quad ; \quad r_A \equiv \frac{A(x)}{\delta m^2_{31}} \tag{1.92}$$

Note that we have used $\tilde{s}_{13} \equiv \sin\tilde{\theta}_{13} = s_{13}/(1-r_A)$ to the leading order in s_{13}, and $\chi = \phi_{e\mu} + \delta_{13}$, $\omega = \phi_{e\tau} + \delta_{13}$. Only the parameters $\varepsilon_{e\mu}$ and $\varepsilon_{e\tau}$ enter in the leading order expression [70].

The survival probability for $\nu_\mu \to \nu_\mu$ is given by

$$\begin{aligned} P(\nu_\mu \to \nu_\mu) \simeq\ & 1 - s^2_{2\times 23}\left[\sin^2\frac{\lambda L}{2}\right] \\ & - |\varepsilon_{\mu\tau}|\cos\phi_{\mu\tau}s_{2\times 23}\left[s^2_{2\times 23}(r_A\lambda L)\sin\lambda L + 4c^2_{2\times 23}r_A\sin^2\frac{\lambda L}{2}\right] \\ & + (|\varepsilon_{\mu\mu}| - |\varepsilon_{\tau\tau}|)s^2_{2\times 23}c_{2\times 23}\left[\frac{r_A\lambda L}{2}\sin\lambda L - 2r_A\sin^2\frac{\lambda L}{2}\right] \end{aligned} \tag{1.93}$$

where $s_{2\times 23} \equiv \sin 2\theta_{23}$ and $c_{2\times 23} \equiv \cos 2\theta_{23}$. Note that the NSI parameters involving the electron sector do not enter this channel and the survival probability depends only on the three parameters $\varepsilon_{\mu\mu}, \varepsilon_{\mu\tau}, \varepsilon_{\tau\tau}$ [68, 70].

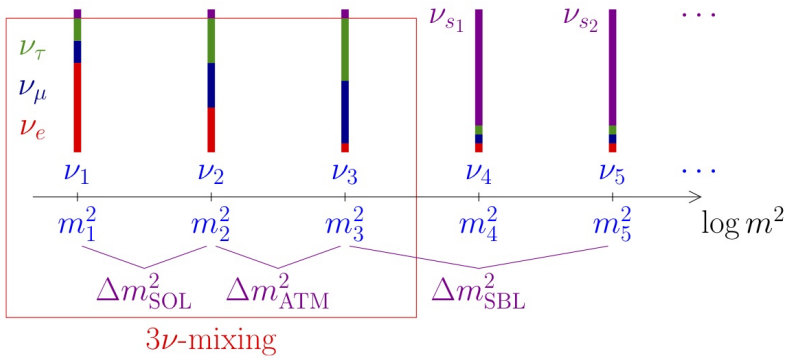

Figure 1.14: Three active and additional sterile neutrinos. Taken from [72, 73].

1.6.2 Additional sterile neutrinos

A sterile neutrino is a neutral lepton introduced by Pontecorvo in 1967 [71] with no usual weak interaction except that induced by mixing. Sterile neutrino arises in most extensions of SM and there is no restriction on its mass. In the minimal Type I Seesaw mechanism [5], one invokes very heavy sterile neutrinos (heaviness being related to the smallness of the neutrino masses) and these are also useful in leptogenesis [6]. However, we are interested in light sterile neutrinos that mix with the ordinary neutrinos and are accessible at neutrino oscillation experiments leading to new oscillation effects (see Fig. 1.14). We know from the precise measurements of the Z_0 width at LEP that there are only three types of weakly interacting neutrino flavors. Thus, any additional neutrino flavors must interact only through oscillation mechanics with the other flavor states and gravity.

There has been interest in light sterile neutrinos due to the long standing anomalies in neutrino experimental data for more than two decades. We briefly describe the anomalies that indicate the existence of an additional sterile neutrino without electroweak interactions. For a review, see [74].

- **LSND :-** The first indication of sterile neutrinos was found in the results of Liquid Scintillator Neutrino Detector (LSND) [54] at the Los Alamos National Laboratory in the mid-nineties. It comprised of a stopped pion source producing intense beam of $\bar{\nu}_\mu$ with energies upto 53 MeV. A liquid scintillator detector (placed at a distance of 30 m from the source) was optimized to observe elec-

tron neutrino events via the inverse beta decay process in carbon, $\bar{\nu}_e p \to e^+ n$, by detecting the Cherenkov and scintillation light produced by the e^+ and the delayed 2.2 MeV photon from neutron capture. Since there are no $\bar{\nu}_e$ in production, this experiment is an ideal set up for studying $\bar{\nu}_\mu \to \bar{\nu}_e$ oscillations at $L/E \simeq 1\text{m}/\text{ MeV}$. The backgrounds to this signal were conventional $\bar{\nu}_e$ production in the beam stop and π^- decay in flight followed by $\bar{\nu}_\mu p \to \mu^+ n$ with μ^+ mis-identified as an e^+. LSND observed an excess of $87.9 \pm 22.4 \pm 6.0$ $\bar{\nu}_e$ events over these backgrounds, a 3.8σ deviation from expectation [54]. Interpretation of this result in terms of neutrino oscillations yields additional mass squared splitting $\delta m^2 \gtrsim \mathcal{O}(0.1)\text{eV}^2$ which can be achieved by invoking additional sterile neutrino (Fig. 1.15).

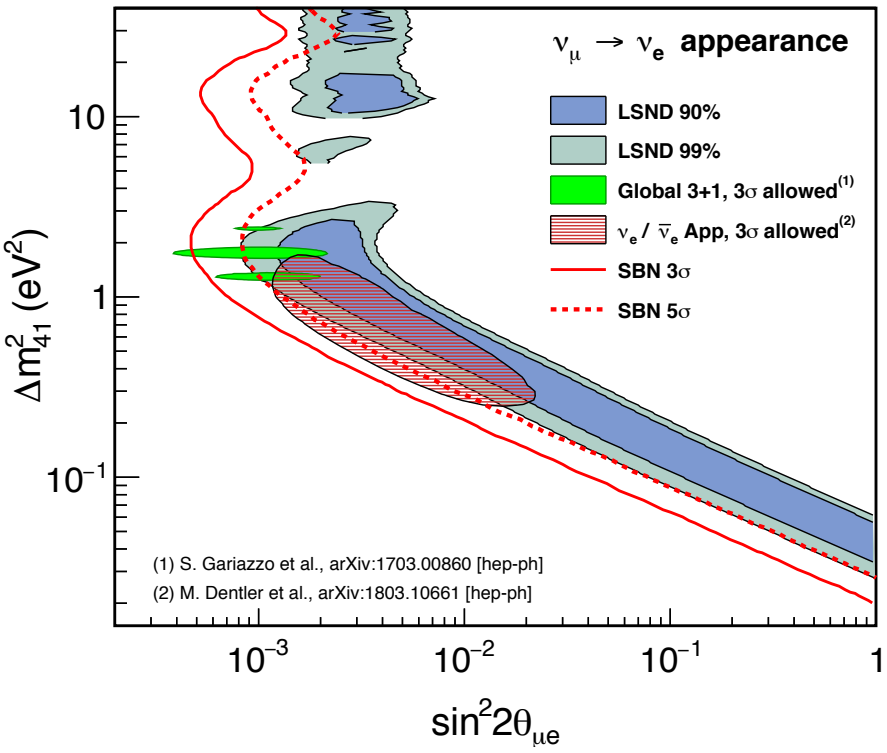

Figure 1.15: Sensitivities to a light sterile neutrino in the $\nu_\mu \to \nu_e$ appearance channel. The LSND preferred region at 90% C.L. (shaded blue) and 99% C.L. (shaded grey) is shown [54]. The sensitivities are reproduced from the SBN proposal. Taken from [75].

- **MiniBooNE :-** The MiniBooNE experiment at Fermilab was proposed to test

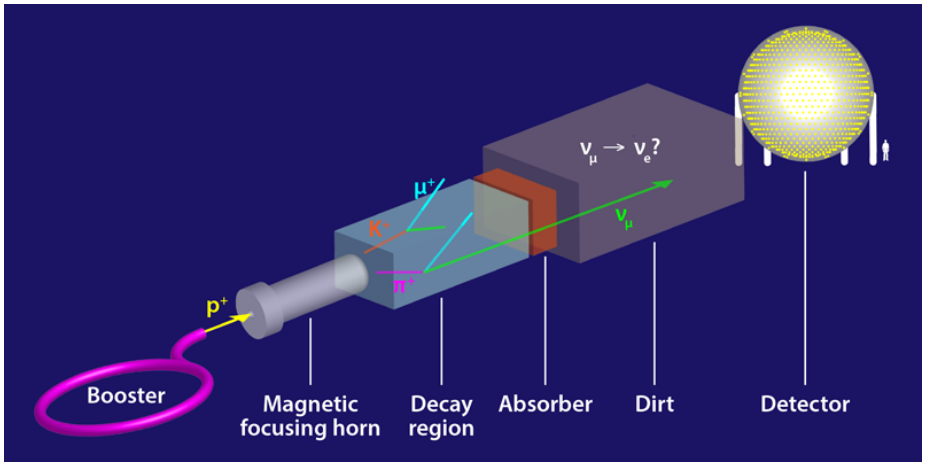

Figure 1.16: Schematic of the MiniBooNE experiment at Fermilab. A high-intensity beam of accelerated protons is focused onto a target, producing pions that decay predominantly into muons and muon neutrinos. The resulting neutrino beam is characterized by the MiniBooNE detector. Taken from [76].

the sterile neutrino hypothesis. Even though the energy and baseline were larger, it is sensitive to the same range of L/E as LSND, which means that MiniBooNE also probes a mass squared splitting of $\mathcal{O}(1)$ eV^2 as LSND. MiniBooNE is located on the Booster Neutrino Beam at Fermilab, which peaks at 700 MeV neutrino energy. A mineral oil detector optimized to observe Cherenkov light emitted by electrons and muons is located 540 m downstream from the neutrino production target. There is a magnetic horn system allowing for focusing negatively or positively charged mesons leading to a mostly ν_μ or $\bar{\nu}_\mu$ neutrino beam (See Fig. 1.16). So, MiniBooNE can run in both neutrino mode and antineutrino mode. The different energy configuration and event signature (Cherenkov ring topology) makes MiniBooNE backgrounds very different from those in LSND. The main backgrounds are : (i) Mis-identification of π^0 as electron like event; (ii) ν_e from kaon and muon decays in the beamline; (iii) single photon production via resonant process $\Delta \rightarrow N\gamma$; and (iv) single photon events from neutrino interactions in dirt and material surrounding detector.

MiniBooNE has reported excess of electron like events after collecting 12.84 (11.27) $\times 10^{20}$ POT in neutrino (antineutrino) modes leading to 4.7σ deviation from the expected backgrounds, thereby strengthening the SBL anomaly [77].

There are two more anomalies that hint towards existence of sterile neutrinos. These are sensitive to disappearance of ν_e.

- **Reactor anomaly :-** In case of reactor neutrino data, the flux re-computation with improved theoretical uncertainties led to a deficit in the experiments in the total number of events with respect to theoretical expectations. Some spectral features have been observed in recent times which are consistent with sterile neutrino oscillations with $\delta m^2 \simeq 1\ eV^2$.

- **Gallium anomaly :-** The number of ν_e events from radioactive sources were found to be less than the theoretical expectations.

The **Short-Baseline Neutrino (SBN) Program** [75] is a joint effort by three collaborations (ICARUS-T600, MicroBooNE, SBND) to use their detectors to perform sensitive searches for ν_e appearance and ν_μ disappearance in the Booster Neutrino Beam at Fermilab. All of the detectors utilize liquid argon time projection chambers (LArTPC), and each contributes to the development of this technology for the long-baseline DUNE experiment at Fermilab. Previous neutrino experiments have seen some hints of yet another sterile neutrino, and SBN will hunt for evidence of this unconfirmed fourth state.

In order to describe oscillations of (3+1) neutrinos, we have the (4×4) unitary matrix for the case of (3+1) flavors

$$U^{sterile} = \begin{pmatrix} U_{e1} & U_{e2} & U_{e3} & U_{e4} \\ U_{\mu 1} & U_{\mu 2} & U_{\mu 3} & U_{\mu 4} \\ U_{\tau 1} & U_{\tau 2} & U_{\tau 3} & U_{\tau 4} \\ U_{s1} & U_{s2} & U_{s3} & U_{s4} \end{pmatrix} \tag{1.94}$$

which can be parameterised as

$$U^{sterile} = O_{34}(\theta_{34}, \delta_{34}) O_{24}(\theta_{24}, \delta_{24}) O_{14}(\theta_{14}) O_{23}(\theta_{23}) O_{13}(\theta_{13}, \delta_{13}) O_{12}(\theta_{12}) \tag{1.95}$$

Here, $O_{ij}(\theta_{ij}, \delta_{ij})$ denotes a rotation in the ij plane by an angle θ_{ij} and phase δ_{ij}.

$$O_{24}(\theta_{24}, \delta_{24}) = \begin{pmatrix} 1 & 0 & 0 & 0 \\ 0 & \cos\theta_{24} & 0 & e^{-i\delta_{24}}\sin\theta_{24} \\ 0 & 0 & 1 & 0 \\ 0 & -e^{i\delta_{24}}\sin\theta_{24} & 0 & \cos\theta_{24} \end{pmatrix}$$

$$O_{14}(\theta_{14}) = \begin{pmatrix} \cos\theta_{14} & 0 & 0 & \sin\theta_{14} \\ 0 & 1 & 0 & 0 \\ 0 & 0 & 1 & 0 \\ -\sin\theta_{14} & 0 & 0 & \cos\theta_{14} \end{pmatrix}$$

The standard formula in 3 flavor formalism can be obtained by setting $\theta_{i4} = 0$ for $i = 1, 2, 3$ and identifying δ_{13} as the standard Dirac CP phase in the framework for three flavors. Note that the δ_{12} becomes unphysical in this case. Now, we know that δm^2_{41} is larger than δm^2_{31} or δm^2_{21} and we can get appropriate two flavor oscillation formulae to describe the SBL oscillations given by

$$P(\nu_\alpha \to \nu_\beta) \;=\; \delta_{\alpha\beta} - 4|U_{\alpha\beta}|^2(\delta_{\alpha\beta} - |U_{\alpha\beta}|^2)\sin^2\left(\frac{\delta m^2_{41}E}{4L}\right) \tag{1.96}$$

where L and E stand for the baseline and neutrino energy respectively. One can identify the effective mixing angle governing different oscillation channels

$$\begin{aligned} \nu_\mu \to \nu_e : \sin^2 2\theta_{\mu e} &\equiv |U_{\mu 4}|^2|U_{e4}|^2 \quad \text{(LSND, MiniBooNE)} \\ \nu_e \to \nu_e : \sin^2 2\theta_{ee} &\equiv |U_{e4}|^2(1 - |U_{e4}|^2) \quad \text{(Reactor, Gallium)} \\ \nu_\mu \to \nu_\mu : \sin^2 2\theta_{\mu\mu} &\equiv |U_{\mu 4}|^2(1 - |U_{\mu 4}|^2) \quad \text{(None)} \end{aligned} \tag{1.97}$$

Now, if we are interested in an expression that can reveal impact of sterile neutrinos at long baselines, we can use the fact that oscillation effects due to the fourth state will be averaged and this leads to the following tractable expression in vacuum [78].

$$\begin{aligned} P(\nu_\mu \to \nu_e) &= 4|U_{\mu 4}U_{e4}|^2 \times (1/2) \\ &- 4Re(U_{\mu 1}U^*_{e1}U^*_{\mu 2}U_{e2})\sin^2\frac{\Delta_{21}}{2} + 2Im(U_{\mu 1}U^*_{e1}U^*_{\mu 2}U_{e2})\sin\Delta_{21} \\ &- 4Re(U_{\mu 1}U^*_{e1}U^*_{\mu 3}U_{e3})\sin^2\frac{\Delta_{31}}{2} + 2Im(U_{\mu 1}U^*_{e1}U^*_{\mu 3}U_{e3})\sin\Delta_{31} \\ &- 4Re(U_{\mu 2}U^*_{e2}U^*_{\mu 3}U_{e3})\sin^2\frac{\Delta_{32}}{2} + 2Im(U_{\mu 2}U^*_{e2}U^*_{\mu 3}U_{e3})\sin\Delta_{32} \end{aligned} \tag{1.98}$$

since $\sin^2 \frac{\Delta_{4i}}{2}$ averages out to 1/2, and $\sin \Delta_{4i}$ averages out to be 0, when $i = 1, 2, 3$. Upon substituting the values of the $U_{\alpha i}$ in terms of the mixing angles, we obtain :

$$\begin{aligned}
P(\nu_\mu \to \nu_e) &= \frac{1}{2}\sin^2 2\theta^{4\nu}_{\mu e} \\
&+ (a^2 \sin^2 2\theta^{3\nu}_{\mu e} - \frac{1}{4}\sin^2 2\theta_{13} \sin^2 2\theta^{4\nu}_{\mu e})\big[\cos^2\theta_{12}\sin^2\frac{\Delta_{31}}{2} + \sin^2\theta_{12}\sin^2\frac{\Delta_{32}}{2}\big] \\
&+ \cos(\delta_{13})ba^2 \sin 2\theta^{3\nu}_{\mu e}\big[\cos 2\theta_{12}\sin^2\frac{\Delta_{21}}{2} + \sin^2\frac{\Delta_{31}}{2} - \sin^2\frac{\Delta_{32}}{2}\big] \\
&+ \cos(\delta_{24})ba \sin 2\theta^{4\nu}_{\mu e}\big[\cos 2\theta_{12}\cos^2\theta_{13}\sin^2\frac{\Delta_{21}}{2} - \sin^2\theta_{13}(\sin^2\frac{\Delta_{31}}{2} - \sin^2\frac{\Delta_{32}}{2})\big] \\
&+ \cos(\delta_{13}+\delta_{24})a \sin 2\theta^{3\nu}_{\mu e}\sin 2\theta^{4\nu}_{\mu e}\big[-\frac{1}{2}\sin^2 2\theta_{12}\cos^2\theta_{13}\sin^2\frac{\Delta_{21}}{2} \\
&+ \cos 2\theta_{13}(\cos^2\theta_{12}\sin^2\frac{\Delta_{31}}{2} + \sin^2\theta_{12}\sin^2\frac{\Delta_{32}}{2})\big] \\
&- \frac{1}{2}\sin(\delta_{13})ba^2 \sin 2\theta^{3\nu}_{\mu e}\big[\sin\Delta_{21} - \sin\Delta_{31} + \sin\Delta_{32}\big] \\
&+ \frac{1}{2}\sin(\delta_{24})ba \sin 2\theta^{4\nu}_{\mu e}\big[\cos^2\theta_{13}\sin\Delta_{21} + \sin^2\theta_{13}(\sin\Delta_{31} - \sin\Delta_{32})\big] \\
&+ \frac{1}{2}\sin(\delta_{13}+\delta_{24})a \sin 2\theta^{3\nu}_{\mu e}\sin 2\theta^{4\nu}_{\mu e}\big[\cos^2\theta_{12}\sin\Delta_{31} + \sin^2\theta_{12}\sin\Delta_{32}\big] \\
&+ (b^2a^2 - \frac{1}{4}a^2\sin^2 2\theta_{12}\sin^2 2\theta^{3\nu}_{\mu e} - \frac{1}{4}\cos^4\theta_{13}\sin^2 2\theta_{12}\sin^2 2\theta^{4\nu}_{\mu e})\sin^2\frac{\Delta_{21}}{2}
\end{aligned} \tag{1.99}$$

where,

$$\sin 2\theta^{3\nu}_{\mu e} = \sin 2\theta_{13}\sin\theta_{23} \tag{1.100}$$

$$b = \cos\theta_{13}\cos\theta_{23}\sin 2\theta_{12} \tag{1.101}$$

$$\sin 2\theta^{4\nu}_{\mu e} = \sin 2\theta_{14}\sin\theta_{24} \tag{1.102}$$

$$a = \cos\theta_{14}\cos\theta_{24} \tag{1.103}$$

This gives us insight as to which terms are important when we are discussing the role of sterile neutrinos at long baselines.

Let us now discuss the implications of the $3+1$ case on CP violating probability difference, $\Delta P_{\alpha\beta}$. We can draw very clear inferences if we assume CPT invariance and unitarity. In vacuum, CPT invariance implies that $P(\nu_\beta \to \nu_\alpha) = P(\bar{\nu}_\alpha \to \bar{\nu}_\beta)$, which in turn implies that $\Delta P_{\beta\alpha} = -\Delta P_{\alpha\beta}$, and in particular that $\Delta P_{\alpha\beta} = 0$ when $\beta = \alpha$. Thus, when there are only three neutrino flavors, there are only three independent

potentially non-zero CP-violating differences $\Delta P_{\alpha\beta}$ to be measured: $\Delta P_{e\mu}$, $\Delta P_{\mu\tau}$ and $\Delta P_{\tau e}$. From the conservation of probability, we have for any number of flavors,

$$\sum_{\beta} P(\nu_\alpha \to \nu_\beta) = 1 \quad \text{and} \quad \sum_{\beta} P(\bar{\nu}_\alpha \to \bar{\nu}_\beta) = 1$$

From this, it immediately follows that $\sum_\beta \Delta P_{\alpha\beta} = 0$. Now, since $\Delta P_{\alpha\beta} = 0$ when $\beta = \alpha$, we can safely conclude that

$$\sum_{\beta \neq \alpha} \Delta P_{\alpha\beta} = 0 \tag{1.104}$$

For three flavor case, this constraint implies that $\Delta P_{e\mu} + \Delta P_{e\tau} = 0$ and that $\Delta P_{\mu e} + \Delta P_{\mu\tau} = 0$. Since $\Delta P_{\beta\alpha} = -\Delta P_{\alpha\beta}$, i.e. the three independent CP-violating differences are equal (Eq. 1.73). In particular, if there are only three flavors, it is not possible for CP invariance to hold in one oscillation channel, such as $\overset{(-)}{\nu}_\mu \to \overset{(-)}{\nu}_e$, and yet be violated in another channel, such as $\overset{(-)}{\nu}_\mu \to \overset{(-)}{\nu}_\tau$.

In the 3+1 scenario, however, there will be six independent differences $\Delta P_{\alpha\beta}$: $\Delta P_{e\mu}$, $\Delta P_{\mu\tau}$, $\Delta P_{\tau e}$, ΔP_{es}, $\Delta P_{\mu s}$ and $\Delta P_{\tau s}$, where s refers to the sterile flavor. Now the above constraint gives rise only to relations like

$$\Delta P_{e\mu} = \Delta P_{\mu\tau} + \Delta P_{\mu s} \tag{1.105}$$

It is now possible for $\Delta P_{\mu e} (= -\Delta P_{e\mu})$ to be zero, while the differences $\Delta P_{\mu\tau}$ and $\Delta P_{\mu s}$ in other oscillation channels are large. Experimentally, the first one that can be measured is the $\Delta P_{\mu e}$ while the other ones will be much harder. But, the main point is that we will not have a clear picture on CP violation in the leptonic sector unless we measure all these differences if indeed there were sterile neutrinos.

1.7 Layout of the chapters

In this thesis, we have explored how LBL experiments can be used to explore new physics (e.g. non-standard interactions or sterile neutrinos) in the neutrino sector. We consider NSI and theories with additional sterile neutrinos as possible candidates for probing new physics in the neutrino sector. We have performed detailed simulations using GLoBES software [79] to substantiate our claims.

In Chapter 2 we analyze impact of new physics on the violation of discrete symmetries and testing non-unitarity at LBL experiments.

In Chapter 3 we present our summarize the results obtained so far. We present the current experimental status of neutrino mass and mixing in terms of flavor diagram. Towards the end, we also briefly describe the work that we are presently engaged in.

Chapter 2

Violation of discrete symmetries and testing non-unitarity at long baseline neutrino experiments

One of the fundamental parameters entering neutrino oscillation framework is the leptonic CP phase δ_{13} and its measurement is an important goal of the planned LBL experiments. It should be noted that ordinary matter effects complicate the determination of this parameter and there are studies in literature that deal with separation of intrinsic versus extrinsic CP violation. It is important to investigate the consequences of new physics effects that can not only hamper the measurement of δ_{13}, but also impact the consequences of discrete symmetries such as CP, T and unitarity in different oscillation channels. In the present chapter, we explore these discrete symmetries and implications on unitarity in presence of two new physics scenarios (NSI in propagation and presence of sterile neutrinos) that serve as good examples of going beyond the standard scenario in different directions. We uncover the impact of new physics scenarios on disentangling intrinsic and extrinsic CP violation. Some of the results presented in this chapter are published in **Phys. Rev. D95, 075035 (2017)**.

The outline of this chapter is as follows. After an introduction comprising of a review of current status of neutrino parameters, in Section 2.2.1, we give general def-

initions of CP, T and CPT asymmetries and unitarity condition. In Section 2.2.2, we give the three flavor framework in vacuum (Section 2.2.2) and in NSI along with the choice of NSI parameters (Section 2.2.2). In Section 2.2.3, we describe the framework and choice of parameters for the sterile case. Our results are discussed in Section 2.3. The CP and T asymmetries are described for the three physics scenarios as a function of E and L in Section 2.3.1. For a test of non-unitarity in the sterile case, we use oscillograms as our main tool (see Section 2.3.2). In Section 2.3.3, we discuss the spectral differences in oscillogram patterns for the three physics scenarios considered [1]. Finally, we discuss prospects of CP violation and implications of our studies for LBL experiments with particular emphasis on T2K, T2HK, NOvA and DUNE in Section 2.4. We conclude in Section 2.5.

2.1 Introduction

The possibility of neutrino oscillations was first raised in a seminal paper by Pontecorvo [12] and almost sixty years later the experimental confirmation of neutrino oscillations was rewarded with a Nobel prize [13]. The standard three flavor neutrino mixing parameters are - three angles $(\theta_{12}, \theta_{13}, \theta_{23})$, two mass splittings $(\delta m^2_{31}, \delta m^2_{21})$ and one phase (δ_{13}) that is responsible for CP violation in the leptonic sector. While the mixing angles and the mass-squared differences (and absolute value of only one of them) have been measured with varying degrees of precision (see Table 2.1), the measured value of θ_{13} allows for an early measurement of the leptonic CP violation [80–82].

The three flavor neutrino mixing matrix U is parameterized by three angles $\theta_{12}, \theta_{23}, \theta_{13}$ and one phase δ_{13} [2]. In the PMNS parametrization [9, 11], U is given by Eq. 1.28. The validity of the three flavor neutrino paradigm relies very heavily on the assumption of 3×3 unitarity of the mixing matrix. Most of the information

[1] For simplicity, we assume CP conserving new physics scenarios (*i.e.*, all NSI and sterile phases are set to zero) while obtaining the oscillograms.

[2] For N flavors, the leptonic mixing matrix, U can be expressed with $(N-1)(N-2)/2$ Dirac-type CP violating phases and $(N-1)$ additional Majorana type phases.

about the parameters of the neutrino mixing matrix is gleaned from a vast variety of experiments. We should realize that much of the information originates from ν_μ and ν_e sector via disappearance ($\bar{\nu}_e \to \bar{\nu}_e$ in case of reactor experiments and $\bar{\nu}_\mu \to \bar{\nu}_\mu$ in case of atmospheric and LBL experiments) and appearance ($\nu_\mu \to \nu_e$) measurements in the ongoing and future LBL neutrino oscillation experiments. The remaining elements in the mixing matrix are fixed assuming unitarity i.e. probability conservation [83]. Clearly, data from neutrino experiments is not sufficient to constrain all the elements of the leptonic mixing matrix [84]. On the other hand, the assumption of unitarity in the quark sector is well justified by data.

Parameter	Best-fit value	3σ range	Precision (%)
$\sin^2\theta_{12}$	0.304	$0.270 \to 0.344$	12
$\sin^2\theta_{13}$	0.0218	$0.0186 \to 0.0250$	14
	0.0219	$0.0188 \to 0.0251$	14
$\sin^2\theta_{23}$	0.452	$0.382 \to 0.643$	25
	0.579	$0.389 \to 0.644$	24
δm^2_{21} $[10^{-5}\ eV^2]$	7.50	$7.02 \to 8.09$	
δm^2_{3l} $[10^{-3}\ eV^2]$	$+2.457$	$7\ +2.317 \to +2.607$	6
	-2.449	$-2.590 \to -2.307$	6
δ_{13}	$*$	$[-\pi : \pi]$	$*$

Table 2.1: The best-fit values, 3σ ranges and precision (in percentage) of the six parameters from the global fit to neutrino data [82]. For entries with two rows, the first (second) row corresponds to NH (IH). For NH, $\delta m^2_{3l} \equiv \delta m^2_{31} > 0$ and for IH, $\delta m^2_{3l} \equiv \delta m^2_{32} < 0$.

Within the SM, the CP symmetry is broken by complex phases in the Yukawa couplings. After removing the unphysical phases in the SM, there is only one physical phase which is the CP violating parameter. This economical description of CP violation in the SM is referred to as the Kobayashi-Maskawa (KM) mechanism [85]. But if neutrinos are Majorana particles, there can be two additional Majorana-type phases in the three flavor case which can not be probed via oscillation experiments.

In vacuum, the lone CP phase given by KM mechanism accounts for the CP violation signal. However SI along with the inherent CP asymmetry present in the Earth matter introduces effects that mimic CP violation. These are referred to as fake/extrinsic CP violating effects as opposed to the genuine/intrinsic CP violating effect due to the presence of δ_{13} [86–91]. Earlier attempts have proposed experimental arrangements [92] and observables useful in disentangling the intrinsic and extrinsic CP violation components [91] however standard physics was assumed there. Our work differs in the fact that we analyse this question in the backdrop of three distinct physics scenarios (SI and two possible sub-dominant new physics effects) and quantitatively demonstrate that new physics further hinders clean extraction of the intrinsic component. We also quantify our results in terms of event rates and make realistic inferences about separability between the intrinsic and extrinsic CP violating effects.

In the era of precision measurements in neutrino oscillation physics, we need to consider subdominant new physics scenarios such as NSI or sterile neutrinos and discuss the capabilities of our planned experiments for some bench mark values of new physics parameters. We study how neutrino oscillations have the potential to shed light on these crucial questions relating CP and T symmetries as well as the unitarity of the neutrino mixing matrix. We also probe deviations due to new physics scenarios. We go beyond the SM in two respects - one in which we introduce subdominant effects due to a possible source of new physics dubbed as NSI [93–102] and another where the presence of extra sterile state can lead to non-unitarity in the 3×3 part even though the overall mixing matrix is still unitary [78, 103–109] and examine consequences relevant to LBL experiments (For other new physics scenarios such as non-unitarity, see [110–114]). We highlight the regions in $L - E$ space where the effects due to CP and T violation are drastically modified due to new physics. Our discussion is mostly targeted towards accelerator based neutrino experiments with $L/E \sim 500$ km/GeV but can easily be extended to SBL experiments and very LBL experiments.

2.2 Framework

2.2.1 Observables

C, P and T are discrete symmetries that refer to charge conjugation, parity and time reversal respectively. CP, T and CPT violation signal in any neutrino oscillation experiment is characterised via a comparison of probability for a given pair of initial and final flavors $\nu_\alpha \to \nu_\beta$ with their CP, T or CPT conjugate counterparts

$$\begin{aligned} \text{CP}: &\qquad \nu_{\alpha,\beta} \Longrightarrow \bar{\nu}_{\alpha,\beta} \\ \text{T}: &\qquad \nu_{\alpha,\beta} \Longrightarrow \nu_{\beta,\alpha} \\ \text{CPT}: &\qquad \nu_{\alpha,\beta} \Longrightarrow \bar{\nu}_{\beta,\alpha} \end{aligned} \tag{2.1}$$

The action of CP and T are equivalent to complex conjugation of $U_{\alpha i}$. For theoretical discussions on CP, T and CPT in neutrino oscillations, see [24, 115–118]. There can be no CP violation in the two flavor case in vacuum as the unitary matrix in two flavor case can always be made real. In matter with varying density, this need not be the case (for geometric visualization, see [119, 120]). Some theoretical consequences of the value of CP violating phase were discussed in [121]. The cosmological effect of CP violation was discussed in [122].

Let us define the following asymmetries [3] which involve both neutrinos and antineutrinos :

$$A^{CP}_{\alpha\beta} = \frac{P_{\alpha\beta} - \bar{P}_{\alpha\beta}}{P_{\alpha\beta} + \bar{P}_{\alpha\beta}} = \frac{\Delta P^{CP}_{\alpha\beta}}{\sum P^{CP}_{\alpha\beta}} \tag{2.2}$$

$$A^{T}_{\alpha\beta} = \frac{P_{\alpha\beta} - P_{\beta\alpha}}{P_{\alpha\beta} + P_{\beta\alpha}} = \frac{\Delta P^{T}_{\alpha\beta}}{\sum P^{T}_{\alpha\beta}} \tag{2.3}$$

$$A^{CPT}_{\alpha\beta} = \frac{P_{\alpha\beta} - \bar{P}_{\beta\alpha}}{P_{\alpha\beta} + \bar{P}_{\beta\alpha}} = \frac{\Delta P^{CPT}_{\alpha\beta}}{\sum P^{CPT}_{\alpha\beta}} \tag{2.4}$$

where $P_{\alpha\beta}$ is the probability for transition $\nu_\alpha \to \nu_\beta$ and $\bar{P}_{\alpha\beta}$ is the probability for transition $\bar{\nu}_\alpha \to \bar{\nu}_\beta$. The probability expression is given by

[3] The denominator $\sum P_{\alpha\beta}\,(\delta_{13})$ merely rescales the asymmetry curves.

$$P_{\alpha\beta} = \sum_{i,j} U_{\alpha i} U^{\star}_{\beta i} U^{\star}_{\alpha j} U_{\beta j} \exp\left\{-i\frac{\delta m^2_{ij} L}{2E}\right\} \tag{2.5}$$

Obviously, these asymmetries present themselves in different channels (appearance and disappearance) that can be employed to study CP, T and CPT violation. If CP were exact, the laws of nature would be same for matter and antimatter. While most phenomena are CP symmetric, weak interactions violation C and P in the strongest possible way. T violation is expected as a corollary of CP violation if the combined CPT transformation is a fundamental symmetry of Nature.

For three flavor case, there are 9 + 9 appearance and disappearance probability channels for neutrinos and antineutrinos. Further, the unitarity of the 3×3 mixing matrix (excluding the case of additional sterile neutrino)

$$\sum_i U_{\alpha i} U^{*}_{\beta i} = \delta_{\alpha\beta} \tag{2.6}$$

can be translated in terms of probability conservation conditions

$$\sum_\beta P_{\alpha\beta} = \sum_\alpha P_{\alpha\beta} \;\; = \;\; 1 \tag{2.7}$$

$$\sum_\beta \bar{P}_{\alpha\beta} = \sum_\alpha \bar{P}_{\alpha\beta} \;\; = \;\; 1 \tag{2.8}$$

which are $6 + 6$ conditions of which $5 + 5$ are independent. This tells us that $4(= 9-5)+4$ neutrino and antineutrino oscillation probabilities are independent. Furthur it may be possible to reduce the number of independent channels to just two for neutrino (and two for anti-neutrino) oscillation probabilities in case of SI. In the parametrization considered (Eq. 1.28), the 23 rotation matrix commutes with the matter part in the Hamiltonian. Denoting the θ_{23} transformed probabilities by

$$\tilde{P}_{\alpha\beta} \equiv P_{\alpha\beta}(s^2_{23} \leftrightarrow c^2_{23}, \sin 2\theta_{23} \rightarrow -\sin 2\theta_{23}) \;, \alpha, \beta = e, \mu, \tau \tag{2.9}$$

we can show that

$$P_{e\tau} = \tilde{P}_{e\mu} \;, P_{\tau\mu} = \tilde{P}_{\mu\tau} \text{ and } P_{\tau\tau} = \tilde{P}_{\mu\mu} \tag{2.10}$$

and P_{ee} turns out to be independent of θ_{23}. Due to unitarity, only two of these are independent [24]. Moreover since the antineutrino probabilities are related to neutrino probabilities by $\delta_{13} \rightarrow -\delta_{13}$ and $A \rightarrow -A$, we are left with just two independent

probabilities (one possible choice could be $P_{e\mu}$ and $P_{\mu\tau}$ [4]). The unitarity condition

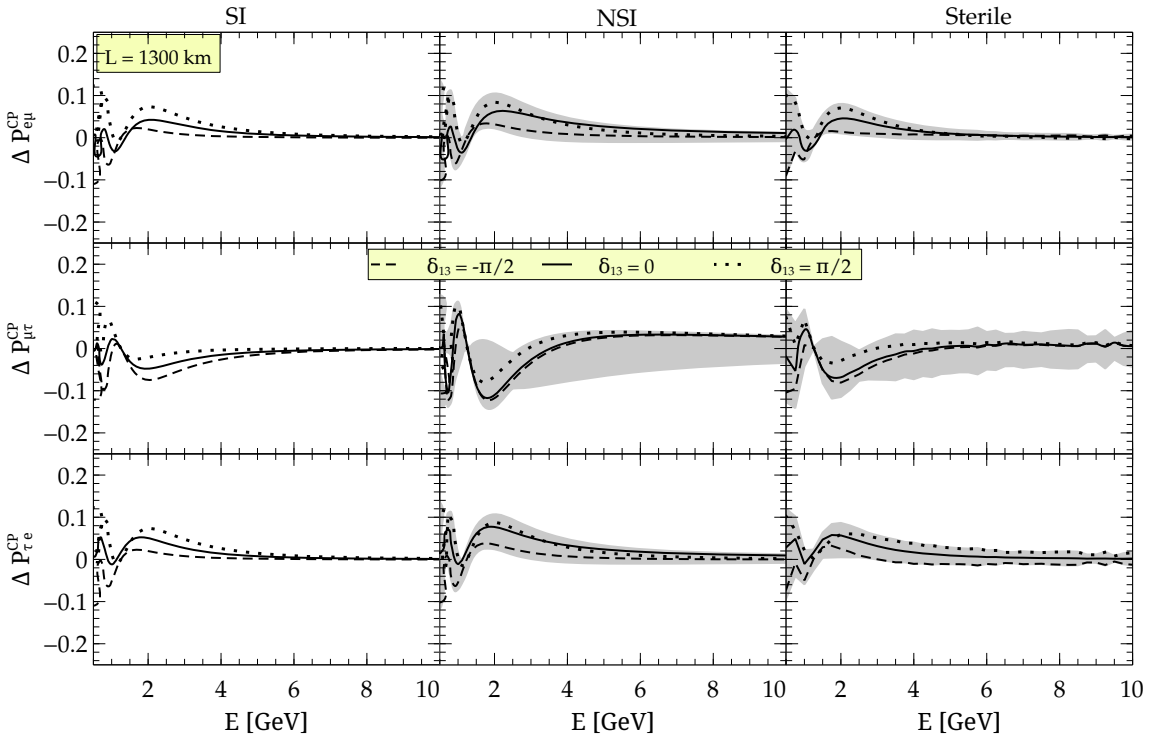

Figure 2.1: CP odd probability difference ($\Delta P^{CP}_{\alpha\beta}$) plotted as a function of energy at a fixed baseline of $L = 1300$ km. The three rows correspond to the different channels considered while the three columns refer to effects due to SI, NSI and Sterile. The solid line corresponds to the case when all CP violating phases are set to zero including δ_{13}. The dotted (dashed) line corresponds to the case when $\delta_{13} = \pi/2 (\delta_{13} = -\pi/2)$ and all additional phases set to zero. The grey bands in the case of NSI and Sterile refer to the variation in phases of the additional parameters introduced in their allowed ranges along with the SI phase δ_{13} (see Tables 2.1, 2.2 and 2.3 for the values of the parameters used).

leads to the following conditions involving CP asymmetries since $\sum_\beta (P_{\alpha\beta} - \bar{P}_{\alpha\beta}) = 0$

[4]The choice of these independent probabilities should be such that they should have θ_{23} dependence and the pair should not be connected by time reversal.

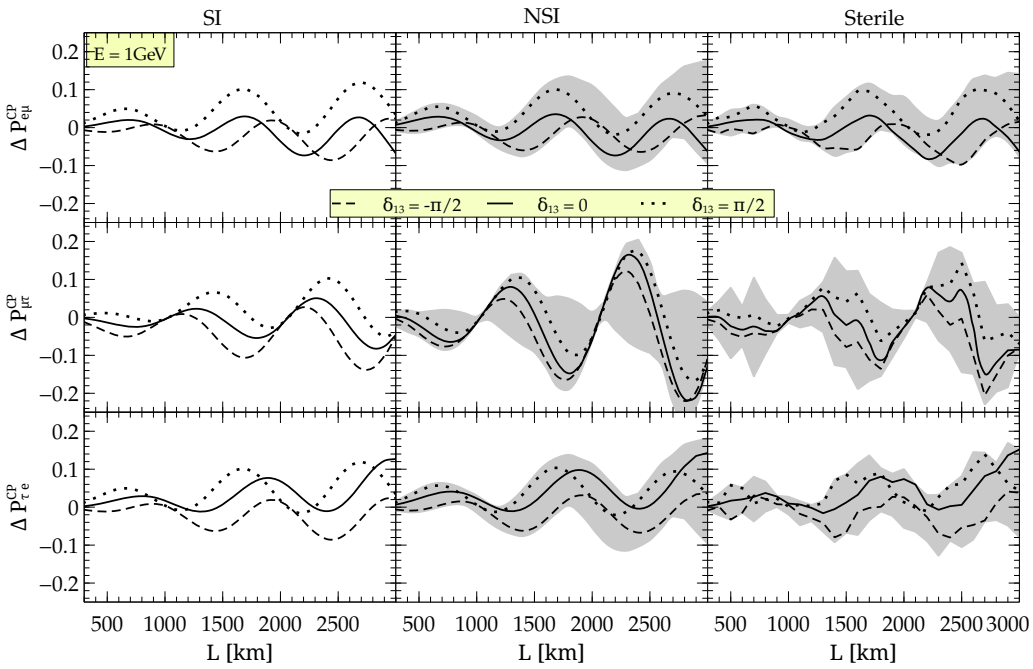

Figure 2.2: CP odd probability difference ($\Delta P^{CP}_{\alpha\beta}$) plotted as a function of baseline at a fixed energy of $E = 1$ GeV. The three rows correspond to the different channels considered while the three columns refer to effects due to SI, NSI and Sterile. The solid line corresponds to the case when all CP violating phases are set to zero including δ_{13}. The dotted (dashed) line corresponds to the case when $\delta_{13} = \pi/2(\delta_{13} = -\pi/2)$ and all additional phases set to zero. The grey bands in the case of NSI and Sterile refer to the variation in phases of the additional parameters introduced in their allowed ranges along with the SI phase δ_{13} (see Tables 2.1, 2.2 and 2.3 for the values of the parameters used).

and $\sum_\alpha (P_{\alpha\beta} - \bar{P}_{\alpha\beta}) = 0$

$$\begin{aligned}
\Delta P^{CP}_{ee} + \Delta P^{CP}_{e\mu} + \Delta P^{CP}_{e\tau} &= 0 \\
\Delta P^{CP}_{\mu e} + \Delta P^{CP}_{\mu\mu} + \Delta P^{CP}_{\mu\tau} &= 0 \\
\Delta P^{CP}_{\tau e} + \Delta P^{CP}_{\tau\mu} + \Delta P^{CP}_{\tau\tau} &= 0 \\
\Delta P^{CP}_{ee} + \Delta P^{CP}_{\mu e} + \Delta P^{CP}_{\tau e} &= 0 \\
\Delta P^{CP}_{e\mu} + \Delta P^{CP}_{\mu\mu} + \Delta P^{CP}_{\tau\mu} &= 0 \\
\Delta P^{CP}_{e\tau} + \Delta P^{CP}_{\mu\tau} + \Delta P^{CP}_{\tau\tau} &= 0
\end{aligned} \tag{2.11}$$

Similarly, in terms of T asymmetries since $\sum_\beta (P_{\alpha\beta} - P_{\beta\alpha}) = 0$ and $\sum_\alpha (P_{\alpha\beta} -$

$P_{\beta\alpha}) = 0$

$$\begin{aligned}
\Delta P^T_{ee} + \Delta P^T_{e\mu} + \Delta P^T_{e\tau} &= 0 \\
\Delta P^T_{\mu e} + \Delta P^T_{\mu\mu} + \Delta P^T_{\mu\tau} &= 0 \\
\Delta P^T_{\tau e} + \Delta P^T_{\tau\mu} + \Delta P^T_{\tau\tau} &= 0 \\
\Delta P^T_{ee} + \Delta P^T_{\mu e} + \Delta P^T_{\tau e} &= 0 \\
\Delta P^T_{e\mu} + \Delta P^T_{\mu\mu} + \Delta P^T_{\tau\mu} &= 0 \\
\Delta P^T_{e\tau} + \Delta P^T_{\mu\tau} + \Delta P^T_{\tau\tau} &= 0
\end{aligned} \tag{2.12}$$

2.2.2 Three active neutrinos only

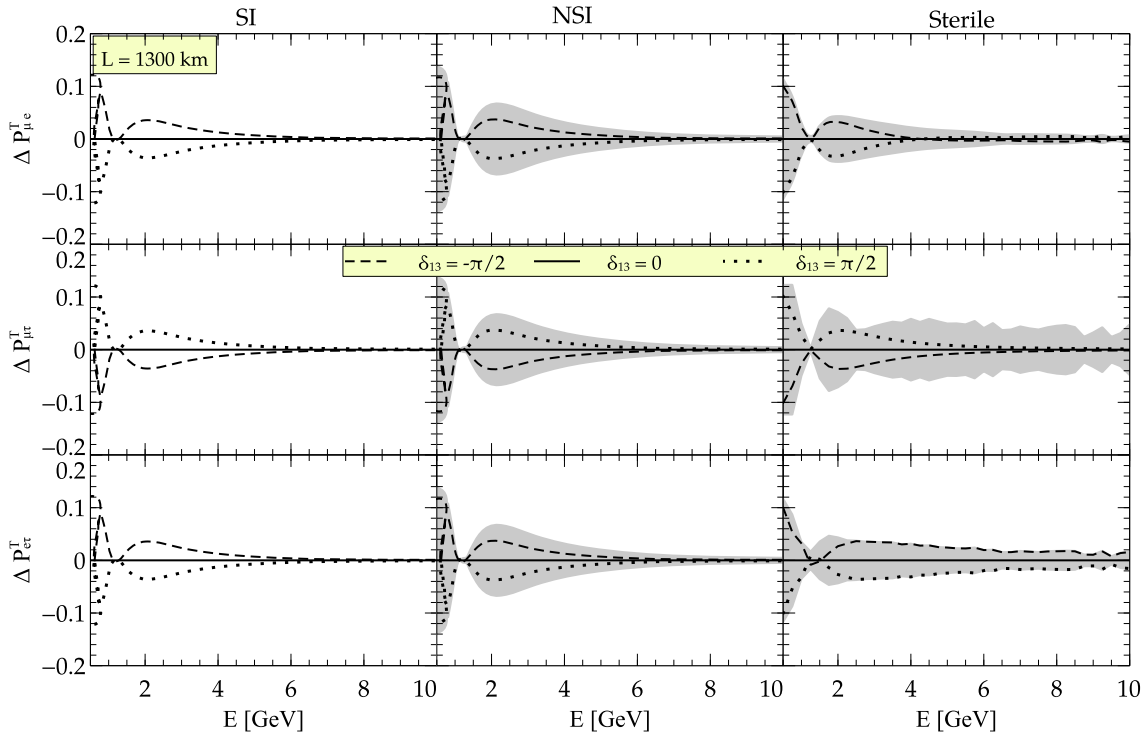

Figure 2.3: Same as Fig. 2.1 but for T asymmetry.

As is well-known, the three neutrino flavor states can be mapped to a three-level quantum system with distinct energy eigenvalues, $E_i = p + m_i^2/2p$ in the ultra-relativistic limit in vacuum along with the assumption of equal fixed momenta (or energy). In the presence of matter, the relativistic dispersion relation $E_i = f(p, m_i)$ gets modified due to the neutrino matter interactions during propagation.

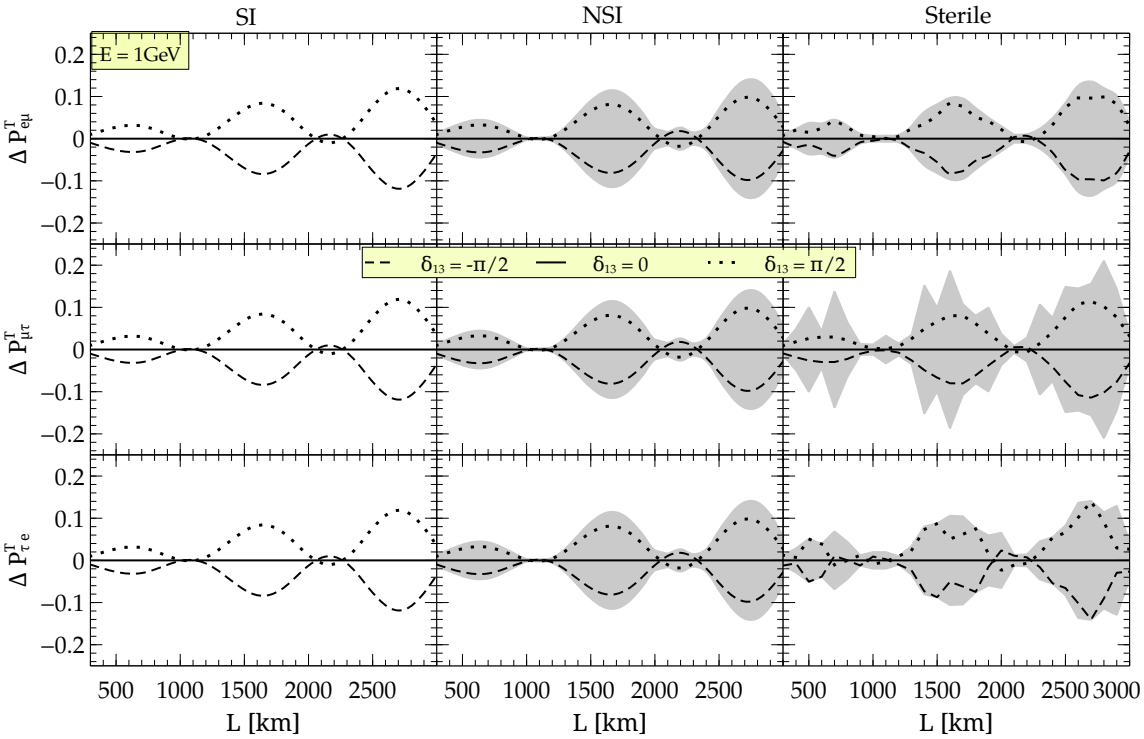

Figure 2.4: Same as Fig. 2.2 but for T asymmetry.

• Propagation in vacuum

The effective Hamiltonian is given by

$$H_{\nu} \;=\; \lambda \left\{ U \begin{pmatrix} 0 & & \\ & r_\lambda & \\ & & 1 \end{pmatrix} U^\dagger \right\} \tag{2.13}$$

where

$$\lambda \equiv \frac{\delta m^2_{31}}{2E} \qquad ; \qquad r_\lambda \equiv \frac{\delta m^2_{21}}{\delta m^2_{31}} \tag{2.14}$$

We first briefly review the case of CPT conservation (CPTC) *i.e.*, $A^{CPT}_{\alpha\beta} = 0$ which immediately relates CP and T asymmetries as

$$A^{CP}_{\alpha\beta} = -A^{CP}_{\beta\alpha} = A^{T}_{\alpha\beta} = -A^{T}_{\beta\alpha} \qquad \text{and} \qquad A^{CP}_{\alpha\alpha} = 0 = A^{T}_{\alpha\alpha} \tag{2.15}$$

Due to this, the CP asymmetry vanishes when $\alpha = \beta$ (disappearance channels). Further, if we assume unitarity of the mixing matrix, the CP and T asymmetries in

the appearance channels are equal to one another in vacuum

$$\begin{aligned} & A^{CP}_{e\mu} = A^{CP}_{\mu\tau} = A^{CP}_{\tau e} = A^{T}_{e\mu} = A^{T}_{\mu\tau} = A^{T}_{\tau e} \\ \Rightarrow \quad & \Delta P^{CP}_{\alpha\beta} = \Delta P^{T}_{\alpha\beta} = \Delta P \end{aligned} \tag{2.16}$$

where the probability difference in the appearance channels responsible for CP (T) violation is given by ΔP. Now in vacuum, we showed that Eq. 2.16 holds which means that the CP and T violating probability differences in appearance channels are equal to one another. The numerator in the CP asymmetry (defined in Eq. 2.2) is given by

$$\begin{aligned} \Delta P^{CP}_{\alpha\beta} &= 8\,\mathcal{J}\left[\sin(r_\lambda \lambda L)\sin^2\frac{\lambda L}{2} - \sin(\lambda L)\sin^2\frac{r_\lambda \lambda L}{2}\right] \\ &= 4\,\sin\delta_{13}\,J_r\,\left[\sin\lambda L/2\sin r_\lambda \lambda L/2\sin(1-r_\lambda)\lambda L/2\right] \end{aligned} \tag{2.17}$$

where $\mathcal{J} = s_{12}c_{12}s_{23}c_{23}s_{13}c^2_{13}\sin\delta_{13}$ is the Jarlskog invariant and $J_r = \mathcal{J}/\sin\delta_{13}$. In order to have observable effects, we should have substantial interference terms that contain the CP violating phase δ_{13}. This implies that both $\lambda L/2$ as well as $r_\lambda \lambda L/2$ must be taken into account. Naturally, the $A^{CP}_{\alpha\beta}(\delta_{13})$ vanishes as $\delta_{13} \to 0, \pi$ and when $\delta_{13} = \pm\pi/2$, $A^{CP}_{\alpha\beta}(\delta_{13})$ attains maximal values. Also it can be noted that the normalized $A^{CP}_{\alpha\beta}(\delta_{13})$ grows linearly with L/E. CPT invariance implies CP violation implies T violation and vice versa.

Since the three CP/T odd probability differences (involving different channels) are equal to one another, it suffices to look for CP violation in only one of the three possible channels (say $\nu_\mu \to \nu_e$) and the conclusions drawn (i.e. whether CP/T is conserved or violated) can be safely extended to include the remaining channels which may be difficult to explore otherwise (for example, $\nu_\mu \to \nu_\tau$ etc). Therefore CP conservation or violation in case of vacuum can be established by looking at any one of the asymmetries.

• Propagation in matter with effects due to NSI switched on

The effective Hamiltonian in flavor basis entering the Schrödinger equation for neutrino propagation is given by

$$\begin{aligned} H &= H_{\rm v} + H_{\rm SI} + H_{\rm NSI} \\ &= \lambda \left\{ U \begin{pmatrix} 0 & & \\ & r_\lambda & \\ & & 1 \end{pmatrix} U^\dagger + r_A \begin{pmatrix} 1 & 0 & 0 \\ 0 & 0 & 0 \\ 0 & 0 & 0 \end{pmatrix} + r_A \begin{pmatrix} \varepsilon_{ee} & \varepsilon_{e\mu} & \varepsilon_{e\tau} \\ \varepsilon_{e\mu}{}^\star & \varepsilon_{\mu\mu} & \varepsilon_{\mu\tau} \\ \varepsilon_{e\tau}{}^\star & \varepsilon_{\mu\tau}{}^\star & \varepsilon_{\tau\tau} \end{pmatrix} \right\} \end{aligned} \tag{2.18}$$

where

$$r_A \equiv \frac{A(x)}{\delta m^2_{31}} \tag{2.19}$$

and $A(x) = 2\sqrt{2}EG_F n_e(x)$ where n_e is the electron number density.

ε_{ee}	$\lvert\varepsilon_{e\mu}\rvert$	$\lvert\varepsilon_{e\tau}\rvert$	$\lvert\varepsilon_{\mu e}\rvert$	$\varepsilon_{\mu\mu}$	$\lvert\varepsilon_{\mu\tau}\rvert$	$\lvert\varepsilon_{\tau e}\rvert$	$\lvert\varepsilon_{\tau\mu}\rvert$	$\varepsilon_{\tau\tau}$
< 4.2	< 0.3	< 3.0	< 0.3	$*$	< 0.04	< 3.0	< 0.04	< 0.15

Table 2.2: The current bounds on NSI parameters taken from [63] (see also [62, 67]). The phases $\varphi_{\alpha\beta}$ of the off-diagonal parameters are unconstrained and can lie the allowed range, $\varphi_{\alpha\beta} \in [-\pi, \pi]$.

The three terms in Eq. 2.18 are due to vacuum, matter with SI and matter with NSI respectively. For the NSI case, the $\varepsilon_{\alpha\beta}\,(\equiv |\varepsilon_{\alpha\beta}|\, e^{i\varphi_{\alpha\beta}})$ are complex parameters which appear in H_{NSI}. As a result of the hermiticity of the Hamiltonian, we have nine additional parameters (three phases and six amplitudes appearing in H_{NSI}).

Switching on matter effects destroys nice feature of the equality of CP and T asymmetries in case of vacuum (see Eq. 2.13) due to the fact that matter effects can fake the CP violation signal. In such a scenario, establishing CP conservation/violation in a particular channel is not enough to conclude overall CP/T violation in the leptonic

sector in general and one needs to examine asymmetries in all possible channels. Even if it the case, one needs to make sure whether the source of CP violation is genuine or fake (depending on the baseline) [123]. In presence of NSI, this is further disturbed due to the presence of additional parameters (see [93, 96, 97]). On top of that in case of NSI, there are new genuine sources of CP violation as well as new fake sources of CP violation (aka matter effects) that can change the asymmetries even further. For models with possibilties of large NSI, see [124–127].

2.2.3 Three active and one sterile neutrino

This case corresponds to a four level quantum system with the 4×4 unitary matrix given by

$$U^{sterile} = O_{34}(\theta_{34}, \delta_{34})O_{24}(\theta_{24}, \delta_{24})O_{14}(\theta_{14})O_{23}(\theta_{23})O_{13}(\theta_{13}, \delta_{13})O_{12}(\theta_{12}) \tag{2.20}$$

Here, $O_{ij}(\theta_{ij}, \delta_{ij})$ denotes a rotation in the ij plane by an angle θ_{ij} and phase δ_{ij}.

$$O_{24}(\theta_{24}, \delta_{24}) = \begin{pmatrix} 1 & 0 & 0 & 0 \\ 0 & c_{24} & 0 & e^{-i\delta_{24}} s_{24} \\ 0 & 0 & 1 & 0 \\ 0 & -e^{i\delta_{24}} c_{24} & 0 & c_{24} \end{pmatrix}$$

$$O_{14}(\theta_{14}, \delta_{14}) = \begin{pmatrix} c_{14} & 0 & 0 & s_{14} \\ 0 & 1 & 0 & 0 \\ 0 & 0 & 1 & 0 \\ -s_{14} & 0 & 0 & c_{14} \end{pmatrix} \tag{2.21}$$

In presence of an additional sterile neutrino, the conditions for unitarity

$$\sum_{\beta} P_{\alpha\beta} = 1 = \sum_{\beta} \bar{P}_{\alpha\beta} \tag{2.22}$$

are valid if β takes values e, μ, τ, s ("s" stands for sterile). The unitarity condition

leads to the following conditions involving CP asymmetries since $\sum_\beta (P_{\alpha\beta} - \bar{P}_{\alpha\beta}) = 0$

$$\begin{aligned}
\sum_{\alpha=e,\mu,\tau} \Delta P^{CP}_{e\alpha} + \Delta P^{CP}_{es} &= 0 \\
\sum_{\alpha=e,\mu,\tau} \Delta P^{CP}_{\mu\alpha} + \Delta P^{CP}_{\mu s} &= 0 \\
\sum_{\alpha=e,\mu,\tau} \Delta P^{CP}_{\tau\alpha} + \Delta P^{CP}_{\tau s} &= 0 \\
\sum_{\alpha=e,\mu,\tau} \Delta P^{CP}_{s\alpha} + \Delta P^{CP}_{ss} &= 0
\end{aligned} \tag{2.23}$$

and $\sum_\alpha (P_{\alpha\beta} - \bar{P}_{\alpha\beta}) = 0$ would give four more conditions. Similarly, we can get conditions in terms of T asymmetries as $\sum_\beta (P_{\alpha\beta} - P_{\beta\alpha}) = 0$ and $\sum_\alpha (P_{\alpha\beta} - P_{\beta\alpha}) = 0$. Since we can only detect the active flavors, the presence of sterile neutrinos can be felt via flavor dependent measure of non-unitarity. The choice of parameters used is given in Table 2.3.

θ_{14} [°]	θ_{24} [°]	θ_{34} [°]	δ_{13} [°]	δ_{24} [°]	δ_{34} [°]	δm^2_{41} [eV^2]
8.0	5.0	15.0	$[-\pi, \pi]$	$[-\pi, \pi]$	$[-\pi, \pi]$	1.0

Table 2.3: The current bounds on sterile parameters taken from [128–132].

2.3 Results and Discussion

2.3.1 CP and T asymmetries as a function of E and L

The CP asymmetries in three appearance channels are plotted as a function of E and L in Fig. 2.1 and 2.2 for fixed baseline of L = 1300 km and fixed energy of E = 1 GeV respectively. Also, the T asymmetries are plotted in Fig. 2.3 and 2.4. In all the figures, the three rows correspond to the three different channels while the three columns correspond to the case of SI, NSI and sterile neutrinos. The solid line refers

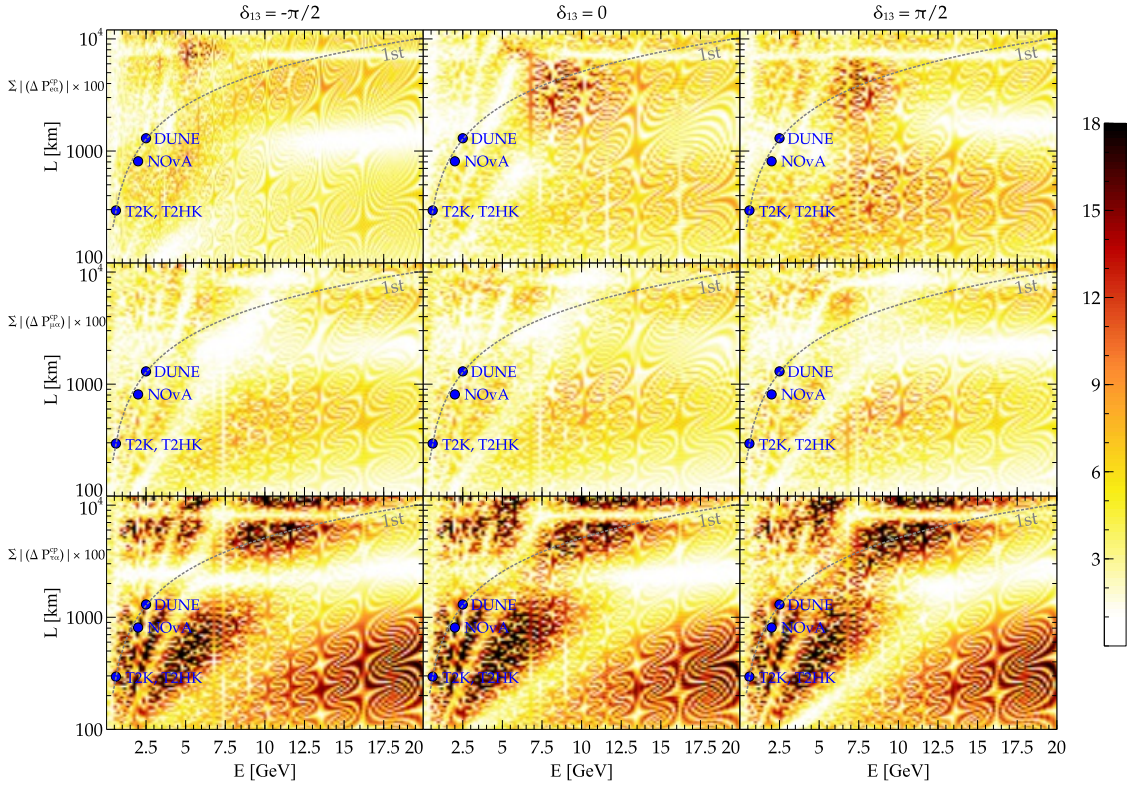

Figure 2.5: Measure of non-unitarity ($\sum_\alpha |\Delta P^{CP}_{e\alpha}|$, $\sum_\alpha |\Delta P^{CP}_{\mu\alpha}|$, $\sum_\alpha |\Delta P^{CP}_{\tau\alpha}|$) in sterile neutrino case shown in the plane of $E - L$. The additional phases δ_{24}, δ_{34} are set to zero. The location of first oscillation maximum (for $P(\nu_\mu \to \nu_e)$) is depicted by dashed grey curve. Darker regions imply larger amount of non-unitarity present (in percentage) for those values of E and L.

to the case when all CP violating phases including δ_{13} are set to zero. The dotted (dashed) lines refer to $\delta_{13} = \pi/2 (\delta_{13} = -\pi/2)$ and all additional phases set to zero. The grey bands correspond to the variation in phases of additional parameters in presence of new physics (see previous section). We can infer the following from these plots.

- *CP asymmetry :* One would expect the CP asymmetry to vanish when $\delta_{13} = 0$ in vacuum (see Eq. 2.17). From Fig. 2.1 and 2.2, we note that in all the three physics scenarios, we get non-trivial effects. The size of the effect depends upon the channel and the choice of parameters considered. For example, for a fixed baseline of 1300 km as considered in Fig. 2.1 and $\nu_\mu \to \nu_e$ channel, we notice that for $\delta_{13} = 0$, there is a non-trivial effect due to matter even in the case of

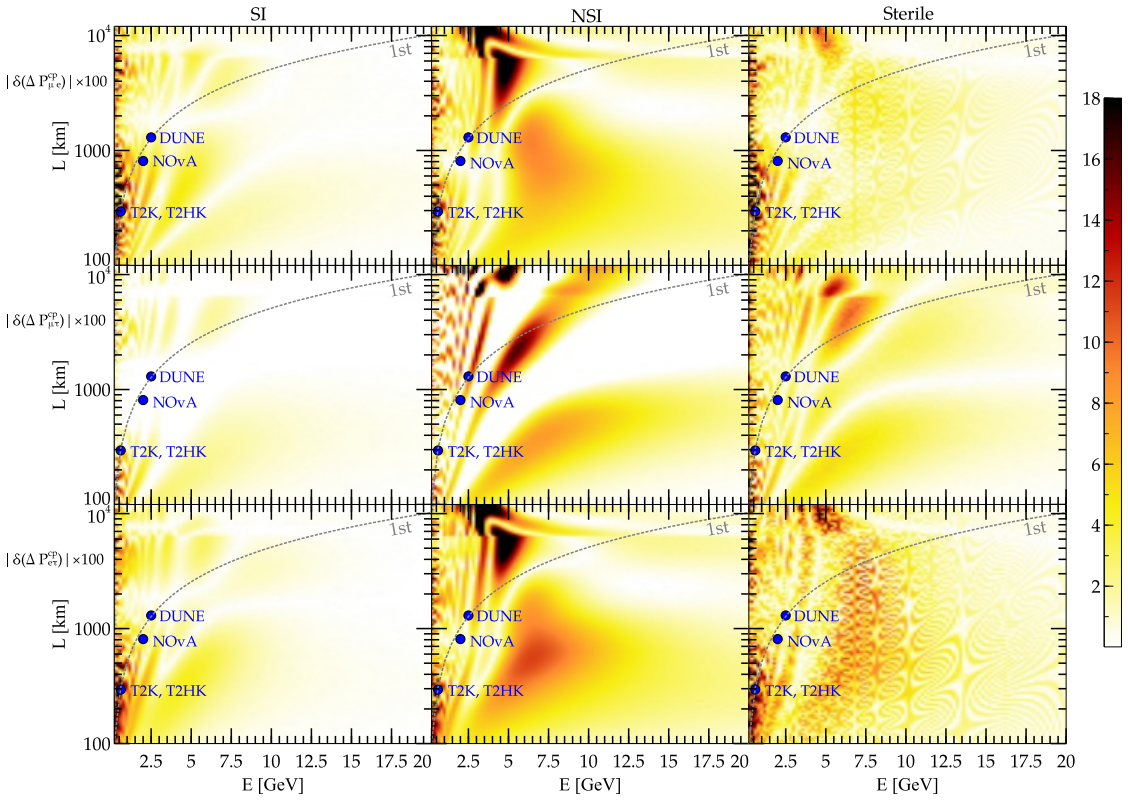

Figure 2.6: Oscillogram of absolute relative CP asymmetry for the appearance channels. The location of first oscillation maximum (for $P(\nu_\mu \to \nu_e)$) is depicted by dashed grey curve. Darker regions imply larger amount absolute relative CP asymmetry (in percentage) for those values of E and L.

SI which is prominent near lower energies (around 4-8% near the peak). The magnitude is similar in case of NSI and Sterile near the peak. However there are spectral differences in the three cases which may or may not be visible depending on the particular channel.

In Fig. 2.2, we plot the CP asymmetry as a function of L for a fixed value of E = 1 GeV. The three curves (solid, dashed and dotted) are oscillatory in nature and we note that there exist specific values of baselines for which one cannot distinguish the curves for the cases $\delta_{13} = \pm\pi/2$ and $\delta_{13} = 0$. These lie near 1000 km and 2000 km. In $\Delta P^{CP}_{\mu\tau}$, we note that surprisingly all the three curves meet near these values of baseline.

Here again for $\delta_{13} = 0$, there is non-trivial effect due to Earth matter and the

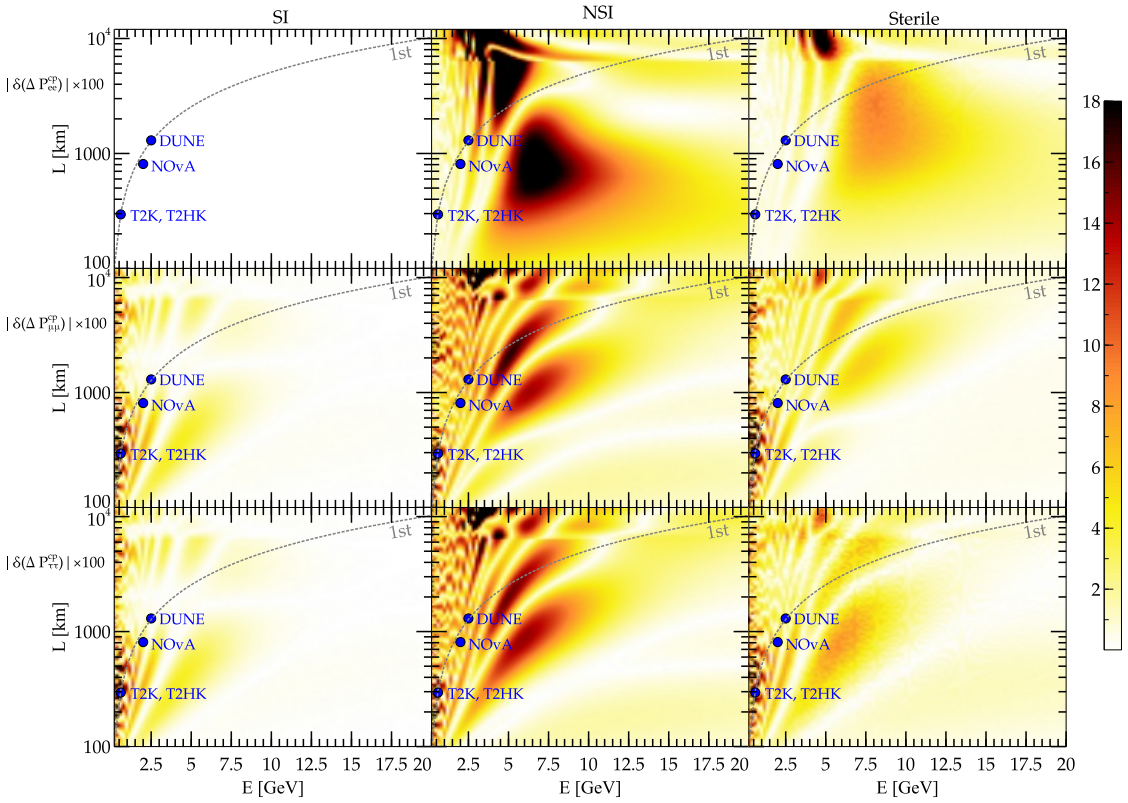

Figure 2.7: Oscillogram of absolute relative CP asymmetry for the disappearance channels. The location of first oscillation maximum (for $P(\nu_\mu \to \nu_e)$) is depicted by dashed grey curve. Darker regions imply larger amount absolute relative CP asymmetry (in percentage) for those values of E and L.

size of the effects increases with baseline and prominently for the new physics scenarios. The spectral differences are also visible here.

- *T asymmetry :* We note that $\delta_{13} = 0$ (solid line in Fig. 2.3) leads to vanishing asymmetry in all the three cases (SI, NSI and sterile). Also, the dotted and dashed lines are similar in all the three physics cases except for the $e-\tau$ channel in sterile neutrino case. Of course, if additional phases are present, there are non-trivial spectral differences which can be seen as grey bands.

  In Fig. 2.4, we plot the T asymmetry as a function of L for a fixed value of E = 1 GeV. The three curves (solid, dashed and dotted) are oscillatory in nature and we note that at specific values (or range of values) of baselines, the three cases ($\delta_{13} = \pm\pi/2$, $\delta_{13} = 0$) are indistinguishable. The spectral differences

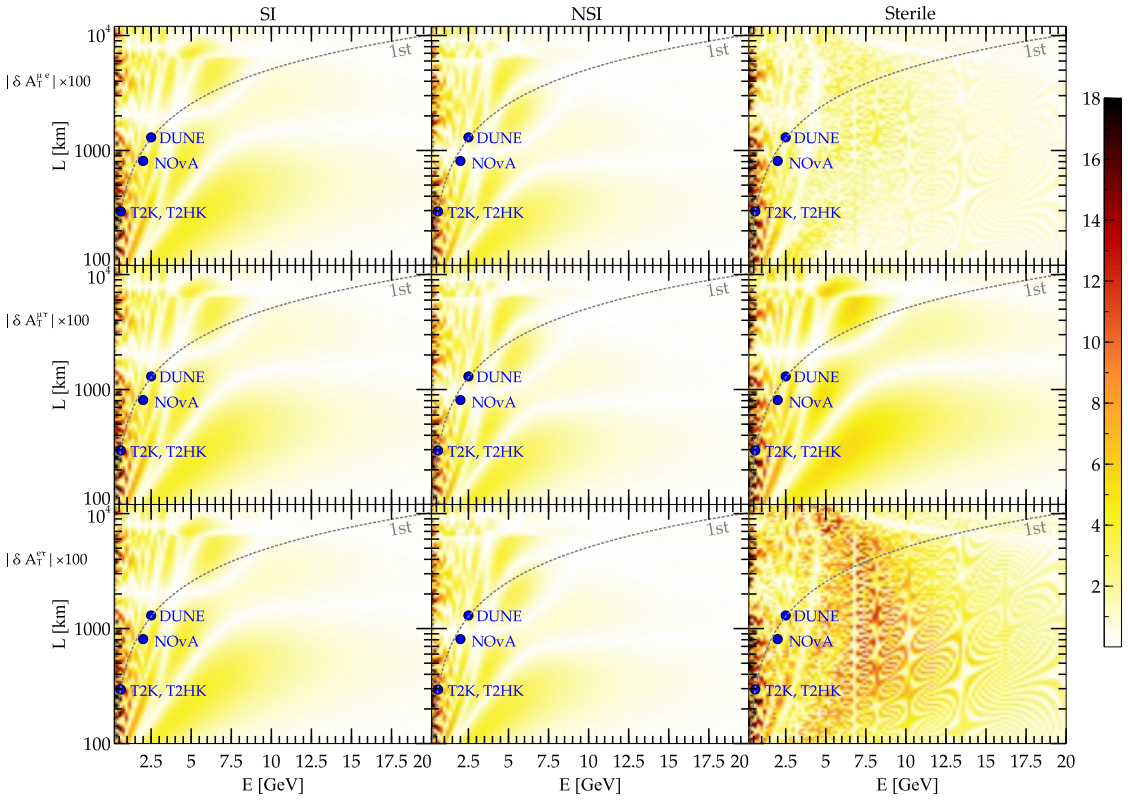

Figure 2.8: Oscillogram of absolute relative T asymmetry for the appearance channels. The location of first oscillation maximum (for $P(\nu_\mu \to \nu_e)$) is depicted by dashed grey curve. Darker regions imply larger amount absolute relative T asymmetry (in percentage) for those values of E and L.

are also visible more prominently in the sterile case.

2.3.2 Test of unitarity violation - oscillograms

We use coloured oscillograms in the plane of E and L as our tool to depict our observations. For the case of SI and NC NSI, the three flavor unitarity is maintained and therefore if we plot the sum of CP odd probability differences, we expect to get blank regions in these cases. However, for the case of one additional sterile neutrino, we obtain what is shown in Fig. 2.5. As we can see, there is pattern appearing in the plot and this has been explained in Appendix B.1. Darker regions imply larger amount of non-unitarity present (in percentage) for those values of E and L as depicted by the colour bar on the right. Primarily, the wiggles are arising due

to the large δm^2 oscillations in the $1-4$ sector. For LBL neutrino experiments, $\sin^2(\lambda L/2) \simeq \mathcal{O}(1)$ which gives

$$\frac{\lambda L}{2} \simeq 1.57 \left[\frac{\delta m^2_{31}}{2.5\times 10^{-3}\ eV^2}\frac{2.5\text{ GeV}}{E}\frac{L}{1300\ km}\right] \qquad \text{for DUNE} \qquad (2.24)$$

for the first oscillation maximum (minimum) in the appearance (disappearance) channel. We note that E = 1.5 GeV, L = 810 km for NOvA and E = 0.6 GeV, L = 295 km for T2K (and also T2HK) also lead to $\lambda L \sim \pi$. The location of first oscillation maximum (using $P(\nu_\mu \to \nu_e)$) is also shown on the plot. Obviously, most of the ongoing or planned LBL experiments lie on or close to [5] this curve.

The different colours depict the amount of unitarity violation. We can note that for the $\nu_e \to \nu_\alpha$ and the $\nu_\tau \to \nu_\alpha$ channel (where $\alpha = e, \mu, \tau$), the violation of unitarity is larger compared to the $\nu_\mu \to \nu_\alpha$ channel. This feature can be ascribed to the larger values of θ_{14} and θ_{34} used in comparison to θ_{24} (see Table 2.3). There is also a mild dependence on the value of δ_{13} as can be seen from different columns. Also, if we look at middle row ($\nu_\mu \to \nu_\alpha$ channel), it seems that none of the ongoing LBL experiments can detect the presence of non-unitarity better than $\sim 6\%$ or so.

2.3.3 Distinguishing between intrinsic and extrinsic CP effects

In the context of LBL experiments where matter can induce extrinsic CP effects, a non-zero value of $\Delta P^{CP}_{\alpha\beta}$ does not unequivocally imply intrinsic CP violation arising due to the Dirac CP phase (δ_{13}). To get over the problem of finding the source of CP violation (i.e. whether due to intrinsic CP phase and due to the matter effects), other observables have been introduced [91] which can prove useful not only to establish whether CP violation effects arise purely due to the Dirac type CP phase (δ_{13}) or a combination of the intrinsic and extrinsic CP effects. We can define an observable quantity which is obtained by taking difference of the CP probability differences computed at different values of δ_{13} for the appearance as well as disappearance channels

[5] NOvA is an off-axis experiment.

as follows [86, 89, 91]

$$\begin{aligned}\delta[\Delta P^{CP}_{\alpha\beta}] &= [\Delta P^{CP}_{\alpha\beta}](\delta_{13}=\pi/2) - [\Delta P^{CP}_{\alpha\beta}](\delta_{13}=0) \\ &= [P_{\alpha\beta} - \bar{P}_{\alpha\beta}](\delta_{13}=\pi/2) - [P_{\alpha\beta} - \bar{P}_{\alpha\beta}](\delta_{13}=0) \end{aligned} \quad (2.25)$$

The choices of δ_{13} in the above equation allow for better observability of the intrinsic CP effects. Obviously, in vacuum, the second term on the RHS vanishes and the first term gives completely intrinsic CP contribution which will be non-zero for $\delta_{13} = \pi/2$. If matter effects are switched off, Eq. 2.25 reduces to the expression for vacuum asymmetry corresponding to CP violation (see Eqs. 2.16 and 2.17). In standard matter, both first and second terms on RHS will be non-zero in general. The second term being non-zero in matter signals the presence of purely extrinsic effects. Under certain conditions [6], the matter contributions are independent of δ_{13} (i.e., not arising due to the intrinsic CP phase, δ_{13}, see Eq. 2.26 below) and above quantity is helpful to extract the intrinsic contribution [25].

From Ref. [25], one can analytically see that for $\nu_\mu \to \nu_e$ oscillation,

$$\Delta P^{CP}_{\mu e} = \Delta P^{CP}_{\mu e}(\sin\delta_{13}) + \Delta P^{CP}_{\mu e}(\text{matter}, \delta_{13}\text{-indep}) + \ldots \quad (2.26)$$

which implies decoupling of the intrinsic and extrinsic effects may be possible near the peak energy. Of course, the decoupling is not expected to work in general.

In Figs. 2.6-2.8, we show the oscillograms of $\delta[\Delta P^{CP/T}_{\alpha\beta}]$ in the plane of E and L for the appearance and the disappearance channels. The three rows correspond to the different appearance or disappearance channels (as mentioned in the subscripts of quantities plotted on the $y-$axes of the plots) while the columns are for SI, NSI and sterile cases. Unless otherwise stated, in this and the remaining plots, we take the additional phases in NSI and sterile cases to be zero for the sake of simplicity. These plots depict how new physics effects impact the inferences about intrinsic CP effects in the region in $\mathrm{E} - \mathrm{L}$ plane. Fig. 2.8 is similar to Fig. 2.6 but shows the T asymmetry.

[6] As we shall see, both vacuum and matter effects lead to same difference in probability differences due to interesting conspiracy near the first peak [25]. Note that this cancellation is perfect in case of standard matter effects but starts getting imperfect in case of new physics scenarios. This is due to the fact that δ_{13} and new physics terms appear in a coupled way in the probability expressions.

The following observations can be made in connection with the difference in CP asymmetries for the three appearance channels (see Fig. 2.6).

- $\nu_\mu \to \nu_e$ channel : In the SI case, we note that the regions of large asymmetry ($\gtrsim 18\%$) are more concentrated at lower energies ($\lesssim 2$ GeV). Any experiment operating at higher energies and longer baselines cannot probe intrinsic CP violation via the quantity considered. The whitish region around a baseline of ~ 8000 km is due to the fact that it is near the magic baseline where the CP dependence vanishes [18]. For NSI and sterile cases, we see the pattern in the oscillogram changes. However in case of NSI, the changes are more drastic. The new significant dark patches in the NSI case can be accounted for by assuming non-zero value of a particular NSI parameter (see Appendix B.2). Origin of different colours can be attributed to different parameters. For instance, in the $\nu_e \to \nu_\mu$ and $\nu_e \to \nu_\tau$ channels, the orangish patch ($\sim 8 - 10\%$) that lies in E $\in (5 - 9)$ GeV, L $\in (300 - 2000)$ km is due to the presence of ε_{ee}. The sterile case is similar to SI with new features in the entire oscillogram plot. The wiggles arise due to the fast oscillations induced by δm^2_{41} which is large in comparison to the other mass squared splittings. Among the considered experiments, T2K or T2HK seem to have the potential to extract the intrinsic CP phase from the probability level discussion as far as the $\nu_\mu \to \nu_e$ channel is concerned.

- $\nu_\mu \to \nu_\tau$ channel : Using this channel, extracting intrinsic CP violation is hard as can be seen from large whitish regions in the oscillogram for the SI case. Again the pattern is very different for NSI and sterile cases. From the probability level oscillogram in the $\nu_\mu \to \nu_\tau$ channel, we note that in NSI case, DUNE lies on a darker patch. This gives an impression that in presence of NSI, extraction of intrinsic CP phase may be easier as compared to SI case. However this is misleading since the source of intrinsic CP violation remains the same in both cases (NSI phases are set to zero). The substructures cancel in sterile case due to the fact that the wiggles are independent of δ_{13} (see Fig. B.6 in Appendix B.3).

- $\nu_e \to \nu_\tau$ channel : The gross features are similar to $\nu_\mu \to \nu_e$ channel. The darker regions can be understood from the size of the wiggles in Fig. B.6 in Appendix B.3.

The following observations can be made in connection with CP plots for the three disappearance channels (see Fig. 2.7).

- $\nu_e \to \nu_e$ channel : There is no δ_{13} dependence in the $\nu_e \to \nu_e$ channel [21] and hence the SI oscillogram is blank. NSI introduces significant effect in this channel. The features can be understood from Appendix B.2. Also, in sterile case, there are smaller dark patches as well as wiggles.

- $\nu_\mu \to \nu_\mu$ channel : Here the dependence on δ_{13} is mild for SI case [21]. Again, differences arise in case of NSI and sterile.

- $\nu_\tau \to \nu_\tau$ channel : Here the dependence on δ_{13} is mild and similar to the case of $\nu_\mu \to \nu_\mu$ channel for SI case [21]. For NSI and sterile, we see darker regions and wiggles respectively.

The following observations can be made in connection with T asymmetry plots for the three appearance channels (Fig. 2.8). The oscillograms show features similar in nature to the CP case but there are fewer dark patches than CP case. Though the SI and NSI cases are indistinguishable, wiggles appear in sterile case.

2.4 Implications for long baseline accelerator experiments

Below we give a very brief description of the LBL experiments considered to describe the implications of our results at the level of event rates. For more details, please see Table 2.4 (see also [96]). We have incorporated realistic efficiencies (Table 2.5) and errors (Table 2.6) in computation of events in Table 2.7.

DUNE : We consider a design that uses 120 GeV proton beam with a power of 1.0 MW which corresponds to

$$\frac{\text{P.O.T./year}}{[5.0\times10^{20}]} \sim \frac{\text{Proton beam power}}{[1\text{ MW}]} \times \frac{T}{[10^7\text{ sec}]} \times \frac{[120\text{ GeV}]}{E_p} \tag{2.27}$$

We assume 5 and 5 years of run time in neutrino and antineutrino modes respectively. The total exposure comes is around 350 Kt.MW.years.

NOvA experiment : We consider a design that uses 120 GeV proton beam with a power of 0.7 MW which corresponds to

$$\frac{\text{P.O.T./year}}{[3.0\times10^{20}]} \sim \frac{\text{Proton beam power}}{[0.7\text{ MW}]} \times \frac{T}{[10^7\text{ sec}]} \times \frac{[120\text{ GeV}]}{E_p} \tag{2.28}$$

We assume 3 and 3 years of run time in neutrino and antineutrino modes respectively. The total exposure comes around 84 Kt.MW.years.

T2K experiment : We consider a design that uses 50 GeV proton beam with a power of 0.770 MW which corresponds to

$$\frac{\text{P.O.T./year}}{[4.15\times10^{20}]} \sim \frac{\text{Proton beam power}}{[0.770\text{ MW}]} \times \frac{T}{[10^7\text{ sec}]} \times \frac{[50\text{ GeV}]}{E_p} \tag{2.29}$$

We assume 3 and 3 years of run time in neutrino and antineutrino modes respectively. The total exposure comes around 103.95 Kt.MW.years.

T2HK experiment : We consider a design that uses 30 GeV proton beam with a power of 7.5 MW which corresponds to

$$\frac{\text{P.O.T./year}}{[8.0\times10^{21}]} \sim \frac{\text{Proton beam power}}{[7.5\text{ MW}]} \times \frac{T}{[10^7\text{ sec}]} \times \frac{[30\text{ GeV}]}{E_p} \tag{2.30}$$

We assume 3 and 1 year of run time in neutrino and antineutrino modes respectively. The total exposure comes around 16.8 Mt.MW.years.

We present our results at the level of event rates using the following quantity

$$\delta[\Delta N^{CP}_{\alpha\beta}] = [\Delta N^{CP}_{\alpha\beta}](\delta_{13}=\pi/2) - [\Delta N^{CP}_{\alpha\beta}](\delta_{13}=0) \tag{2.31}$$

Here the first term on the RHS corresponds to the case of maximal CP violation ($\delta_{13}=\pi/2$) while the second term corresponds to CP conservation ($\delta_{13}=0$). Since

DUNE	**T2K**
$E = 2.5$ GeV, $L = 1300$ km	$E = 0.6$ GeV, $L = 295$ km
Runtime (yr) = 5 ν + 5 $\bar{\nu}$	Runtime (yr) = 3 ν + 3 $\bar{\nu}$
35 Kt, LArTPC	22.5 Kt, WC
$\varepsilon_{app} = 80\%$, $\varepsilon_{dis} = 85\%$	$\varepsilon_{app} = 50\%$, $\varepsilon_{dis} = 90\%$
$R_\mu = 0.20/\sqrt{E}$, $R_e = 0.15/\sqrt{E}$	$R_\mu = 0.085/\sqrt{E}$, $R_e = 0.085/\sqrt{E}$
$E \in [0.5 - 10.0]$ GeV,	$E \in [0.4 - 1.2]$ GeV,
Bin width = 250 MeV	Bin width = 40 MeV
NOvA	**T2HK**
$E = 1.6$ GeV, $L = 810$ km	$E = 0.6$ GeV, $L = 295$ km
Runtime (yr) = 3 ν + 3 $\bar{\nu}$	Runtime (yr) = 1 ν + 3 $\bar{\nu}$
14 Kt, TASD	560 Kt, WC
$\varepsilon_{app} = 55\%$, $\varepsilon_{dis} = 85\%$	$\varepsilon_{app} = 50\%$, $\varepsilon_{dis} = 90\%$
$R_\mu = 0.06/\sqrt{E}$, $R_e = 0.085/\sqrt{E}$	$R_\mu = 0.085/\sqrt{E}$, $R_e = 0.085/\sqrt{E}$
$E \in [0.5 - 4.0]$ GeV,	$E \in [0.4 - 1.2]$ GeV,
Bin width = 125 MeV	Bin width = 40 MeV

Table 2.4: Detector configuration, efficiencies, resolutions and relevant energy ranges for DUNE**,** NOvA**,** T2K**,** T2HK**.**

all the accelerator experiments mentioned above can produce ν_μ only at the source (pion decay), we discuss the implications of our results at the level of event rates using $\nu_\mu \to$ any flavor. Note that the binning and energy range of the experiments are different (see Table. 2.4).

- $\nu_\mu \to \nu_e$: Among all the considered experiments, the total event rate is highest for T2HK by a large margin. This high statistics is due to large detector size and beam power. Moreover, this means that one would be able to disentangle intrinsic and extrinsic sources of CP violation better with T2HK. The much shorter baseline ensures that matter effects are small which in turn simplifies the extraction of intrinsic CP phase. We can note that NSI and sterile scenarios also retain this feature as long as additional phases are set to zero (see Table 2.7

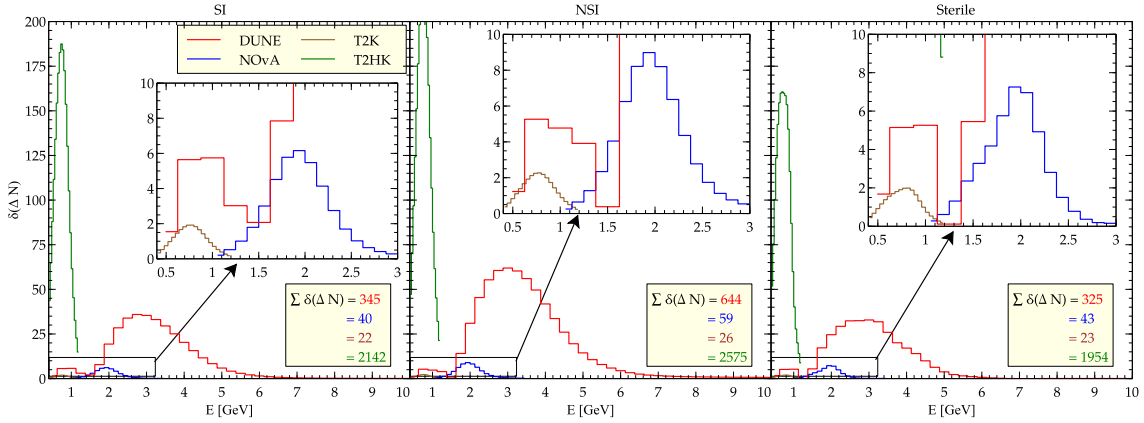

Figure 2.9: $|\delta[\Delta N^{CP}_{\mu e}]|$ plotted as a function of E. The binning for the four experiments is different.

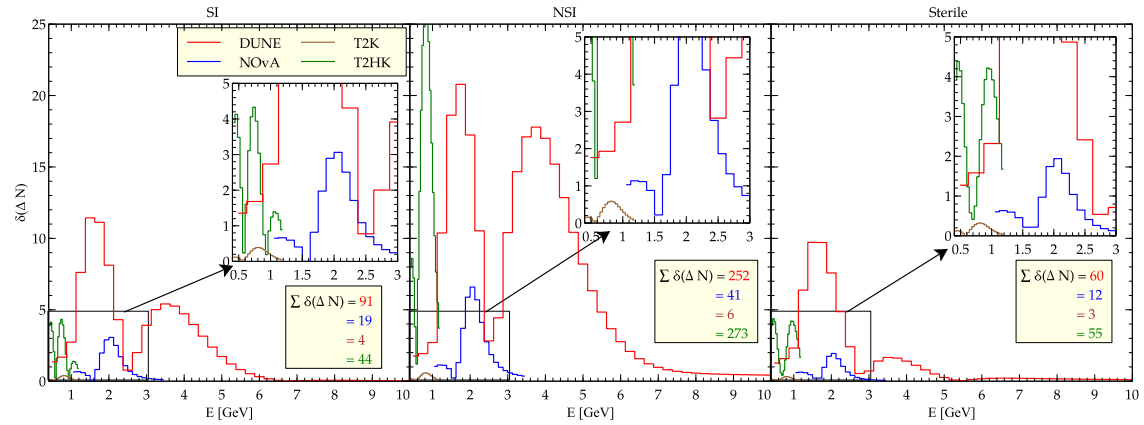

Figure 2.10: $|\delta[\Delta N^{CP}_{\mu\mu}]|$ plotted as a function of E. The binning for the four experiments is different.

and Fig. 2.9).

- $\nu_\mu \to \nu_\mu$: Here, in case of SI, DUNE seems to be the best choice. But, in presence of new physics such as NSI or sterile, T2HK seems to do slightly better though DUNE is also competitive (see Table 2.7 and Fig. 2.10).

- $\nu_\mu \to \nu_\tau$: The number of events are scarce even after using a higher energy beam tune and evidently we can not draw useful conclusions from this channel (see Table 2.7 and Fig. 2.11).

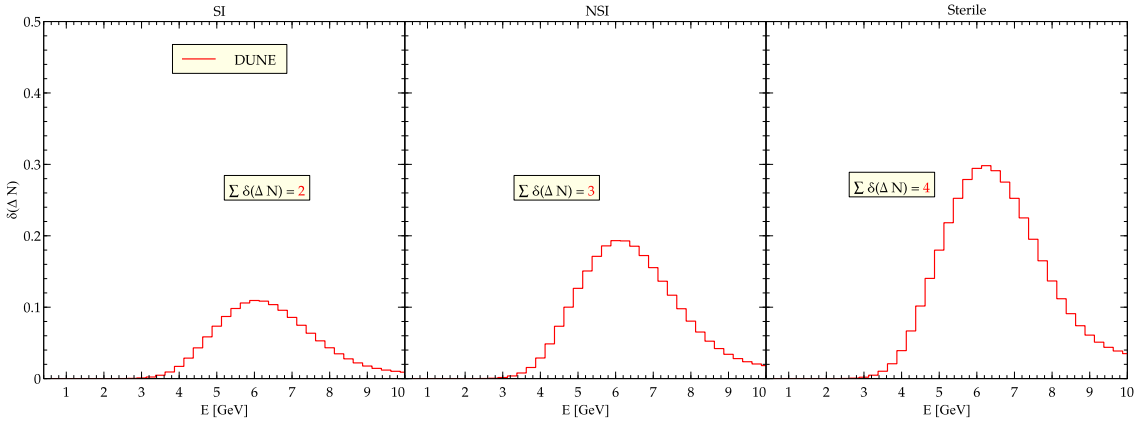

Figure 2.11: $|\delta[\Delta N_{\mu\tau}^{CP}]|$ plotted as a function of E. We get handful events for DUNE and none for the rest.

2.5 Conclusion

It is fair to say that neutrino oscillation physics has entered a precision era and the upcoming LBL experiments are expected to shed some light on one of the crucial unknown parameters in the oscillation framework - the leptonic CP phase. Going beyond the recent studies revealing how potential new physics scenarios can hinder the clean determination of this important parameter [78, 93–109], we address the issue of clean separation of the intrinsic leptonic CP phase from the extrinsic contribution arising due to SI as well as new physics[7]. We also show the impact of new physics on testing non-unitarity.

Accelerator-based LBL experiments are plagued with the problem of clean separation of intrinsic and extrinsic CP violating terms due to the fact that neutrinos propagate through Earth matter. Resolution of this is a difficult task and there are several suggestions including new observables in literature. In order to elucidate and quantify our results, we use an observable quantity given by Eq. 2.25 (see [86, 89, 91]) and scan the range of energies and path lengths relevant to LBL experiments. We consider two new physics scenarios - NSI in propagation and additional sterile neu-

[7]We assume that only source of intrinsic CP violation is due to δ_{13} which is very optimistic. In principle, the new physics scenarios considered here can also bring in more sources of intrinsic CP violation via pure phase terms.

trinos. We depict our outcome in the form of oscillogram plots in L – E space where we unravel the regions where the impact of new physics on the oscillograms could be potentially large. We also highlight the differences in the different physics cases for some benchmark values of new physics parameters. Our discussion is mostly targeted towards accelerator based neutrino experiments with L/E $\sim$ 500 km/GeV but can easily be extended to short baseline (SBL) experiments and very LBL experiments. Other than the question of separating the intrinsic CP contribution, we also discuss the impact of additional sterile neutrinos on the unitarity conditions.

For the sake of simplicity, we set the additional intrinsic CP phases (induced by new physics) to zero and discuss the impact of additional parameters appearing in NSI and sterile cases that are extrinsic in nature. Furthur through the event rates (see Eq. 2.31) for realistic configurations for some of the ongoing and planned LBL experiments, we show which experiment has better potential to answer the questions that we have posed in this article. We have considered four LBL experiments - T2K, T2HK, DUNE and NOvA and also taken into account both the appearance ($\nu_\mu \to \nu_e$) and disappearance ($\nu_\mu \to \nu_\mu$) channels for each of them (see Sec. 2.4). We demonstrate how even the restricted class of CP conserving new physics effects complicate the separation of intrinsic CP phase from the extrinsic CP effects that can come from SI or new physics. Our main results can be summarised as follows :

- *Non-unitarity :* Deviation from unitarity (in the sterile case) at the probability level can be discernible by looking at various E and L ranges where one gets darker regions. Fig. 2.5 shows the deviation from unitarity for three different values of δ_{13}. Obviously, in vacuum, one would expect to get blank region whenever the source of CP violating phase vanishes (δ_{13} being the only source of CP violation, see Eq. 2.11). This corresponds to the middle column of Fig. 2.5. Instead we see some pattern even for $\delta_{13} = 0$ and this can be attributed to the SI with matter which contributes to non-unitarity. We can note that only in channels involving ν_τ, it might be possible for DUNE or NOvA or T2HK to reveal some signature of non-unitarity. However this is not expected to be useful at the level of events. Non-unitarity is very hard to probe in the ν_τ

channel using any of the LBL experiments primarily because one is statistically limited in case of tau events (see Fig. 2.5).

- *Extraction of intrinsic CP violating component and comparison of new physics scenarios with SI :* At the probability level, the darker shaded regions imply larger influence of new physics. This dark region should not be thought of as aiding the extraction of intrinsic CP component in any given channel, rather it makes the situation more complicated. Some of the ongoing and future experiments are shown as bulleted points along the curve representing the first oscillation maximum. For lower values of E and L, it is expected that the NSI effects would be small and hence one could in principle have a clean detection of intrinsic component. From the oscillograms, we can note that the impact of new physics scenarios is more prominent at larger values of E and L. Also, note that NOvA and DUNE lie on lighter shaded region of the oscillogram while T2K (and T2HK) is at a darker patch. Hence the baseline choice of T2K or T2HK is desirable in order to extract the intrinsic component from the probability level analysis. Finally, at the level of events, T2HK wins due to the large statistics in order to cleanly extract the intrinsic contribution (see Fig. 2.6 - 2.8).

- *Event analysis :* At the level of event rates, we find that T2HK offers best statistics among all the considered experiments in case of $\nu_\mu \to \nu_e$ channel. But, DUNE is competitive with T2HK if we consider $\nu_\mu \to \nu_\mu$ channel. Tau appearance channel is mostly not useful due to limited statistics (see Figs. 2.9 - 2.11 and Table 2.7).

Finally some comments concerning the validity of our approach are in order. We assume that only source of intrinsic CP violation is due to δ_{13} which is very optimistic. In principle, the new physics scenarios considered here can also bring in more sources of intrinsic CP violation via pure phase terms. Any source of new physics therefore has both intrinsic (i.e. phases) and extrinsic components and discussing the problem with both components is rather cumbersome. In fact, the separation of intrinsic contribution using a quantity like $\delta(\Delta P^{CP}_{\alpha\beta})$ is feasible only when there is one source

of intrinsic CP violation (δ_{13}) present. For a more general scenario with phases introduced in the new physics sector, one needs to think of appropriate observables to be able to separate out the intrinsic contribution.

Nonetheless we would like to stress that our overall approach to survey the impact of CP conserving new physics scenarios is quite general and can be applied to other new physics scenarios or other regimes in $\mathrm{E}-\mathrm{L}$ space. The discussion in the present work is targeted towards accelerator-based neutrino experiments with $\mathrm{L/E} \sim 500$ km/GeV but the ideas can easily be extended to SBL experiments or very LBL experiments.

Experiment	Channel	Signal (sg)/Background (bg)	Efficiency (%)
DUNE	$\nu_\mu \to \nu_e$	sg: ν_e	80
		bg:	
		(a) ν_e beam	46
		(b) ν_μ CC misidentification rate	0.8
		(c) ν_μ NC misidentification rate	0.6
	$\nu_\mu \to \nu_\mu$	sg: ν_μ	85
		bg: ν_μ NC misidentification rate	0.5
NOvA	$\nu_\mu \to \nu_e$	sg: ν_e	24
		bg:	
		(a) ν_e beam	12
		(b) ν_μ CC misidentification rate	0.04
		(c) ν_μ NC misidentification rate	0.15
	$\nu_\mu \to \nu_\mu$	sig: ν_μ	80
		bg: ν_μ NC misidentification rate	0.15
T2K and T2HK	$\nu_\mu \to \nu_e$	sg: ν_e	50
		bg:	
		(a) ν_e beam	50
		(b) ν_μ CC misidentification rate	0.03
		(c) ν_μ NC misidentification rate	0.5
	$\nu_\mu \to \nu_\mu$	sg: ν_μ	90
		bg: ν_μ NC misidentification rate	0.5

Table 2.5: Signal (sg) and Background (bg) efficiencies for the experiments considered (DUNE, T2K, T2HK and NOvA).

Experiment	Channel	sg error (%)	bg error (%)
DUNE	$\nu_\mu \to \nu_e$	5	10
	$\nu_\mu \to \nu_\mu$	5	45
NOvA	$\nu_\mu \to \nu_e$	5	5
	$\nu_\mu \to \nu_\mu$	5	5
T2K and T2HK	$\nu_\mu \to \nu_e$	10	5
	$\nu_\mu \to \nu_\mu$	2.5	20

Table 2.6: Signal (sg) and Background (bg) error for the experiments considered (DUNE, T2K, T2HK and NOvA).

Experiment	SI		NSI		Sterile	
	$\nu_\mu \to \nu_e$	$\nu_\mu \to \nu_\mu$	$\nu_\mu \to \nu_e$	$\nu_\mu \to \nu_\mu$	$\nu_\mu \to \nu_e$	$\nu_\mu \to \nu_\mu$
DUNE (NH, $\pi/2$)	345	91	644	252	325	60
DUNE (NH, $-\pi/2$)	328	91	261	252	197	60
DUNE (IH, $\pi/2$)	231	41	141	187	227	28
DUNE (IH, $-\pi/2$)	310	41	514	187	278	28
NOvA (NH, $\pi/2$)	40	19	59	41	43	12
NOvA (NH, $-\pi/2$)	34	19	16	41	22	12
NOvA (IH, $\pi/2$)	33	12	15	36	38	9
NOvA (IH, $-\pi/2$)	36	12	53	36	43	9
T2K (NH, $\pi/2$)	22	4	26	6	23	3
T2K (NH, $-\pi/2$)	15	4	11	6	8	3
T2K (IH, $\pi/2$)	14	3	11	5	22	3
T2K (IH, $-\pi/2$)	21	3	24	5	21	3
T2HK (NH, $\pi/2$)	2142	44	2575	273	1954	55
T2HK (NH, $-\pi/2$)	2001	44	1567	273	1492	55
T2HK (IH, $\pi/2$)	2021	32	1574	217	2552	71
T2HK (IH, $-\pi/2$)	2094	32	2531	217	2658	71

Table 2.7: $|\delta[\Delta N^{CP}_{\alpha\beta}]| = |[\Delta N^{CP}_{\alpha\beta}](\delta_{13} = \pm\pi/2) - [\Delta N^{CP}_{\alpha\beta}](\delta_{13} = 0)|$ **summed over energy bins for different experiments for NH and IH. For NSI, we show the collective case when the NSI parameters** $|\varepsilon_{e\mu}| = 0.04, |\varepsilon_{e\tau}| = 0.04, |\varepsilon_{\mu\tau}| = 0.03, \varepsilon_{\mu\mu} = 0.06, \varepsilon_{\tau\tau} = 0.1, \varepsilon_{ee} = 0.4$, $\varphi_{e\mu} = 0$, $\varphi_{e\tau} = 0$, $\varphi_{\mu\tau} = 0$ **are considered. The sterile parameters are as mentioned in Table 2.3.**

Chapter 3

Summary and future prospects

Neutrino physics represents a major frontier of high energy physics and astroparticle physics research today. A succession of seminal results from low energy experiments involving neutrinos from a variety of sources (solar, atmospheric, reactor and accelerator) have established the phenomenon of neutrino flavor oscillations on a firm footing which in turn implies existence of tiny non-zero neutrino masses. A vibrant global experimental program in neutrino physics is underway, with the goal of answering several outstanding fundamental questions which crucially impact our search for a theory beyond the SM. This includes the LBL experiments and SBL experiments. The important long and SBL experiments are :

- DUNE [52] is a leading-edge experiment for neutrino science and proton decay studies. This experiment, together with the facility that will support it, the Long-Baseline Neutrino Facility (LBNF), will be an internationally designed, coordinated and funded program, hosted at the Fermi National Accelerator Laboratory (Fermilab) in Batavia, Illinois. A ceremonial groundbreaking for the International LBNF/DUNE project took place in July at the Sanford Underground Research Facility. DUNE will attempt to answer some of the yet unresolved questions in neutrino physics such as whether CP is violated, if the neutrino mass hierarchy is normal or inverted and what is the correct octant of θ_{23}.

- The SBN Program [75] is a joint effort (ICARUS-T600, MicroBooNE, SBND)

to use their detectors to perform sensitive searches for ν_e appearance and ν_μ disappearance in the Booster Neutrino Beam at Fermilab. All of the detectors utilize liquid argon time projection chambers (LArTPC), and each contributes to the development of this technology for the long-baseline DUNE experiment at Fermilab. Previous neutrino experiments have seen some hints of yet another sterile neutrino, and SBN will hunt for evidence of this unconfirmed fourth state.

On the theoretical front, it is well known that the phenomenon of neutrino oscillations cannot be accommodated within the SM of particle physics. The neutrino sector in the SM has only left-handed neutrinos and right-handed anti-neutrinos. The absence of right-handed neutrinos in the SM doesnot allow for a Dirac mass term unlike other fermions. Thus the neutrinos are massless in the SM. For the above mentioned reasons, neutrinos provide an unmatched window to probe physics beyond the SM, also referred to as new physics. In the minimal extension to account for neutrino masses, we need to include 3 right handed neutrinos : ν_{eR}, $\nu_{\mu R}$ and $\nu_{\tau R}$ in the theory. These are singlets under $\mathrm{SU(3)_c}$ and $\mathrm{SU(2)_L}$ and carry no hypercharge, $Y = 0$.

In this thesis, we go beyond the minimal model of new physics required to explain neutrino masses and we are concerned with the phenomenological aspects of neutrino oscillations in presence of new physics (NSI and sterile neutrinos) at LBL neutrino experiments. This thesis is divided into two chapters. We have carried out the study both analytically as well as numerically with the use of GLoBES software [79]. We first summarize the inferences obtained thus far. Then we will discuss the ideas that we are currently investigating.

- **Chapter 1** serves as the introduction to the thesis, and also reviews the basic requirements necessary to study a class of exotic processes via new physics in neutrino sector. The Chapter starts with an introduction to the basic features of the SM and the need for new physics (particularly relevant for the problems discussed in this thesis). We introduce the neutrino oscillations formalism in vacuum and matter and discuss the salient features in each case. We then

present the current state of the art in neutrino oscillation physics. We also give experimental details and cover the wide range of sources and variety of detectors that are in use to study neutrino oscillations. We give an overview of the physics goals of the LBL neutrino experiments with particular emphasis on the DUNE experiment. We discuss the oscillation probabilities that can be studied at LBL in vacuum and in matter. Towards the end, we introduce and motivate the two new physics scenarios that we have studied in this thesis - NSI and sterile neutrinos.

- **Chapter 2** deals with probing discrete symmetries and their violations at LBL accelerator experiments in presence of new physics. We define the observable for quantifying the CP (C-Charge conjugation, P-Parity) and T (T-Time reversal) violations. In presence of sterile neutrino, we also study the effects due to non-unitarity in neutrino mixing. We then present our results in terms of oscillograms to depict the impact of new physics on the observable defined above. Finally, we also discuss the issue of extraction of intrinsic CP phase at LBL experiments.

3.1 Summary of work done

It is fair to say that neutrino oscillation physics has entered a precision era and the upcoming LBL experiments are expected to shed some light on one of the crucial unknown parameters in the oscillation framework - the leptonic CP phase. Going beyond the recent studies revealing how potential new physics scenarios can hinder the clean determination of this important parameter [78, 93–109], we address the issue of clean separation of the intrinsic leptonic CP phase from the extrinsic contribution arising due to SI as well as new physics[1]. We also show the impact of new physics on testing non-unitarity.

[1]We assume that only source of intrinsic CP violation is due to δ_{13} which is very optimistic. In principle, the new physics scenarios considered here can also bring in more sources of intrinsic CP violation via pure phase terms.

Accelerator-based LBL experiments are plagued with the problem of clean separation of intrinsic and extrinsic CP violating terms due to the fact that neutrinos propagate through Earth matter. Resolution of this is a difficult task and there are several suggestions including new observables in literature. In order to elucidate and quantify our results, we use an observable quantity given by Eq. 2.25 (see [86, 89, 91]) and scan the range of energies and path lengths relevant to LBL experiments. We consider two new physics scenarios - NSI in propagation and additional sterile neutrinos. We depict our outcome in the form of oscillogram plots in $\mathrm{L} - \mathrm{E}$ space where we unravel the regions where the impact of new physics on the oscillograms could be potentially large. We also highlight the differences in the different physics cases for some benchmark values of new physics parameters. Our discussion is mostly targeted towards accelerator based neutrino experiments with $\mathrm{L/E} \sim 500$ km/GeV but can easily be extended to SBL experiments and very LBL experiments. Other than the question of separating the intrinsic CP contribution, we also discuss the impact of additional sterile neutrinos on the unitarity conditions.

For the sake of simplicity, we set the additional intrinsic CP phases (induced by new physics) to zero and discuss the impact of additional parameters appearing in NSI and sterile cases that are extrinsic in nature. Furthur through the event rates (see Eq. 2.31) for realistic configurations for some of the ongoing and planned LBL experiments, we show which experiment has better potential to answer the questions that we have posed in this article. We have considered four LBL experiments - T2K, T2HK, DUNE and NOvA and also taken into account both the appearance ($\nu_\mu \to \nu_e$) and disappearance ($\nu_\mu \to \nu_\mu$) channels for each of them (see Sec. 2.4). We demonstrate how even the restricted class of CP conserving new physics effects complicate the separation of intrinsic CP phase from the extrinsic CP effects that can come from SI or new physics. Our main results can be summarised as follows

3.1.1 Deviation from unitarity in presence of additional sterile neutrino

Deviation from unitarity (in the sterile case) at the probability level can be discernible by looking at various E and L ranges where one gets darker regions. Fig. 2.5 shows the deviation from unitarity for three different values of δ_{13}. Obviously, in vacuum, one would expect to get blank region whenever the source of CP violating phase vanishes (δ_{13} being the only source of CP violation, see Eq. 2.11). This corresponds to the middle column of Fig. 2.5. Instead we see some pattern even for $\delta_{13} = 0$ and this can be attributed to the SI with matter which contributes to non-unitarity. We can note that only in channels involving ν_τ, it might be possible for DUNE or NOvA or T2HK to reveal some signature of non-unitarity. However this is not expected to be useful at the level of events. Non-unitarity is very hard to probe in the ν_τ channel using any of the LBL experiments primarily because one is statistically limited in case of tau events (see Fig. 2.5).

3.1.2 Extracting the intrinsic CP violating component in presence of new physics

At the probability level, the darker shaded regions imply larger influence of new physics. This dark region should not be thought of as aiding the extraction of intrinsic CP component in any given channel, rather it makes the situation more complicated. Some of the ongoing and future experiments are shown as bulleted points along the curve representing the first oscillation maximum. For lower values of E and L, it is expected that the NSI effects would be small and hence one could in principle have a clean detection of intrinsic component. From the oscillograms, we can note that the impact of new physics scenarios is more prominent at larger values of E and L. Also, note that NOvA and DUNE lie on lighter shaded region of the oscillogram while T2K (and T2HK) is at a darker patch. Hence the baseline choice of T2K or T2HK is desirable in order to extract the intrinsic component from the probability level analysis. Finally, at the level of events, T2HK wins due to the large statistics

in order to cleanly extract the intrinsic contribution (see Fig. 2.6 - 2.8).

3.1.3 Discussion at the level of event rates

At the level of event rates, we find that T2HK offers best statistics among all the considered experiments in case of $\nu_\mu \to \nu_e$ channel. But, DUNE is competitive with T2HK if we consider $\nu_\mu \to \nu_\mu$ channel. Tau appearance channel is mostly not useful due to limited statistics (see Figs. 2.9 - 2.11 and Table 2.7).

Finally some comments concerning the validity of our approach are in order. We assume that only source of intrinsic CP violation is due to δ_{13} which is very optimistic. In principle, the new physics scenarios considered here can also bring in more sources of intrinsic CP violation via pure phase terms. Any source of new physics therefore has both intrinsic (i.e. phases) and extrinsic components and discussing the problem with both components is rather cumbersome. In fact, the separation of intrinsic contribution using a quantity like $\delta(\Delta P^{CP}_{\alpha\beta})$ is feasible only when there is one source of intrinsic CP violation (δ_{13}) present. For a more general scenario with phases introduced in the new physics sector, one needs to think of appropriate observables to be able to separate out the intrinsic contribution.

Nonetheless we would like to stress that our overall approach to survey the impact of CP conserving new physics scenarios is quite general and can be applied to other new physics scenarios or other regimes in $E - \mathrm{L}$ space. The discussion in the present work is targeted towards accelerator-based neutrino experiments with L/E $\sim$ 500 km/GeV but the ideas can easily be extended to SBL experiments or very LBL experiments.

3.2 Experimental Status : neutrino mixing

Neutrino mixing among the three neutrino flavors is described by 3×3 unitary matrix

$$U = \begin{pmatrix} c_{12}c_{13} & s_{12}c_{13} & s_{13}e^{-i\delta_{13}} \\ -s_{12}c_{23} - c_{12}s_{13}s_{23}e^{i\delta_{13}} & c_{12}c_{23} - s_{12}s_{13}s_{23}e^{i\delta_{13}} & c_{13}s_{23} \\ s_{12}s_{23} - c_{12}s_{13}c_{23}e^{i\delta_{13}} & -c_{12}s_{23} - s_{12}s_{13}c_{23}e^{i\delta_{13}} & c_{13}c_{23} \end{pmatrix}$$

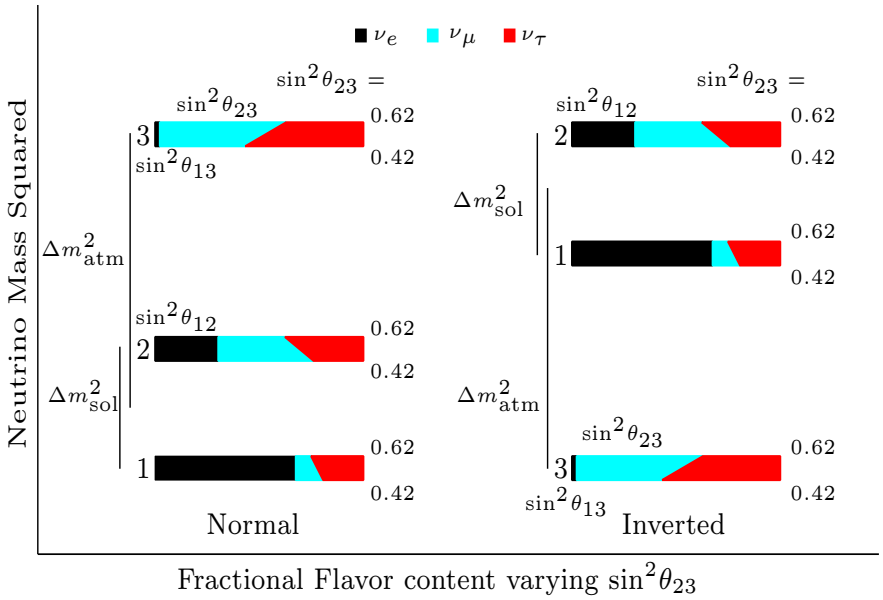

Figure 3.1: Flavor content of neutrinos for the current values of oscillation parameters for NH (left) and IH (right). Adapted from [133] to include the current best-fit values.

where $s_{ij} = \sin\theta_{ij}, c_{ij} = \cos\theta_{ij}$ and δ_{13} is the Dirac CP phase.
We can readily see that the angles of the mixing matrix can be defined through the elements of the mixing matrix :

$$\begin{aligned} c^2_{12} &= \frac{|U_{e1}|^2}{1-|U_{e3}|^2} \quad ; \quad s^2_{12} = \frac{|U_{e2}|^2}{1-|U_{e3}|^2} \\ s^2_{13} &= |U_{e3}|^2 \\ s^2_{23} &= \frac{|U_{\mu 3}|^2}{1-|U_{e3}|^2} \quad ; \quad c^2_{23} = \frac{|U_{\tau 3}|^2}{1-|U_{e3}|^2} \end{aligned} \tag{3.1}$$

In Table 1.4 and 1.5, we have summarized the present status of the known three flavor neutrino oscillation parameters [26] obtained from a global analysis of data available from solar, atmospheric, reactor and accelerator experiments. The unknown parameters are sign(δm^2_{31}) and δ_{13}. We summarize our current knowledge about neutrino mass and mixing parameters [26] in terms of a flavor diagram (Fig. 3.1) which depicts how much of the individual flavors (shown in different colours) are contained in each mass state. The probability that a neutrino of given mass m^2_i contains flavors of ν_e, ν_μ, ν_τ is proportional to the length of the respective coloured band. The vertical height takes into account the θ_{23} variation. Neutrino oscillation experiments

are sensitive to mass squared differences and not absolute masses. Presently, there can be two possibilities - NH or IH. In the case of NH, m_1^2 is one of the lowest states and m_3^2 is highest and this gets reversed when we have IH.

3.3 Ongoing work and future prospects

We briefly mention the ongoing work that we are presently engaged in. The first one concerns the optimal beam tune to study the current unknowns in neutrino oscillations. The key goal is to measure CP violation and it is well-known that even tiny effects can obscure the determination of this important parameter. In any experimental collaboration, detailed optimization techniques are used to optimize the signal for our need. Here the question concerns sensitivity to CP violation.

3.3.1 Beam optimization in presence of NSI

Usually, in the standard case, the beam optimization is carried out with a genetic algorithm [134] that uses "survival of the fittest" concept to identify the primary beam, horn and target parameters that maximize sensitivity to CP violation. Such optimizations have been carried out for several target options and horn shapes which produce several beam options all of which give rise to neutrino fluxes and projected sensitivities to CP violation that are drastically improved over the reference beam that is considered in the DUNE CDR [52]. This is handled by DUNE Beam Optimization Task Force (BOTF) [135].

Since we are interested in studying oscillations at far detector, we would like to optimize the beam of neutrinos for direction and energy relevant to the physics goals. The process involved is

- The primary beam strikes (neutrino production) target in the target hall.
- The product of the interaction of primary beam with the target produces pions and kaons which get collected in the target hall and focussed towards the far detector.

- Among all pions and kaons, only those that are pointed correctly enter the long decay pipe where neutrinos are produced.

The LBNF beamline design has been planned to optimize neutrino flux in appropriate energy range so as to meet the the physics goal of DUNE. In Fig. 3.2, the $\nu_\mu \rightarrow \nu_e$

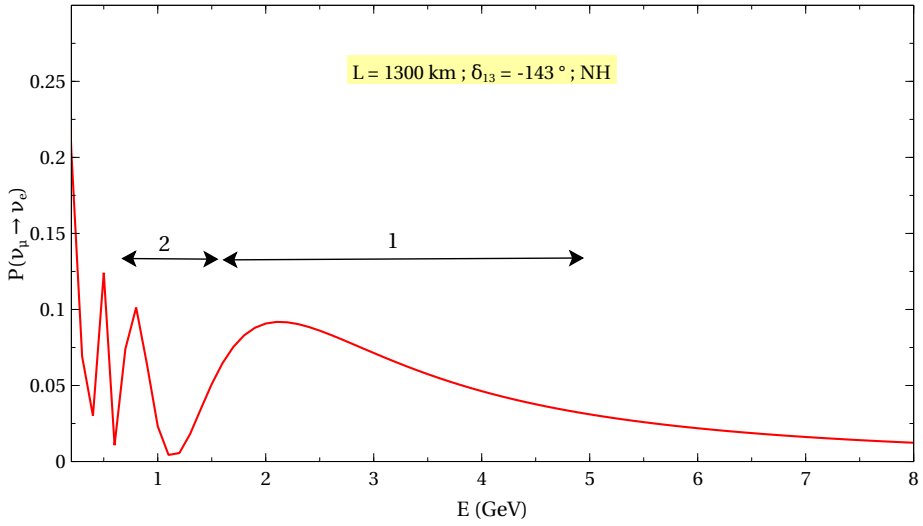

Figure 3.2: Probability of $\nu_\mu \rightarrow \nu_e$ oscillation as a function of energy.

oscillation probability is depicted in the energy range (0.1-8) GeV for a fixed (1300 km) baseline same as the DUNE. One can identify two energy ranges that are useful. The first one corresponds to the region of first oscillation maximum shown as "1" which covers energies between $1.5 - 5$ GeV and the other one corresponds to the region of second oscillation maximum represented as "2" which covers lower energy region in $0.1 - 1.5$ GeV. The neutrino flux must be maximized in the energy range corresponding to the two regions of interest. The higher energy spectrum is produced by pions and kaons of $3.5 - 12$ GeV while the lower energy spectrum by pions and kaons of energies less than a few GeV. The focusing of the charged pions and kaons requires at least two magnetic horns. The focused pions and kaons are collected in the decay pipe where they decay into neutrinos. High energy pions and kaons are mostly collimated with LBNF beamline axis and normally require longer pipe length and smaller pipe diameter where as low energy pions and kaons are widely distributed and require larger pipe diameter. The reference design has a 194 long decay pipe of diameter 4 m, which matches well with the physics of DUNE [52]. The remaining

protons that do not interact with target along with the residual kaons and pions are absorbed in the hadron absorber which is specially designed with aluminium, steel and concrete pile to prevent the radioactivity in the surrounding soil.

After carrying out the optimization procedure, the best-fit beam is depicted in Fig. 3.3 along with the reference beam for comparison. The parameters are given in Table 3.1.

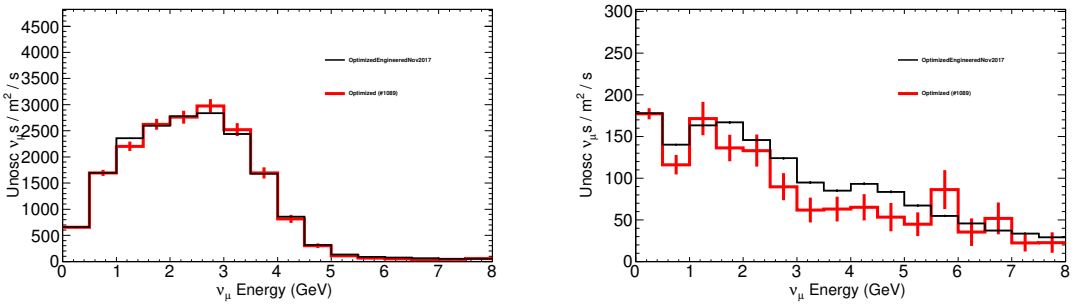

Figure 3.3: ν_μ **in neutrino mode (left) and antineutrino mode (right)**

Parameter	Reference value	Best-fit value
Horn Current (kA)	294	$\approx$ 293
Proton Energy (GeV)	120	$\approx$ 113
Horn B Longitudinal Position (mm)	2957	$\approx$ 3673
Horn C Longitudinal Position (mm)	17477	$\approx$ 14963

Table 3.1: The beam parameters for reference and best-fit beam.

The CP violation sensitivity for the two fluxes is shown in Fig. 3.4. The total runtime is 7 years with 3.5 year in neutrino mode and 3.5 year in antineutrino mode. We have used a 40 Kt liquid Argon detector.

We now come to the discussion of NSI and its impact on the beam optimization procedure. In order to examine the impact of NSI, it is instructive to look at the plot of CP asymmetry as shown in Fig. 3.5 [136].

The CP asymmetry,

$$A_{\mu e}^{CP} = \frac{P(\nu_\mu \to \nu_e) - \bar{P}(\nu_\mu \to \nu_e)}{P(\nu_\mu \to \nu_e) + \bar{P}(\nu_\mu \to \nu_e)} \tag{3.2}$$

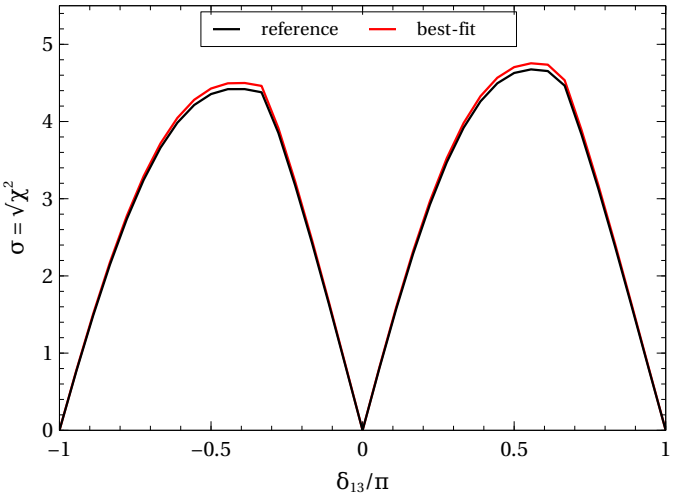

Figure 3.4: CP violation sensitivity for the two fluxes shown above.

is plotted in Fig. 3.5 against the neutrino energy for a fixed baseline of 1300 km. The black solid curve denotes the CP asymmetry for the case of SI with $\delta_{13} = 0$ and the black dashed curve denotes the CP asymmetry in presence of NSI ($|\varepsilon_{e\mu}| = 0.1$) with $\delta_{13}, \phi_{e\mu} = 0$. The two bands, cyan and grey denote the CP asymmetry in the SI and NSI ($\varepsilon_{e\mu} = 0.1$) cases respectively where the phases have been taken in the allowed range (Fig. 3.5). From Fig. 3.5, we find that the difference of CP asymmetry between the SI and NSI case is not too large at around 2.5 GeV. Since the reference flux of 120 GeV optimized engineered beam is peaked around 2.5 GeV, it is expected that the reference beam will give better sensitivity to CP violation. However we also note that the difference between SI and NSI is significantly large at higher energies [136]. This calls for optimizing the neutrino flux at high energies in order to study effects due to NSI and also to disentangle SI from NSI.

3.3.2 Role of the second oscillation maximum at DUNE

The LBL neutrino experiments are planned to exploit the first oscillation maximum of the $\nu_\mu \to \nu_e$ probability (i.e. $L/E \simeq 500$ km/GeV) and the neutrino flux is typically tuned to be peaked at a value of energy corresponding the first oscillation maximum for a given baseline. The location of the dominant phase term in the probability dictates the value of energy since the present unknowns are expected to

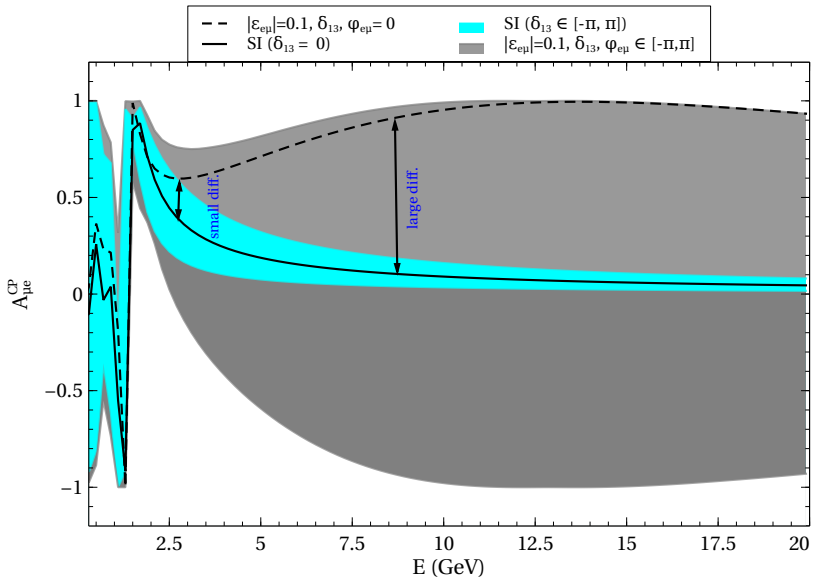

Figure 3.5: CP asymmetry plotted as a function of energy for a baseline of 1300 km relevant for DUNE. The solid (dashed) black curve is for SI case with $\delta_{13} = 0$ (NSI case with non-zero moduli but zero phases). The cyan band is for SI with δ_{13} taking all possible values in the allowed range. The grey band is for NSI with all phases in allowed ranges

be best extracted by using that combination of E and L.

We attempt to elucidate the role of second oscillation maximum in investigating the sensitivity to the standard unknowns in oscillation physics i.e., CP violation, mass hierarchy and octant of θ_{23}. We utilise an optimal beam tune so that the flux at second oscillation maximum is large.

The next generation neutrino oscillation experiments would allow us to precisely determine the known parameters and determine the remaining unknowns in the neutrino oscillation formalism. The LBL neutrino experiments are designed such that the desirable physics outcome is achieved. Typically, the optimal combination is for a value of baseline (L) and energy (E) for which $P_{\mu e}$ has its first peak [137]. This is referred to as the first oscillation maximum. Typically, for shorter baselines, the higher oscillation maximas are unaccessible as the energies at which these occur are too small. For longer baselines, it may be possible to access the information from the second (and higher) oscillation maxima.

A promising future experiment is the Deep Underground Neutrino Experiment

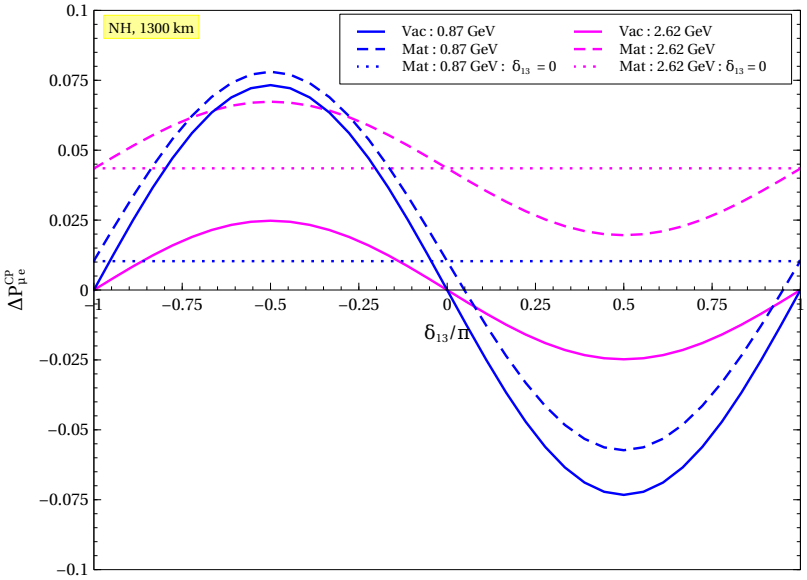

Figure 3.6: $\Delta P^{CP}_{\mu e}$ plotted in vacuum and in matter (for NH) as a function of δ for a fixed baseline of 1300 km and for two fixed energy values corresponding to first and second oscillation maxima.

(DUNE). Neutrino beam will be produced at Fermilab and will travel 1300 km to a liquid Argon (LAr) far detector placed at an on-axis location at Sanford Underground Research Facility (SURF). The primary aim of DUNE is to address the question of CP violation and identify the neutrino mass hierarchy [52]. A wide-band neutrino beam originating from the Fermilab proton complex is considered for DUNE. A systematic evaluation of optimal baseline for discovery of CP violation, determination of the mass hierarchy and resolution of the θ_{23} octant in a LBL oscillation experiment was carried out by Bass et al. [137] and it was concluded that for achieving unambiguous measurement of these parameters, one needed a baseline atleast of the order of 1000 km. It was further shown from the asymmetry plot that CP measurement was better achieved in the vicinity of second oscillation maximum irrespective of the mass hierarchy and results for sensitivities to standard three flavor oscillation parameters were presented. The authors had considered two detector types - Water Cherenkov (WC) and LAr and performed the study for the erstwhile LBNE [52].

Overall, one sees that the probability difference is larger for the energy corresponding to second oscillation maximum ($E = 0.87$ GeV) in comparison to the case

when the energy is pinned to the value at first oscillation maximum ($E = 2.62$ GeV). This holds both in vacuum and in matter for all values of δ. The difference is maximum when δ takes values $\pm\pi/2$. (see Fig. 3.6).

The idea of using the second oscillation maximum is not new. The prospect of using high intensity low energy neutrino beam using Project X was studied in [138] and it was demonstrated the simultaneous operation of 8 GeV and 60 GeV beams in conjunction with a WC detector allows for sensitivity to $\nu_\mu \rightarrow \nu_e$ oscillation at the second oscillation maximum. The focus of the study was to attain high precision measurement of θ_{13} and δ_{CP}. With the goal of enhancing the mass hierarchy sensitivity, the authors of [139] introduced a second detector at an off-axis location (same beam was used) and obtained marginal improvement for certain values of δ_{CP} in the worse half plane of δ_{CP} values. It was shown that one could utilize the larger CP violation signal at the second oscillation maximum at yet another facility called the European Spallation Source (ESS) neutrino Super Beam (ESSnuSB) with a large underground Water Cherenkov detector located at 540 km from Lund, Sweden [140]. Their conclusion was that the second oscillation maximum was advantageous from the view point of discovery of CP violation.

However, it should be noted that, a comprehensive and detailed assessment of the role of different oscillation maxima for a given experiment such as DUNE has not been addressed in the earlier works and this is the main motivation of the ongoing work.

Bibliography

[1] S. L. Glashow, "Partial Symmetries of Weak Interactions," Nucl. Phys. **22**, 579 (1961) ;
S. Weinberg, "A Model of Leptons," Phys. Rev. Lett. **19**, 1264 (1967) ;
A. Salam, Proceedings of the Nobel symposium held 1968 at Lerum, Sweden, Stockholm 1968, 367-377 (Nobel prize 1979 for physics).

[2] L. B. Okun, "Leptons and quarks," Amsterdam, Netherlands : North-Holland (1982) ; F. Halzen and A. D. Martin, "Quarks and leptons : An introductory course in modern particle physics," New York, USA : Wiley (1984) ;
L. H. Ryder, "Quantum Field Theory," Cambridge University Press (1985) ;
M. Peskin and D. Schroeder, "An Introduction to Quantum Field Theory," Addison- Wesly (1995) ;
M. Srednicki, "Quantum Field Theory," Cambridge University Press (1985).

[3] C. Giunti and C. W. Kim, "Fundamentals of Neutrino Physics and Astrophysics," Oxford University Press (2017).

[4] C. W. Kim and A. Pevsner, "Neutrinos in physics and astrophysics," Harwood Academic Publishers, Chur, Switzerland (1993).

[5] P. Minkowski, "Mu $\rightarrow$ E Gamma At A Rate Of One Out Of 1-Billion Muon Decays?," Phys. Lett. B **67**, 421 (1977) ;
T. Yanagida, in *Proceedings of the Workshop on Unified Theories and Baryon Number in the Universe*, edited by O. Sawada and A. Sugamoto, (KEK report 79-18, Tsukuba, Japan, 1979), p. 95; M. Gell-Mann, P. Ramond and R. Slansky, *Complex spinors and unified theories*, in *Supergravity*, edited by P. van

Nieuwenhuizen and D. Z. Freedman, (North-Holland, Amsterdam, 1979) p. 315 ;

S. L. Glashow, *The future of elementary particle physics* in *Proceedings of the 1979 Cargèse Summer Institute on Quarks and Leptons*, edited by M. Lévy *et.al.* , (Plenum Press, New York, USA, 1980), p. 687-713 ; and

R. N. Mohapatra and G. Senjanovic, "Neutrino mass and spontaneous parity nonconservation," Phys. Rev. Lett. **44**, 912 (1980).

[6] S. Davidson, E. Nardi and Y. Nir, "Leptogenesis," Phys. Rept. **466**, 105 (2008).

[7] J. Schechter and J. W. F. Valle, "Neutrinoless Double beta Decay in SU(2) x U(1) Theories," Phys. Rev. D **25**, 2951 (1982).

[8] M. C. Gonzalez-Garcia and Y. Nir, "Neutrino masses and mixing: Evidence and implications," Rev. Mod. Phys. **75**, 345 (2003).

[9] M. Tanabashi *et al.* [Particle Data Group], "Review of Particle Physics," Phys. Rev. D **98**, no. 3, 030001 (2018).

[10] S. F. King, "Unified Models of Neutrinos, Flavour and CP Violation," Prog. Part. Nucl. Phys. **94**, 217 (2017).

[11] B. Pontecorvo, "Neutrino Experiments and the Problem of Conservation of Leptonic Charge," Sov. Phys. JETP **26**, 984 (1968) [Zh. Eksp. Teor. Fiz. **53**, 1717 (1967)] ;

Z. Maki, M. Nakagawa and S. Sakata, "Remarks on the unified model of elementary particles," Prog. Theor. Phys. **28**, 870 (1962).

[12] B. Pontecorvo, "Mesonium and anti-mesonium," Sov. Phys. JETP **6**, 429 (1957) [Zh. Eksp. Teor. Fiz. **33**, 549 (1957)].

[13] T. Kajita and A. B. McDonald, "The Nobel Prize in Physics 2015," (2015).

[14] G. G. Raffelt, "Stars as laboratories for fundamental physics : The astrophysics of neutrinos, axions, and other weakly interacting particles," Chicago, USA: University Press (1996).

[15] C. Jarlskog, "Commutator of the Quark Mass Matrices in the Standard Electroweak Model and a Measure of Maximal CP Violation," Phys. Rev. Lett. **55**, 1039 (1985).

[16] L. Wolfenstein, "Neutrino Oscillations in Matter," Phys. Rev. D **17**, 2369 (1978); S. P. Mikheyev and A. Y. Smirnov, "Resonance Amplification of Oscillations in Matter and Spectroscopy of Solar Neutrinos," Sov. J. Nucl. Phys. **42**, 913 (1985).

[17] H. A. Bethe, "A Possible Explanation of the Solar Neutrino Puzzle," Phys. Rev. Lett. **56**, 1305 (1986).

[18] V. D. Barger, K. Whisnant, S. Pakvasa and R. J. N. Phillips, "Matter Effects on Three-Neutrino Oscillations," Phys. Rev. D **22**, 2718 (1980).

[19] A. Cervera, A. Donini, M. B. Gavela, J. J. Gomez Cadenas, P. Hernandez, O. Mena and S. Rigolin, "Golden measurements at a neutrino factory," Nucl. Phys. B **579**, 17 (2000) Erratum: [Nucl. Phys. B **593**, 731 (2001)].

[20] M. Freund, "Analytic approximations for three neutrino oscillation parameters and probabilities in matter," Phys. Rev. D **64**, 053003 (2001).

[21] E. K. Akhmedov, R. Johansson, M. Lindner, T. Ohlsson and T. Schwetz, "Series expansions for three flavor neutrino oscillation probabilities in matter," JHEP **0404**, 078 (2004).

[22] R. Gandhi, P. Ghoshal, S. Goswami, P. Mehta and S. U. Sankar, "Large matter effects in nu(mu) $\rightarrow$ nu(tau) oscillations," Phys. Rev. Lett. **94**, 051801 (2005).

[23] R. Gandhi, P. Ghoshal, S. Goswami, P. Mehta and S. U. Sankar, "Earth matter effects at very long baselines and the neutrino mass hierarchy," Phys. Rev. D **73**, 053001 (2006).

[24] E. K. Akhmedov, "Three-flavor effects and CP- and T-violation in neutrino oscillations," Phys. Scripta T **121**, 65 (2005).

[25] W. Marciano and Z. Parsa, "Intense neutrino beams and leptonic CP violation," Nucl. Phys. Proc. Suppl. **221**, 166 (2011).

[26] I. Esteban, M. C. Gonzalez-Garcia, A. Hernandez-Cabezudo, M. Maltoni and T. Schwetz, "Global analysis of three-flavour neutrino oscillations: synergies and tensions in the determination of θ_{23}, δ_{CP}, and the mass ordering," JHEP **1901**, 106 (2019).

[27] P. F. Harrison, D. H. Perkins and W. G. Scott, "Tri-bimaximal mixing and the neutrino oscillation data," Phys. Lett. B **530**, 167 (2002).

[28] M. C. Gonzalez-Garcia and M. Maltoni, "Phenomenology with Massive Neutrinos," Phys. Rept. **460**, 1 (2008) ;
S. M. Bilenky and B. Pontecorvo, "Lepton Mixing and Neutrino Oscillations," Phys. Rept. **41**, 225 (1978).

[29] J. Kelley, UW-Madison, September 2005, "Solar fusion cross sections II: the pp chain and CNO cycles," https://icecube.wisc.edu/ jkelley/atm/proposal.html ; N. G. Cooper, "Solar fusion cross sections II: the pp chain and CNO cycles," Los Alamos Science, Number 25 –1997: Celebrating the neutrino.

[30] M. Honda, T. Kajita, K. Kasahara and S. Midorikawa, "A New calculation of the atmospheric neutrino flux in a 3-dimensional scheme," Phys. Rev. D **70**, 043008 (2004).

[31] G. D. Barr, T. K. Gaisser, P. Lipari, S. Robbins and T. Stanev, "A Three - dimensional calculation of atmospheric neutrinos," Phys. Rev. D **70**, 023006 (2004).

[32] G. Battistoni, A. Ferrari, T. Montaruli and P. R. Sala, "High-energy extension of the FLUKA atmospheric neutrino flux," hep-ph/0305208.

[33] J. N. Bahcall and W. C. Haxton, "Matter Enhanced Neutrino Oscillations in the Standard Solar Model," Phys. Rev. D **40**, 931 (1989).

[34] E. G. Adelberger *et al.*, "Solar fusion cross sections II: the pp chain and CNO cycles," Rev. Mod. Phys. **83**, 195 (2011).

[35] J. G. Learned and K. Mannheim, "High-energy neutrino astrophysics," Ann. Rev. Nucl. Part. Sci. **50**, 679 (2000).

[36] N. Agafonova *et al.* [OPERA Collaboration], "Observation of a first ν_τ candidate in the OPERA experiment in the CNGS beam," Phys. Lett. B **691**, 138 (2010).

[37] S. Amerio *et al.* [ICARUS Collaboration], "Design, construction and tests of the ICARUS T600 detector," Nucl. Instrum. Meth. A **527**, 329 (2004).

[38] M. A. Acero *et al.* [NOvA Collaboration], "New constraints on oscillation parameters from ν_e appearance and ν_μ disappearance in the NOvA experiment," Phys. Rev. D **98**, 032012 (2018) ;
D. S. Ayres *et al.* [NOvA Collaboration], "NOvA: Proposal to Build a 30 Kiloton Off-Axis Detector to Study $\nu_\mu \to \nu_e$ Oscillations in the NuMI Beamline," hep-ex/0503053.

[39] K. Abe *et al.* [T2K Collaboration], "Search for CP Violation in Neutrino and Antineutrino Oscillations by the T2K Experiment with 2.2×10^{21} Protons on Target," Phys. Rev. Lett. **121**, no. 17, 171802 (2018) ;
K. Abe *et al.* [T2K Collaboration], "Neutrino oscillation physics potential of the T2K experiment," PTEP **2015**, no. 4, 043C01 (2015).

[40] M. Apollonio *et al.* [CHOOZ Collaboration], "Limits on neutrino oscillations from the CHOOZ experiment," Phys. Lett. B **466**, 415 (1999) ;
M. Apollonio *et al.* [CHOOZ Collaboration], "Initial results from the CHOOZ long baseline reactor neutrino oscillation experiment," Phys. Lett. B **420**, 397 (1998) doi:10.1016/S0370-2693(97)01476-7 [hep-ex/9711002].

[41] Y. Abe *et al.* [Double Chooz Collaboration], "Improved measurements of the neutrino mixing angle θ_{13} with the Double Chooz detector," JHEP **1410**, 086 (2014); Erratum: [JHEP **1502**, 074 (2015)] ; F. Ardellier *et al.* [Double

Chooz Collaboration], "Double Chooz: A Search for the neutrino mixing angle theta(13)," hep-ex/0606025 ; Y. Abe *et al.* [Double Chooz Collaboration], "Indication of Reactor $\bar{\nu}_e$ Disappearance in the Double Chooz Experiment," Phys. Rev. Lett. **108**, 131801 (2012).

[42] A. Piepke [Palo Verde Collaboration], "Final results from the Palo Verde neutrino oscillation experiment," Prog. Part. Nucl. Phys. **48**, 113 (2002) ; F. Boehm *et al.* [Palo Verde Collaboration], "The Palo Verde reactor neutrino oscillation experiment," Nucl. Phys. Proc. Suppl. **77**, 166 (1999).

[43] K. Eguchi *et al.* [KamLAND Collaboration], "First results from KamLAND: Evidence for reactor anti-neutrino disappearance," Phys. Rev. Lett. **90**, 021802 (2003);
S. Abe *et al.* [KamLAND Collaboration], "Precision Measurement of Neutrino Oscillation Parameters with KamLAND," Phys. Rev. Lett. **100**, 221803 (2008).

[44] F. P. An *et al.* [Daya Bay Collaboration], "Observation of electron-antineutrino disappearance at Daya Bay," Phys. Rev. Lett. **108**, 171803 (2012) ;
X. Guo *et al.* [Daya Bay Collaboration], "A Precision measurement of the neutrino mixing angle θ_{13} using reactor antineutrinos at Daya-Bay," hep-ex/0701029.

[45] J. K. Ahn *et al.* [RENO Collaboration], "Observation of Reactor Electron Antineutrino Disappearance in the RENO Experiment," Phys. Rev. Lett. **108**, 191802 (2012).

[46] A. Bandyopadhyay *et al.* [ISS Physics Working Group], "Physics at a future Neutrino Factory and super-beam facility," Rept. Prog. Phys. **72**, 106201 (2009) ;
C. Albright *et al.*, "Physics at a neutrino factory," hep-ex/0008064 ;
A. De Rujula, M. B. Gavela and P. Hernandez, "Neutrino oscillation physics with a neutrino factory," Nucl. Phys. B **547**, 21 (1999).

[47] Y. Fukuda *et al.* [Super-Kamiokande Collaboration], "Evidence for oscillation of atmospheric neutrinos," Phys. Rev. Lett. **81**, 1562 (1998).

[48] K. Abe *et al.* [Hyper-Kamiokande Collaboration], "Hyper-Kamiokande Design Report," arXiv:1805.04163 [physics.ins-det].

[49] L. Agostino *et al.* [MEMPHYS Collaboration], "Study of the performance of a large scale water-Cherenkov detector (MEMPHYS)," JCAP **1301**, 024 (2013) ;

A. de Bellefon *et al.*, "MEMPHYS: A Large scale water Cerenkov detector at Frejus," hep-ex/0607026.

[50] M. H. Ahn *et al.* [K2K Collaboration], "Measurement of Neutrino Oscillation by the K2K Experiment," Phys. Rev. D **74**, 072003 (2006).

[51] P. Adamson *et al.* [MINOS Collaboration], "Measurement of Neutrino and Antineutrino Oscillations Using Beam and Atmospheric Data in MINOS," Phys. Rev. Lett. **110**, no. 25, 251801 (2013).

[52] T. Alion *et al.* [DUNE Collaboration], "Experiment Simulation Configurations Used in DUNE CDR," 1606.09550 [physics.ins-det] ;

R. Acciarri *et al.* [DUNE Collaboration], "Long-Baseline Neutrino Facility (LBNF) and Deep Underground Neutrino Experiment (DUNE) : Conceptual Design Report, Volume 2: The Physics Program for DUNE at LBNF," arXiv:1512.06148 [physics.ins-det] ;

B. Abi *et al.* [DUNE Collaboration], "The DUNE Far Detector Interim Design Report Volume 1: Physics, Technology and Strategies," arXiv:1807.10334 [physics.ins-det].

[53] M. S. Athar *et al.* [INO Collaboration], "India-based Neutrino Observatory: Project Report. Volume I.," INO-2006-01.

[54] C. Athanassopoulos *et al.* [LSND Collaboration], "Evidence for anti-muon neutrino $\rightarrow$ anti-electron neutrino oscillations from the LSND experiment at LAMPF," Phys. Rev. Lett. **77**, 3082 (1996) ;

A. Aguilar-Arevalo *et al.* [LSND Collaboration], "Evidence for neutrino oscillations from the observation of anti-neutrino(electron) appearance in a anti-neutrino(muon) beam," Phys. Rev. D **64**, 112007 (2001).

[55] C. Adams *et al.* [LBNE Collaboration], "The Long-Baseline Neutrino Experiment: Exploring Fundamental Symmetries of the Universe," arXiv:1307.7335 [hep-ex] ;
M. V. Diwan, V. Galymov, X. Qian and A. Rubbia, "Long-Baseline Neutrino Experiments," Ann. Rev. Nucl. Part. Sci. **66**, 47 (2016).

[56] G. J. Feldman, "History of Long-Baseline Accelerator Neutrino Experiments," arXiv:1901.09431 [hep-ex] ;
U. Dore, P. Loverre and L. Ludovici, "History of accelerator neutrino beams," arXiv:1805.01373 [physics.acc-ph].

[57] A. K. Ichikawa, "High intensity neutrino beams," AIP Conference Proceedings 1666, 130001 (2015).

[58] T. Ohlsson, "Status of non-standard neutrino interactions," Rept. Prog. Phys. **76**, 044201 (2013).

[59] Y. Farzan and M. Tortola, "Neutrino oscillations and Non-Standard Interactions," Front. in Phys. **6**, 10 (2018).

[60] I. Esteban, M. C. Gonzalez-Garcia and M. Maltoni, "On the Determination of Leptonic CP Violation and Neutrino Mass Ordering in Presence of Non-Standard Interactions: Present Status," JHEP **1906**, 055 (2019).

[61] P. S. Bhupal Dev *et al.*, "Neutrino Non-Standard Interactions: A Status Report," [arXiv:1907.00991 [hep-ph]].

[62] S. Davidson, C. Pena-Garay, N. Rius and A. Santamaria, "Present and future bounds on nonstandard neutrino interactions," JHEP **0303**, 011 (2003).

[63] C. Biggio, M. Blennow and E. Fernandez-Martinez, "General bounds on non-standard neutrino interactions," JHEP **0908**, 090 (2009).

[64] G. Mitsuka *et al.* [Super-Kamiokande Collaboration], "Study of Non-Standard Neutrino Interactions with Atmospheric Neutrino Data in Super-Kamiokande I and II," Phys. Rev. D **84**, 113008 (2011).

[65] P. Adamson *et al.* [MINOS Collaboration], "Search for flavor-changing non-standard neutrino interactions by MINOS," Phys. Rev. D **88**, no. 7, 072011 (2013).

[66] J. Kopp, P. A. N. Machado and S. J. Parke, "Interpretation of MINOS Data in Terms of Non-Standard Neutrino Interactions," Phys. Rev. D **82**, 113002 (2010).

[67] M. C. Gonzalez-Garcia and M. Maltoni, JHEP **1309**, 152 (2013).

[68] T. Kikuchi, H. Minakata and S. Uchinami, "Perturbation Theory of Neutrino Oscillation with Nonstandard Neutrino Interactions," JHEP **0903**, 114 (2009).

[69] K. Asano and H. Minakata, "Large-Theta(13) Perturbation Theory of Neutrino Oscillation for Long-Baseline Experiments," JHEP **1106**, 022 (2011).

[70] J. Kopp, M. Lindner, T. Ota and J. Sato, Phys. Rev. D **77**, 013007 (2008).

[71] B. Pontecorvo, "Neutrino Experiments and the Problem of Conservation of Leptonic Charge," Sov. Phys. JETP **26**, 984 (1968).

[72] "Sterile Neutrino Fits" by C. Giunti, https://neutel11.wordpress.com/2011/03/17/sterile-neutrino-fits-by-carlo-giunti.

[73] C. Giunti, "Sterile Neutrino Fits," [arXiv:1106.4479 [hep-ph]].

[74] C. Giunti and T. Lasserre, "eV-scale Sterile Neutrinos," [arXiv:1901.08330 [hep-ph]].

[75] P. A. Machado, O. Palamara and D. W. Schmitz, "The Short-Baseline Neutrino Program at Fermilab," Ann. Rev. Nucl. Part. Sci. **69**.

[76] J. Kopp, "The Plot Thickens for a Fourth Neutrino," APS Physics **11**, 122 (2018).

[77] A. A. Aguilar-Arevalo *et al.* [MiniBooNE Collaboration], "Significant Excess of ElectronLike Events in the MiniBooNE Short-Baseline Neutrino Experiment," Phys. Rev. Lett. **121**, no. 22, 221801 (2018).

[78] R. Gandhi, B. Kayser, M. Masud and S. Prakash, "The impact of sterile neutrinos on CP measurements at long baselines," JHEP **1511**, 039 (2015).

[79] P. Huber, M. Lindner and W. Winter, "Simulation of long-baseline neutrino oscillation experiments with GLoBES (General Long Baseline Experiment Simulator)," Comput. Phys. Commun. **167**, 195 (2005).

[80] F. Capozzi, G. Fogli, E. Lisi, A. Marrone, D. Montanino, et al., "Neutrino Reactions At Accelerator Energies," Phys. Rev. **D89(9)**, 093018 (2014).

[81] D. V. Forero, M. Tortola and J. W. F. Valle, "Neutrino oscillations refitted," Phys. Rev. D **90**, no. 9, 093006 (2014).

[82] I. Esteban, M. C. Gonzalez-Garcia, M. Maltoni, I. Martinez-Soler and T. Schwetz, "Updated fit to three neutrino mixing: exploring the accelerator-reactor complementarity," JHEP **1701**, 087 (2017).

[83] S. Parke and M. Ross-Lonergan, "Unitarity and the three flavor neutrino mixing matrix," Phys. Rev. D **93**, no. 11, 113009 (2016).

[84] Y. Farzan and A. Y. Smirnov, "Leptonic unitarity triangle and CP violation," Phys. Rev. D **65**, 113001 (2002).

[85] M. Kobayashi and T. Maskawa, "CP Violation in the Renormalizable Theory of Weak Interaction," Prog. Theor. Phys. **49**, 652 (1973).

[86] J. Arafune, M. Koike and J. Sato, "CP violation and matter effect in long baseline neutrino oscillation experiments," Phys. Rev. D **56**, 3093 (1997).

[87] S. M. Bilenky, C. Giunti and W. Grimus, "Long baseline neutrino oscillation experiments and CP violation in the lepton sector," Phys. Rev. D **58**, 033001 (1998).

[88] J. Burguet-Castell, M. B. Gavela, J. J. Gomez-Cadenas, P. Hernandez and O. Mena, "On the Measurement of leptonic CP violation," Nucl. Phys. B **608**, 301 (2001).

[89] H. Nunokawa, S. J. Parke and J. W. F. Valle, "CP Violation and Neutrino Oscillations," Prog. Part. Nucl. Phys. **60**, 338 (2008).

[90] G. C. Branco, R. G. Felipe and F. R. Joaquim, "Leptonic CP Violation," Rev. Mod. Phys. **84**, 515 (2012).

[91] T. Ohlsson, H. Zhang and S. Zhou, "Probing the leptonic Dirac CP-violating phase in neutrino oscillation experiments," Phys. Rev. D **87**, no. 5, 053006 (2013).

[92] H. Minakata and H. Nunokawa, "Measuring leptonic CP violation by low-energy neutrino oscillation experiments," Phys. Lett. B **495**, 369 (2000).

[93] M. Masud, A. Chatterjee and P. Mehta, "Probing CP violation signal at DUNE in presence of non-standard neutrino interactions," J. Phys. G **43**, no. 9, 095005 (2016).

[94] A. de Gouvêa and K. J. Kelly, "Non-standard Neutrino Interactions at DUNE," Nucl. Phys. B **908**, 318 (2016).

[95] P. Coloma, "Non-Standard Interactions in propagation at the Deep Underground Neutrino Experiment," JHEP **1603**, 016 (2016).

[96] M. Masud and P. Mehta, "Nonstandard interactions spoiling the CP violation sensitivity at DUNE and other long baseline experiments," Phys. Rev. D **94**, 013014 (2016).

[97] M. Masud and P. Mehta, "Nonstandard interactions and resolving the ordering of neutrino masses at DUNE and other long baseline experiments," Phys. Rev. D **94**, no. 5, 053007 (2016).

[98] M. Blennow, S. Choubey, T. Ohlsson, D. Pramanik and S. K. Raut, "A combined study of source, detector and matter non-standard neutrino interactions at DUNE," JHEP **1608**, 090 (2016).

[99] D. V. Forero and P. Huber, "Hints for leptonic CP violation or New Physics?," Phys. Rev. Lett. **117**, no. 3, 031801 (2016).

[100] A. de Gouvêa and K. J. Kelly, "False Signals of CP-Invariance Violation at DUNE," arXiv:1605.09376 [hep-ph].

[101] S. Fukasawa, M. Ghosh and O. Yasuda, "Sensitivity of the T2HKK experiment to nonstandard interactions," Phys. Rev. D **95**, no. 5, 055005 (2017).

[102] J. Liao, D. Marfatia and K. Whisnant, "Nonstandard neutrino interactions at DUNE, T2HK and T2HKK," JHEP **1701**, 071 (2017).

[103] S. K. Agarwalla, S. S. Chatterjee, A. Dasgupta and A. Palazzo, "Discovery Potential of T2K and NOvA in the Presence of a Light Sterile Neutrino," JHEP **1602**, 111 (2016).

[104] S. K. Agarwalla, S. S. Chatterjee and A. Palazzo, "Physics Reach of DUNE with a Light Sterile Neutrino," JHEP **1609**, 016 (2016).

[105] S. Choubey and D. Pramanik, "Constraints on Sterile Neutrino Oscillations using DUNE Near Detector," Phys. Lett. B **764**, 135 (2017).

[106] D. Dutta, R. Gandhi, B. Kayser, M. Masud and S. Prakash, "Capabilities of long-baseline experiments in the presence of a sterile neutrino," JHEP **1611**, 122 (2016).

[107] S. K. Agarwalla, S. S. Chatterjee and A. Palazzo, "Octant of θ_{23} in danger with a light sterile neutrino," Phys. Rev. Lett. **118**, no. 3, 031804 (2017).

[108] M. Blennow, P. Coloma, E. Fernandez-Martinez, J. Hernandez-Garcia and J. Lopez-Pavon, "Non-Unitarity, sterile neutrinos, and Non-Standard neutrino Interactions," JHEP **1704**, 153 (2017).

[109] K. N. Deepthi, S. Goswami and N. Nath, "Can nonstandard interactions jeopardize the hierarchy sensitivity of DUNE?," Phys. Rev. D **96**, no. 7, 075023 (2017).

[110] S. F. Ge, P. Pasquini, M. Tortola and J. W. F. Valle, "Measuring the leptonic CP phase in neutrino oscillations with nonunitary mixing," Phys. Rev. D **95**, no. 3, 033005 (2017).

[111] D. Dutta and P. Ghoshal, "Probing CP violation with T2K, NOνA and DUNE in the presence of non-unitarity," JHEP **1609**, 110 (2016).

[112] O. G. Miranda, M. Tortola and J. W. F. Valle, "New ambiguity in probing CP violation in neutrino oscillations," Phys. Rev. Lett. **117**, no. 6, 061804 (2016).

[113] F. J. Escrihuela, D. V. Forero, O. G. Miranda, M. Trtola and J. W. F. Valle, "Probing CP violation with non-unitary mixing in long-baseline neutrino oscillation experiments: DUNE as a case study," New J. Phys. **19**, no. 9, 093005 (2017).

[114] C. S. Fong, H. Minakata and H. Nunokawa, "A framework for testing leptonic unitarity by neutrino oscillation experiments," JHEP **1702**, 114 (2017).

[115] E. K. Akhmedov, P. Huber, M. Lindner and T. Ohlsson, "T violation in neutrino oscillations in matter," Nucl. Phys. B **608**, 394 (2001).

[116] Z. z. Xing, "Leptonic commutators and clean T violation in neutrino oscillations," Phys. Rev. D **88**, no. 1, 017301 (2013).

[117] P. I. Krastev and S. T. Petcov, "Resonance Amplification and T Violation Effects in Three Neutrino Oscillations in the Earth," Phys. Lett. B **205**, 84 (1988).

[118] S. Toshev, "On T violation in matter neutrino oscillations," Mod. Phys. Lett. A **6**, 455 (1991).

[119] P. Mehta, "Topological phase in two flavor neutrino oscillations," Phys. Rev. D **79**, 096013 (2009).

[120] P. Mehta, "Geometric imprint of CP violation in two flavor neutrino oscillations," hep-ph/0907.0562.

[121] Y. Farzan and A. Y. Smirnov, "Leptonic CP violation: Zero, maximal or between the two extremes," JHEP **0701**, 059 (2007).

[122] M. Y. Khlopov and S. T. Petcov, "Possible cosmological effect of CP violation in neutrino oscillations," Phys. Lett. **99B**, 117 (1981).

[123] Z. z. Xing, "New formulation of matter effects on neutrino mixing and CP violation," Phys. Lett. B **487**, 327 (2000).

[124] S. Antusch, J. P. Baumann and E. Fernandez-Martinez, "Non-Standard Neutrino Interactions with Matter from Physics Beyond the Standard Model," Nucl. Phys. B **810**, 369 (2009).

[125] Y. Farzan, "A model for large non-standard interactions of neutrinos leading to the LMA-Dark solution," Phys. Lett. B **748**, 311 (2015).

[126] Y. Farzan and I. M. Shoemaker, "Lepton Flavor Violating Non-Standard Interactions via Light Mediators," JHEP **1607**, 033 (2016).

[127] D. V. Forero and W. C. Huang, "Sizable NSI from the $SU(2)_L$ scalar doublet-singlet mixing and the implications in DUNE," JHEP **1703**, 018 (2017).

[128] F. P. An *et al.* [Daya Bay Collaboration], "Search for a Light Sterile Neutrino at Daya Bay," Phys. Rev. Lett. **113**, 141802 (2014).

[129] B. Jones, Results of the Search for Sterile Neutrinos with IceCube, talk at FermiLab, February 12, 2016. https://hep.uchicago.edu/seminars/semwin2016/BenJones1. pdf (2016).

[130] P. Adamson *et al.* [MINOS Collaboration], "Active to sterile neutrino mixing limits from neutral-current interactions in MINOS," Phys. Rev. Lett. **107**, 011802 (2011)

[131] J. Kopp, P. A. N. Machado, M. Maltoni and T. Schwetz, "Sterile Neutrino Oscillations: The Global Picture," JHEP **1305**, 050 (2013).

[132] G. H. Collin, C. A. Argüelles, J. M. Conrad and M. H. Shaevitz, "First Constraints on the Complete Neutrino Mixing Matrix with a Sterile Neutrino," Phys. Rev. Lett. **117**, no. 22, 221801 (2016).

[133] O. Mena and S. J. Parke, "Unified graphical summary of neutrino mixing parameters," Phys. Rev. D **69**, 117301 (2004).

[134] L. Fields, "Genetic Optimization of the LBNF/DUNE Beamline II.", DUNE DocDB 1151. URL - http://docs.dunescience.org:8080/cgi-bin/ShowDocument?docid=1151.

[135] L. Fields and A. Weber, "Beam Optimization Task Force Final Report," June 2017, URL - https://docs.dunescience.org/cgi-bin/private/ShowDocument?docid=2901.

[136] M. Masud, M. Bishai and P. Mehta, "Extricating New Physics Scenarios at DUNE with Higher Energy Beams," Sci. Rep. **9**, no. 1, 352 (2019).

[137] M. Bass *et al.*, "Baseline Optimization for the Measurement of CP Violation, Mass Hierarchy, and θ_{23} Octant in a Long-Baseline Neutrino Oscillation Experiment," Phys. Rev. D **91**, no. 5, 052015 (2015).

[138] M. Bishai, M. Diwan, S. Kettell, J. Stewart, B. Viren, E. Worcester, R. Tschirhart and L. Whitehead, "Precision Neutrino Oscillation Measurements using Simultaneous High-Power, Low-Energy Project-X Beams," arXiv:1307.0807 [hep-ex].

[139] X. Qian, J. J. Ling, R. D. McKeown, W. Wang, E. Worcester and C. Zhang, "A Second Detector Focusing on the Second Oscillation Maximum at an Off-

axis Location to Enhance the Mass Hierarchy Discovery Potential in LBNE10," arXiv:1307.7406 [hep-ex].

[140] E. Wildner *et al.*, "The Opportunity Offered by the ESSnuSB Project to Exploit the Larger Leptonic CP Violation Signal at the Second Oscillation Maximum and the Requirements of This Project on the ESS Accelerator Complex," Adv. High Energy Phys. **2016**, 8640493 (2016).

[141] J. Liao, D. Marfatia and K. Whisnant, "Degeneracies in long-baseline neutrino experiments from nonstandard interactions," Phys. Rev. D **93**, no. 9, 093016 (2016).

Appendix A

A.1 Effective potentials in matter

The interaction of neutrinos while propagating through matter, which could be coherent or incoherent, affects their properties. For purely incoherent inelastic ν-p scattering, the characteristic cross section, which is very small, is given by:

$$\sigma \sim \frac{G_F^2 s}{\pi} \sim 10^{-43}\text{cm}^2 \left(\frac{E}{1\text{ MeV}}\right)^2 . \tag{A.1}$$

The minuteness of this cross section is appreciated by the fact that if a beam of 10^{10} neutrinos with $E \sim 1$ MeV was aimed at the Earth, only one would be deflected. The matter is enhanced by the contribution from forward elastic coherent interactions. The medium remains unchanged in coherent interactions rendering the interference of scattered and unscattered neutrino possile, waves which enhances the effect. Coherence further decouples the evolution equation of the neutrinos from the equations of the medium. Here, the effect of the medium is described by an effective potential which depends on the density and composition of the matter [16].

We derive the effective potential for the evolution of ν_e in a medium. The effective low-energy Hamiltonian describing the relevant neutrino interactions is given by

$$H_W = \frac{G_F}{\sqrt{2}}[J^{(+)\mu}(x)J_\mu^{(-)}(x) + \frac{1}{4}J^{(N)\mu}(x)J_\mu^{(N)}(x)] \tag{A.2}$$

where the J_μ's are the standard fermionic currents,

$$J_\mu^{(+)}(x) = \overline{\nu_e}(x)\gamma_\mu(1-\gamma_5)e(x) \quad (A.3)$$

$$J_\mu^{(-)}(x) = \overline{e}(x)\gamma_\mu(1-\gamma_5)\nu_e(x) \quad (A.4)$$

$$J_\mu^{(N)}(x) = \overline{\nu_e}(x)\gamma_\mu(1-\gamma_5)\nu_e(x) - \overline{e}(x)[\gamma_\mu(1-\gamma_5) - 4\sin^2\theta_W\gamma_\mu]e(x)$$
$$+ \overline{p}(x)[\gamma_\mu(1-g_A^{(p)}\gamma_5) - 4\sin^2\theta_W\gamma_\mu]p(x) - \overline{n}(x)\gamma_\mu(1-g_A^{(n)}\gamma_5)n(x) \quad (A.5)$$

$g_A^{(n,p)}$ are the axial couplings for neutrons and protons, respectively. Now, we concentrate on the effect of the CC interactions. The effective CC Hamiltonian due to electrons in the medium is

$$H_C^{(e)} = \frac{G_F}{\sqrt{2}} \int d^3p_e f(E_e,T) \quad (A.6)$$
$$\times \left\langle \langle e(s,p_e)|\overline{e}(x)\gamma^\mu(1-\gamma_5)\nu_e(x)\overline{\nu_e}(x)\gamma_\mu(1-\gamma_5)e(x)|e(s,p_e)\rangle \right\rangle$$
$$= \frac{G_F}{\sqrt{2}}\overline{\nu_e}(x)\gamma_\mu(1-\gamma_5)\nu_e(x)\int d^3p_e f(E_e,T)\left\langle \langle e(s,p_e)|\overline{e}(x)\gamma_\mu(1-\gamma_5)e(x)|e(s,p_e)\rangle \right\rangle$$

where s is the electron spin and p_e its momentum. The energy distribution function of the electrons in the medium, $f(E_e,T)$, is assumed to be homogeneous and isotropic and is normalized as

$$\int d^3p_e f(E_e,T) = 1 \quad (A.7)$$

By $\left\langle ... \right\rangle$ we denote the averaging over electron spinors and summing over all electrons in the medium. Notice that coherence implies that s, p_e are the same for initial and final electrons.

Expanding the electron fields $e(x)$ in plane waves we find

$$\langle e(s,p_e) \quad | \quad \overline{e}(x)\gamma_\mu(1-\gamma_5)e(x)|e(s,p_e)\rangle$$
$$= \frac{1}{V}\langle e(s,p_e) \quad | \quad \overline{u_s}(p_e)a_s^\dagger(p_e)\gamma_\mu(1-\gamma_5)a_s(p_e)u_s(p_e)|e(s,p_e)\rangle \quad (A.8)$$

where V is a volume normalization factor. The averaging gives

$$\frac{1}{V}\left\langle \langle e(s,p_e)|a_s^\dagger(p_e)a_s(p_e)|e(s,p_e)\rangle \right\rangle = n_e(p_e)\frac{1}{2}\sum_s \quad (A.9)$$

where $n_e(p_e)$ is the number density of electrons with momentum p_e. We assumed here that the medium has equal numbers of spin $+1/2$ and spin $-1/2$ electrons, and we

used the fact that $a_s^\dagger(p_e)a_s(p_e) = \mathcal{N}_e^{(s)}(p_e)$ is the number operator. We thus obtain:

$$\left\langle \langle e(s,p_e)|\overline{e}(x)\gamma_\mu(1-\gamma_5)e(x)|e(s,p_e)\rangle \right\rangle = n_e(p_e)\frac{1}{2}\sum_s \overline{u_{(s)}}(p_e)\gamma_\mu(1-\gamma_5)u_{(s)}(p_e)$$
$$= \frac{n_e(p_e)}{2}\mathrm{Tr}\Big[\frac{m_e+\not{p}}{2E_e}\gamma_\mu(1-\gamma_5)\Big] = n_e(p_e)\frac{p_e^\mu}{E_e} \quad \text{(A.10)}$$

Isotropy implies that $\int d^3p_e\vec{p_e}f(E_e,T) = 0$. Thus, only the p^0 term contributes upon integration, with $\int d^3p_e f(E_e,T)n_e(p_e) = n_e$ (the electron number density). Substituting Eq. A.10 in Eq. A.6 we obtain:

$$H_C^{(e)} = \frac{G_F n_e}{\sqrt{2}}\overline{\nu_e}(x)\gamma_0(1-\gamma_5)\nu_e(x) \quad \text{(A.11)}$$

The effective potential for ν_e induced by its CC interactions with electrons in matter is then given by

$$V_C = \langle\nu_e|\int d^3x\ H_C^{(e)}|\nu_e\rangle = \frac{G_F n_e}{\sqrt{2}}\frac{2}{V}\int d^3x\ u_\nu^\dagger u_\nu = \sqrt{2}G_F n_e \quad \text{(A.12)}$$

For $\overline{\nu_e}$ the sign of V is reversed. This potential can also be expressed in terms of the matter density ρ:

$$V_C = \sqrt{2}G_F n_e \simeq 7.6\,Y_e\,\frac{\rho}{10^{14}\mathrm{g/cm}^3}\ \mathrm{eV} \quad \text{(A.13)}$$

where $Y_e = \frac{n_e}{n_p+n_n}$ is the relative number density.

Three examples that are relevant to observations are the following:

- At the Earth core $\rho \sim 10$ g/cm^3 and $V_C \sim 10^{-13}$ eV;
- At the solar core $\rho \sim 100$ g/cm^3 and $V_C \sim 10^{-12}$ eV
- At a supernova $\rho \sim 10^{14}$ g/cm^3 and $V_C \sim$ eV

Appendix B

B.1 Origin of oscillogram pattern depicting non unitarity in the Sterile case

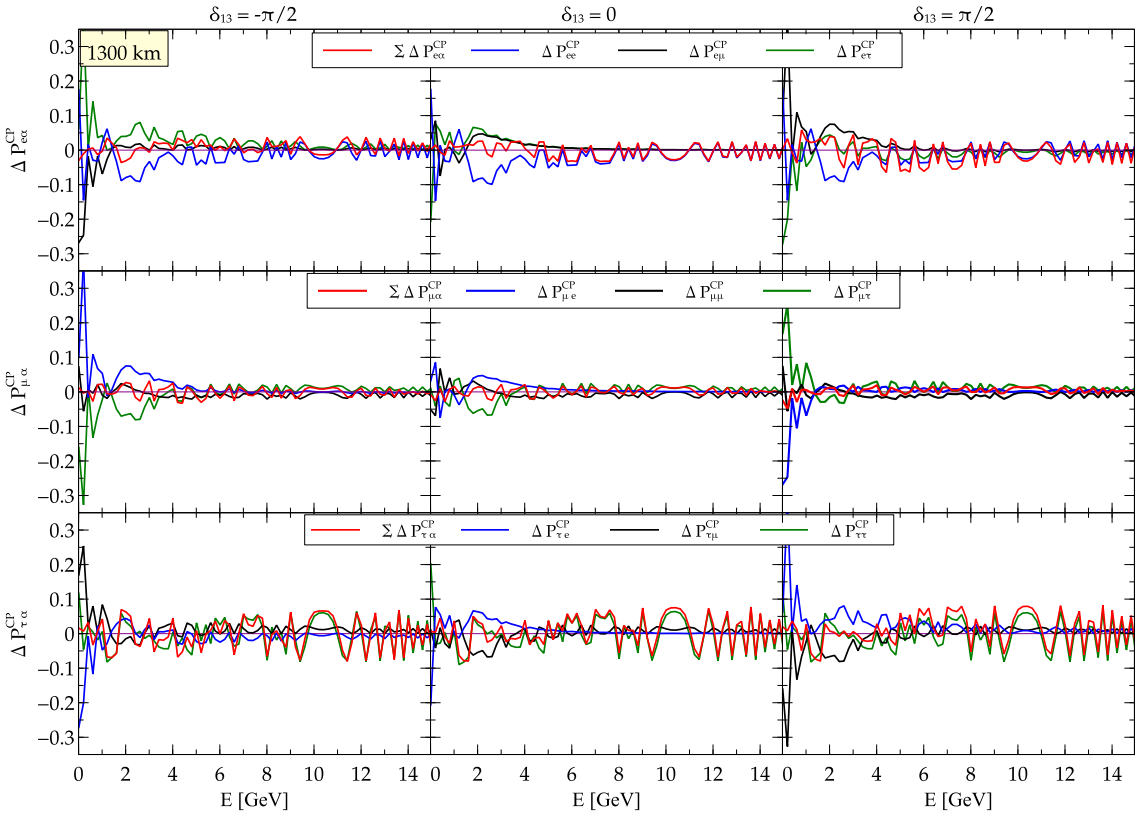

Figure B.1: $\Delta P^{CP}_{e\alpha}$, $\Delta P^{CP}_{\mu\alpha}$ and $\Delta P^{CP}_{\tau\alpha}$ plotted as a function of E for a fixed baseline of 1300 km.

In order to explain the features of different panels in Fig. 2.5, in Fig. B.1 we show

the individual components (blue, black and darkgreen curves) and the sum of the contributions in each row (red curves) appearing in Fig. 2.5 for a fixed baseline of 1300 km. As we can see the red curve is rapidly oscillating which leads to thin light and dark patches in Fig. 2.5 along the horizontal line at 1300 km. The amplitude of the red curve depends on the value of the sterile mixing angle relevant in each channel (see the main text).

B.2 Origin of dark regions in the CP and T oscillograms in NSI case

The approximate analytic expressions for probabilities upto second order in small parameters ($\hat{r_A}, s_{13}, \varepsilon$'s) in different channels in case of NSI are given in [68, 69, 141]. Using the analytic expressions, we attempt to explain the distinct features of the oscillograms (Figs. 2.6, 2.7 and 2.8). In order to simplify the tedious expressions, we assume the following

- NH
- $|\varepsilon_{e\mu}| = |\varepsilon_{e\tau}|$ which is consistent with our choice of parameters in generating the oscillograms. This results in the cancellation of terms $\propto (|\varepsilon_{e\mu}| - |\varepsilon_{e\tau}|)$ and allows for useful simplifications in the analytical formulae.
- the NSI phases are set to zero ($\varphi_{e\mu} = \varphi_{e\tau} = \varphi_{\mu\tau} = 0$)
- Upto second order, the expression for $P(\nu_e \to \nu_\alpha)$ (where, $\alpha = e, \mu, \tau$) contain the NSI parameters $\varepsilon_{e\mu}, \varepsilon_{e\tau}, \varepsilon_{ee}$ [68]. Hence, the mild effect of $\varepsilon_{\mu\tau}, \varepsilon_{\mu\mu}, \varepsilon_{\tau\tau}$ on electron sector cannot be understood from these.
- To get the anti-neutrino probabilities, one needs to do the following replacements $r_A \to -r_A$, $\delta_{13} \to -\delta_{13}, \varepsilon_{\alpha\beta} \to \varepsilon^*_{\alpha\beta}$.

In order to facilitate the presentation, we define the following quantities (the *bars* above indicate the corresponding quantities for antineutrinos.).

1.

$$\begin{aligned} r_A &= \frac{A}{\delta m^2_{31}} \approx 0.03\ E[GeV]\ \rho[gm/cc] \\ \hat{r_A} &= r_A\,(1+\varepsilon_{ee}) \\ \lambda &= \frac{\delta m^2_{31}}{2E} \end{aligned} \tag{B.1}$$

2.

$$\begin{aligned} C &= \frac{\hat{r_A}}{\sqrt{2}}(|\varepsilon_{e\mu}| + |\varepsilon_{e\tau}|)\ ; \bar{C} = -C \\ D_1 &= \frac{\sin((1-\hat{r_A})\lambda L/2)}{1-\hat{r_A}} - \frac{\sin((1+\hat{r_A})\lambda L/2)}{1+\hat{r_A}}\ ; \bar{D_1} = -D_1 \\ D_2 &= \frac{\sin((1-\hat{r_A})\lambda L/2)}{1-\hat{r_A}} + \frac{\sin((1+\hat{r_A})\lambda L/2)}{1+\hat{r_A}}\ ; \bar{D_2} = D_2 \\ D &= \frac{\sin((1-\hat{r_A})\lambda L/2)}{(1-\hat{r_A})^2} - \frac{\sin((1+\hat{r_A})\Delta)}{(1+\hat{r_A})^2}\ ; \bar{D} = -D \end{aligned} \tag{B.2}$$

3.

$$\begin{aligned} \Omega &= |\Omega| e^{i\omega} \quad \text{where} \\ |\Omega| &\approx \sqrt{\frac{s^2_{13} + C^2 + 2 s_{13} C \cos\delta_{13}}{\hat{r_A}^2}} \\ \tan\omega &= \frac{C\sin\delta_{13}}{s_{13} + C\cos\delta_{13}} \\ \text{and } |\bar{\Omega}| &\approx \sqrt{\frac{s^2_{13} + C^2 - 2 s_{13} C \cos\delta_{13}}{\hat{r_A}^2}} \\ \tan\bar{\omega} &= \frac{C\sin\delta_{13}}{s_{13} - C\cos\delta_{13}} \end{aligned} \tag{B.3}$$

Note that, ω vanishes at $\delta_{13} = 0$.

4.

$$\begin{aligned} \Sigma &= |\Sigma|\ \exp\{i\sigma\} \quad \text{where} \\ |\Sigma| &= (r_\lambda/2r_A)\sin 2\theta_{12} + (\propto (|\varepsilon_{e\mu}| - |\varepsilon_{e\tau}|)) \approx (r_\lambda/2r_A)\sin 2\theta_{12}\ , \\ \sigma &\simeq \delta_{13} \quad \text{for } \varphi_{\alpha\beta} = 0\ . \end{aligned} \tag{B.4}$$

Hence, $|\bar{\Sigma}| = -|\Sigma|$ and $\bar{\sigma} = -\sigma$.

Now we give the simplified expressions for the different sectors below.

- $\mu - \tau$ **sector:**

$$\begin{aligned}
\delta\Delta P^{CP}_{\mu\tau} &= \delta(P_{\mu\tau} - \bar{P}_{\mu\tau}) \\
&= (P_{\mu\tau} - \bar{P}_{\mu\tau})|_{\delta_{13}=\pi/2} - (P_{\mu\tau} - \bar{P}_{\mu\tau})|_{\delta_{13}=0} \\
&\approx 4s_{13}C \sin\lambda L/2 \left\{ \cos(\hat{r_A}\lambda L/2)D - \lambda L/2(\cos\lambda L/2)\frac{2r_A}{1-\hat{r_A}^2} \right\} \\
&+ r_\lambda \sin 2\theta_{12} \sin(\hat{r_A}\lambda L/2) \sin\lambda L/2 \sin\theta_{13} D_1 \qquad \text{(B.5)}
\end{aligned}$$

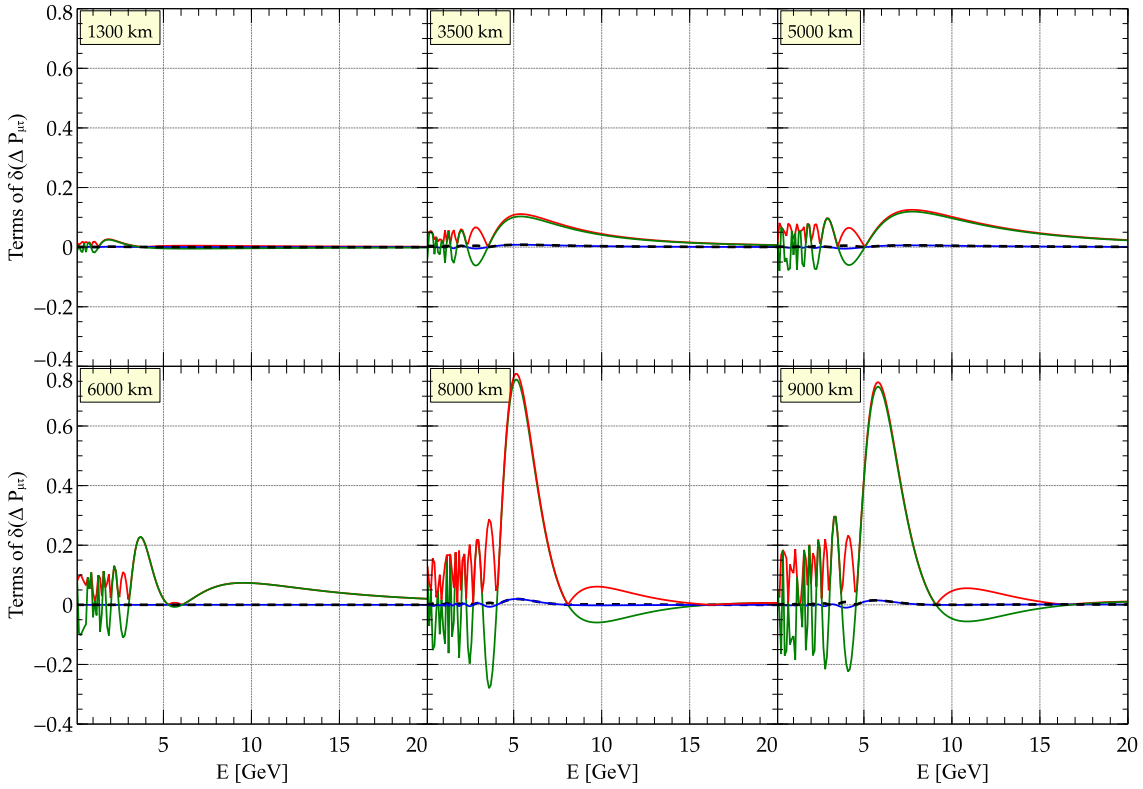

Figure B.2: $\delta(\Delta P^{CP}_{\mu\tau})$ **as a function of E[GeV] for 6 fixed values of the baseline L[km]. The darkgreen (blue) curve corresponds to the first (second) term of Eq. B.5. The red curve is the value of** $|\delta\Delta P^{CP}_{\mu\tau}|$ **in Eq. B.5. The black dashed curve corresponds to the value of** $|\delta\Delta P^{CP}_{\mu\tau}|$ **in the SI case.**

$$
\begin{aligned}
\delta\Delta P^{CP}_{\mu\mu} &= \delta(P_{\mu\mu} - \bar{P}_{\mu\mu}) \\
&= (P_{\mu\mu} - \bar{P}_{\mu\mu})|_{\delta_{13}=\pi/2} - (P_{\mu\mu} - \bar{P}_{\mu\mu})|_{\delta_{13}=0} \\
&\approx 4s_{13}C\left(D_1D_2 + \frac{\hat{r_A}\lambda L/2\sin(\lambda L)}{1-\hat{r_A}^2} - D\cos(\hat{r_A}\lambda L/2)\sin\lambda L/2\right) \\
+\ 2r_\lambda \sin 2\theta_{12}\cos\lambda L/2 &\frac{\sin(\hat{r_A}\lambda L/2)}{\hat{r_A}}\left[s_{13}D_2 + \frac{2C\sin((1+\hat{r_A})\lambda L/2)}{1+\hat{r_A}}\right] \qquad \text{(B.6)}
\end{aligned}
$$

These expressions serve to explain the qualitative features obtained in Fig. 2.6 and 2.7. We note that $\delta\Delta P^{CP}_{\mu\tau}$ and $\delta\Delta P^{CP}_{\mu\mu}$ are shown in the middle row of Fig. 6 and 7 respectively. In Figs. B.2 and B.3, different terms in Eq. B.5 and B.6 have been plotted respectively and we can connect these plots with Fig. 2.6 and 2.7. We observe the following distinct features from Figs. B.2.

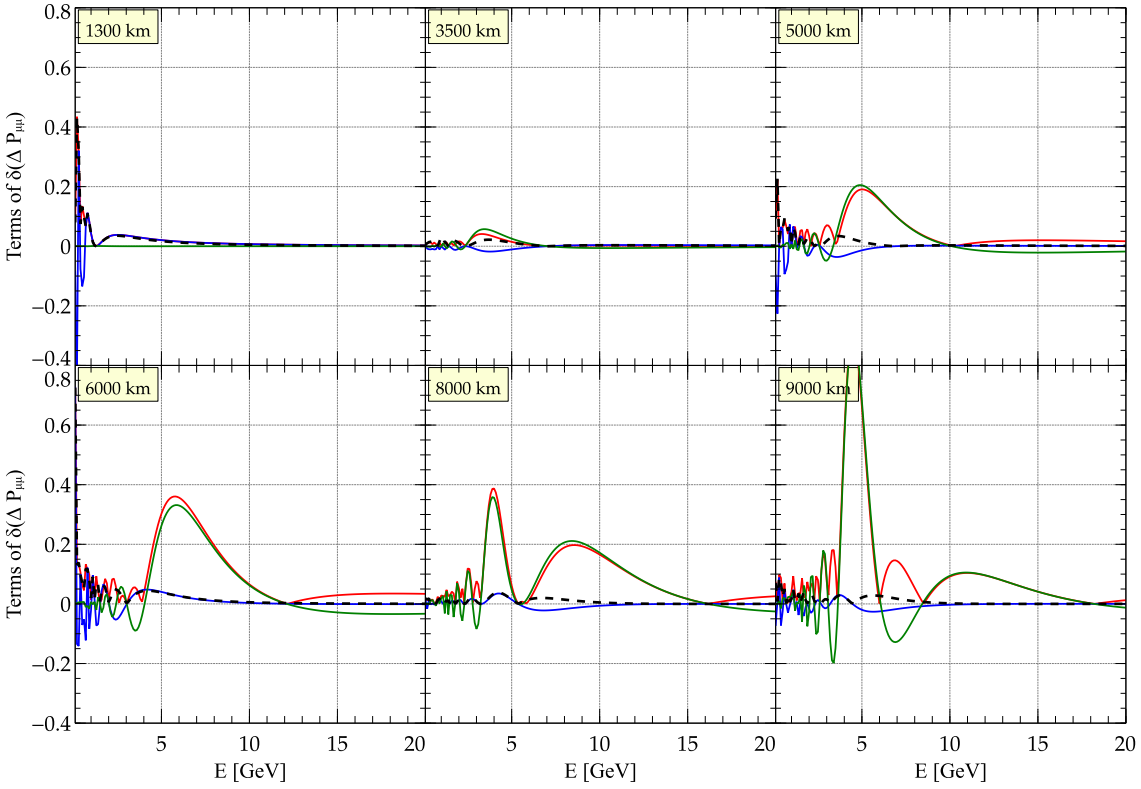

Figure B.3: $\delta(\Delta P^{CP}_{\mu\mu})$ **as a function of E [GeV] for 6 fixed values of the baseline L [km]. The darkgreen (blue) curve corresponds to the first (second) term of Eq. B.6. The red curve is the value of** $|\delta\Delta P^{CP}_{\mu\mu}|$ **in Eq. B.6. The black dashed curve corresponds to the value of** $|\delta\Delta P^{CP}_{\mu\mu}|$ **in the SI case.**

- The gross nature of $|\delta\Delta P^{CP}_{\mu\tau}|$ and $|\delta\Delta P^{CP}_{\mu\mu}|$ (the red curves) is mostly dictated by the first term ($\propto Cs_{13}$) in Eq. B.5 and B.6 respectively. The first term is purely NSI term and is the dominant term in the expression. Note that the second term in Eq. B.5 and B.6 is scaled by r_λ ($\approx 10^{-2}$) which is small in comparison to the first term.

- Let us compare the plots at different baselines. For shorter baselines, $|\delta\Delta P^{CP}_{\mu\tau}|$ is insignificant for all values of energies but for some choice of energies it becomes prominent as the baseline increases. This prominence can be visualized as a series of peaks in the plot. As the baseline increases, these peaks show the following tendencies - shift towards right, becoming broad or narrow and change in prominence (amplitude) among the different peaks. There are two prominent long dark orangish stretches in Fig. 2.6 - one around $E \sim 3.5 - 7.5$ GeV and $L \sim 1000 - 5000$ km and another thinner one around $E \sim 2.5 - 3.5$ GeV and $L \sim 1000 - 5000$ km. These can be explained from the first (right most) peak in Fig. B.2. The slant of these stretches is due to shift in the peak position towards right as the baseline increases. The *sharpness* of the second peak of Fig. B.2 and its relatively mild shift from ~ 3 GeV to ~ 6 GeV as L increases from ~ 3500 km to ~ 9000 km produces the less slanted thin dark stretch in Fig. 2.6. In addition, there are two dark patches at very long baselines in Fig. 2.6 around $E \sim 3-5$ GeV and $L \sim 8000 - 10000$ km. The sudden rise in magnitude of the second peak at around $\gtrsim 8000$ km produces the two dark spots in Fig. 2.6 at longer baseline values.

- The features in Fig. B.3 are grossly similar to Fig. B.2.

  The peaks can be mapped to the dark patches/regions in the NSI plot (middle row and middle panel) of Fig. 2.7.

- We note that there are more white spaces in the middle panel of Fig. B.2 than that in Fig. B.3. Because of the overall $\sin \lambda L/2$ dependence, the first term of $\delta(\Delta P^{CP}_{\mu\tau})$ (dark green curves in Fig. B.2 and Eq. B.5) vanishes if $\lambda L/2 \sim \pi$ or $L/E \sim 1000$ km/GeV. No such overall $\sin \lambda L/2$ is present in the first term of

Eq. B.6 for $\delta(\Delta P^{CP}_{\mu\mu})$, making it less probable to vanish.

- The much smaller dark patches at energies $\lesssim 2$ GeV in the middle panels of Figs. 2.6 and 2.7 arise because of rapid oscillation at lower energies ($\lesssim 2$ GeV) in Fig. B.2 and B.3 respectively.

- In presence of SI only (black dashed curves in Figs. B.2 and B.3), we note that the values of $\delta(\Delta P^{CP}_{\mu\tau})$ and $\delta(\Delta P^{CP}_{\mu\mu})$ are very small. This explains the almost completely white/light yellowish oscillograms in Figs. 2.6 and 2.7 respectively (middle row, left column).

- **$\mu - e$ sector:**

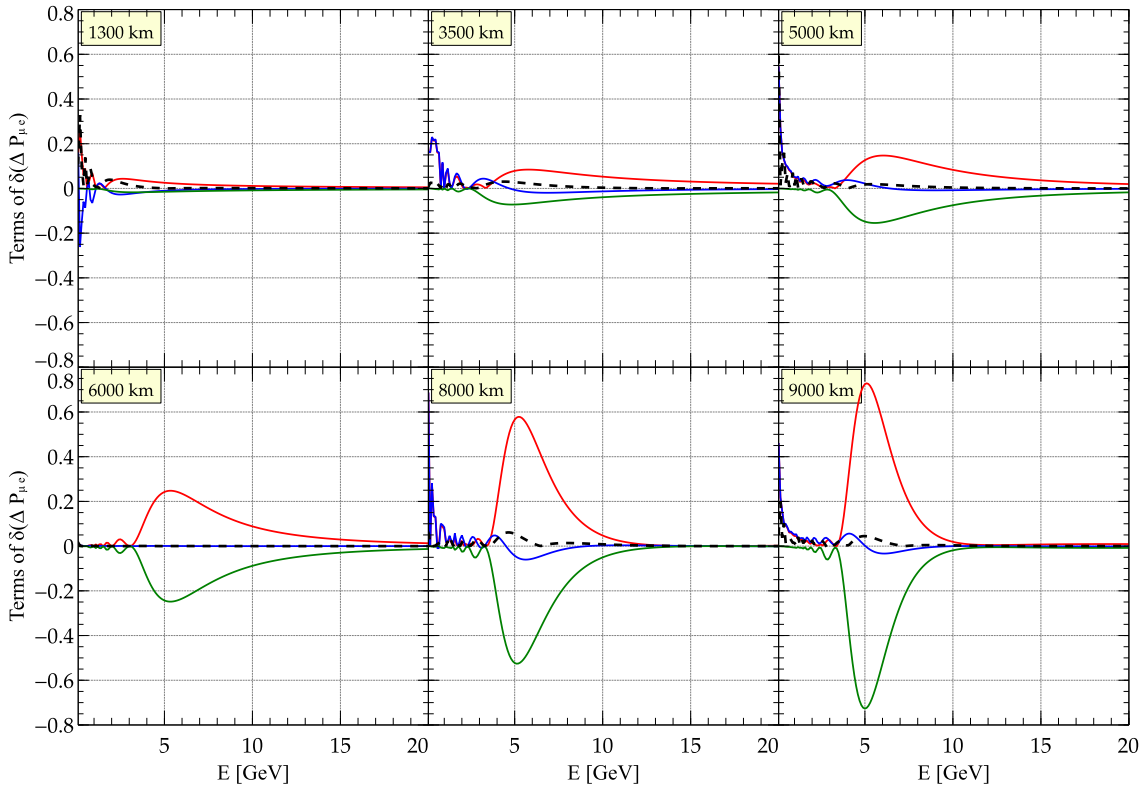

Figure B.4: $\delta(\Delta P^{CP}_{\mu e})$ as a function of E[GeV] for 6 fixed values of the baseline L[km]. The darkgreen (blue) curve corresponds to the first (second) term of Eq. B.7. The red curve is the value of $|\delta\Delta P^{CP}_{\mu e}|$ in Eq. B.7. The black dashed curve corresponds to the value of $|\delta\Delta P^{CP}_{\mu e}|$ in the SI case.

$$
\begin{aligned}
\delta\Delta P^{CP}_{\mu e} &= \delta(P_{\mu e} - \bar{P}_{\mu e}) \\
&= (P_{\mu e} - \bar{P}_{\mu e})|_{\delta_{13}=\pi/2} - (P_{\mu e} - \bar{P}_{\mu e})|_{\delta_{13}=0} \\
&\approx -2\sqrt{2}Cs_{13}\left[\frac{\sin^2((1-\hat{r_A})\lambda L/2)}{(1-\hat{r_A})^2} + \frac{\sin^2((1+\hat{r_A})\lambda L/2)}{(1+\hat{r_A})^2}\right] \\
&+ \frac{2r_\lambda \sin 2\theta_{12}\sin(\hat{r_A}\lambda L/2)}{\hat{r_A}}\Bigg[CD_1\cos\lambda L/2 - s_{13}D_2\sin\lambda L/2 \\
&- \frac{\sin((1-\hat{r_A})\lambda L/2)}{1-\hat{r_A}}(C+s_{13})\cos(\omega-\lambda L/2) \\
&+ \frac{\sin((1+\hat{r_A})\lambda L/2)}{1+\hat{r_A}}(s_{13}-C)\cos(\omega+\lambda L/2)\Bigg]
\end{aligned} \tag{B.7}
$$

We make the following observations from Fig. B.4 which are useful to understand the features in Fig. 2.6 (top row, middle panel).

- In Fig. B.4, we plot $\delta(\Delta P^{CP}_{\mu e})$ as a function of E for different baselines. The overall behaviour is dominated by the first term of Eq. B.7.

- Unlike the case of $\delta(\Delta P^{CP}_{\mu\tau})$ or $\delta(\Delta P^{CP}_{\mu\mu})$, here we have only one primary peak in Fig. B.4. This peak starts appearing roughly at $L \gtrsim 5000$ km and rapidly grows with the baseline. This gives rise to the dark inverted triangular shaped patch in Fig. 2.6 (top row, middle column) at $E \approx 4 - 6\ GeV$.

- The orangish blob in the same panel of Fig. 2.6 (at $L \lesssim 2000$ km and roughly at 5 GeV $< E <$ 9 GeV) is due to the presence of ε_{ee} [1].

- **$e - e$ sector:**

$$
\begin{aligned}
\delta\Delta P^{CP}_{ee} &= \delta(P_{ee} - \bar{P}_{ee}) \\
&= (P_{ee} - \bar{P}_{ee})|_{\delta_{13}=\pi/2} - (P_{ee} - \bar{P}_{ee})|_{\delta_{13}=0} \\
&\approx 8Cs_{13}\left[\frac{\sin^2((1-\hat{r_A})\lambda L/2)}{(1-\hat{r_A})^2} + \frac{\sin^2((1+\hat{r_A})\lambda L/2)}{(1+\hat{r_A})^2}\right]
\end{aligned} \tag{B.8}
$$

From Eq. B.8, we note that $\delta\Delta P^{CP}_{ee}$ contains only one term which is the same as the first term of Eq. B.7 for $\delta\Delta P^{CP}_{\mu e}$ apart from a scaling factor. We note that

[1] we have checked this numerically by assuming only the presence of the parameter ε_{ee}

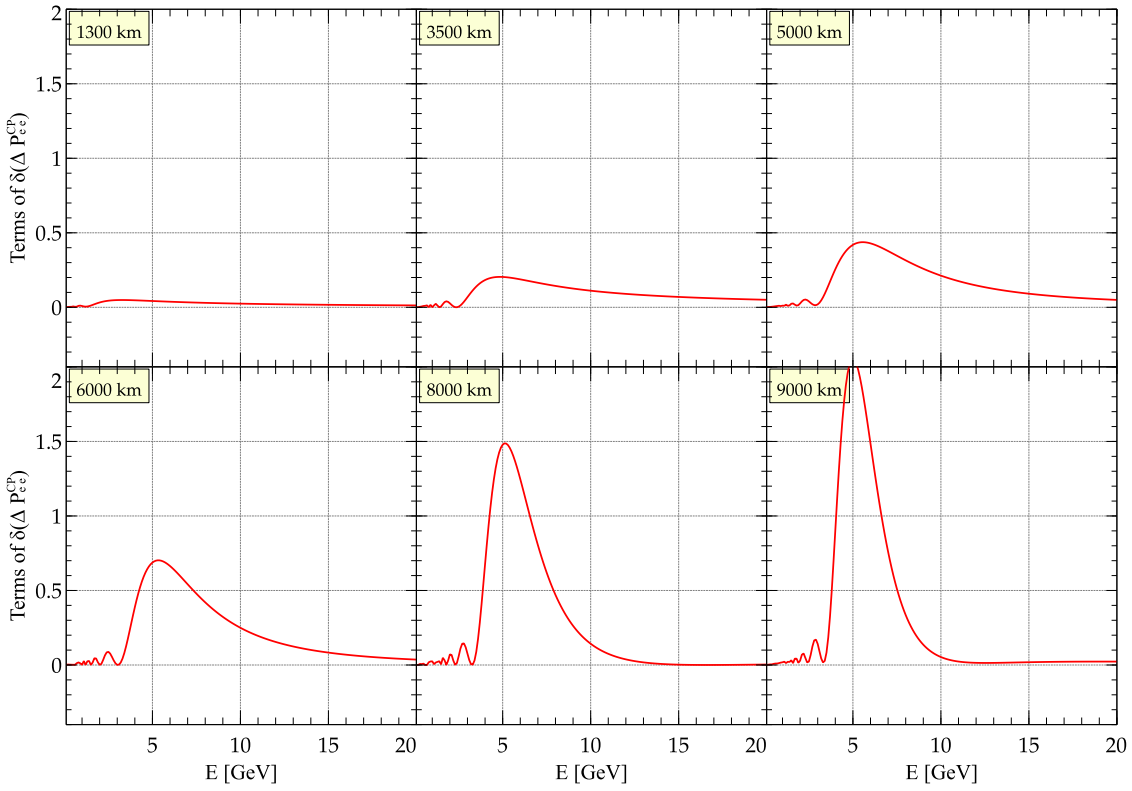

Figure B.5: $|\delta(\Delta P^{CP}_{ee})|$ **as a function of E [GeV] for 6 fixed values of the baseline L[km]. The single term in Eq. B.8 has been plotted as red curves.**

$\delta\Delta P^{CP}_{ee}$ vanishes completely in absence of NSI. Indeed, we see that the top, left panel of Fig. 2.7 is completely white. Also, the second column of the top row of Fig. 2.7 is qualitatively similar [2] to the corresponding oscillogram for $\delta\Delta P^{CP}_{\mu e}$ (top row, second column of Fig. 2.6).

B.3 Pattern of CP and T oscillograms in the Sterile case

In Fig. B.6, we plot the various probability differences (see the legend) that go in the calculation of $\delta\Delta P^{CP}_{\alpha\beta}$ in presence of a sterile neutrino for the channels $\nu_\mu \to \nu_e$, $\nu_\mu \to \nu_\tau$ and $\nu_e \to \nu_\tau$ (corresponding to the three rows of Fig. 2.6). The baseline is taken to be 1300 km. These three panels correspond to the three rows of the

[2] The numerical factor $2\sqrt{2}$ makes the dark patches in the oscillogram for $\delta\Delta P^{CP}_{ee}$ only darker.

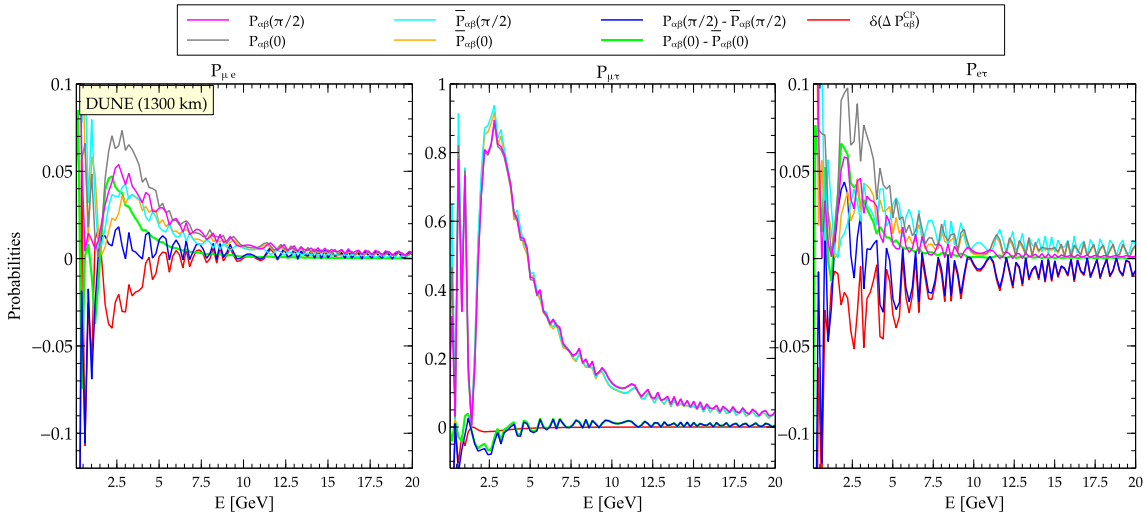

Figure B.6: Probability differences for the appearance channels in sterile case and size of the wiggles for different channels for a fixed baseline of 1300 km.

right column of Fig. 2.6. One can see that $\delta\Delta P^{CP}_{\mu\tau}$ (represented by the red curve in Fig. B.6) is quite smooth, unlike $\delta\Delta P^{CP}_{\mu e}$ or $\delta\Delta P^{CP}_{e\tau}$, that show rapidly oscillating nature[3]. We also note that the amplitude of the wiggles is larger in the $\nu_e \to \nu_\tau$ channel than that in $\nu_\mu \to \nu_e$ channel. Indeed, in Fig. 2.6 (the three rows in the right column), we see that the oscillogram is mostly *smooth* in the $\nu_\mu \to \nu_\tau$ channel. Also, the $\nu_e \to \nu_\tau$ channel seems to be more *wiggly* than the $\nu_\mu \to \nu_e$ channel in the oscillogram [4].

[3]these rapid secondary oscillations are the manifestations of a high $\delta m^2_{41} \sim 1\ eV^2$

[4]Note from Table. 2.3 that, we have considered a value of 15^o for θ_{34}, which is quite large compared to θ_{14} ($\sim 8^o$) and θ_{24} ($\sim 5^o$). The large allowed range for θ_{34} ($< 25^o$) permits us to use such a large value for it. Although θ_{34} has marginal effect on the $\nu_\mu \to \nu_e$ channel, the $\nu_e \to \nu_\tau$ channel depends quite significantly on θ_{34}. This, in turn, produces the large wiggles for $\delta\Delta P^{CP}_{e\tau}$.